Mass Transfer of Hydrogen Sulfide in Sewer Drop Structures

by

Letian Sun

A thesis submitted in partial fulfillment of the requirements for the degree of

Doctor of Philosophy

in

Water Resources Engineering

Department of Civil and Environmental Engineering
University of Alberta

Abstract

Hydrogen sulfide (H_2S) is the primary cause of the widespread odor and corrosion issues in sanitary sewer systems. When wastewater falls in drop structures, the emission of H_2S is expected to be significantly enhanced. This study focuses on the mass transfer coefficient, K_L, for H_2S and other surrogate gases from falling droplets, at turbulent water surface and in drop structures.

When wastewater breaks up into small droplets in drop structures, the emission of H_2S is expected to be significantly enhanced relative to that of the continuously falling sewage. In this study, laboratory experiments of mass transfer from falling liquid droplets to air were conducted with two gases: H_2S and carbon dioxide (CO_2). In the testing range of droplet diameter (3.02-4.68 mm) and free-falling height (0.1-1.5 m), the K_L value at 20℃ was found to be 0.9-4.5 × 10^{-4} m/s, which increased with the falling height (or velocity) while decreased with the droplet size. A modified equation was proposed to better predict K_L. In addition, CO_2 was found to be a suitable surrogate for H_2S in mass transfer due to the toxicity of H_2S.

Laboratory experiments were conducted to study the mass transfer at the pool surface with falling water drops or a single jet. In the test range of falling flow rate of 49-223 mm/h and falling velocity of 3.1-5.2 m/s [kinetic energy flux KEF = 0.11-0.80 J/(m^2s)], K_L for the pool surface was found to be 2.6-14.8 × 10^{-5} m/s for H_2S. K_L was found to be 76% larger when the pool surface was impinged by water drops than by a single jet. In addition, K_L was 27-47% larger in the half of the water surface directly receiving the drops or jet than the other half. The increase of water depth in the pool promoted the mass transfer, especially for the scenario of a falling jet. Equations were proposed to predict K_L under drops or jet. Finally, K_L for H_2S and for O_2 was found almost the same, indicating O_2 can be a safe surrogate gas for H_2S.

Laboratory experiments were conducted using two forms of falling sewage in drop structures: free-falling and attached-falling jets. The results show that K_L and concentration deficit ratio, r, increased with an increase of drop height (0.2 - 1.4 m) and a decrease of flow rate (0.9 - 2.0 L/min). Nonlinear correlations between r and the hydraulic parameters were proposed for both jet scenarios, with good agreements with experimental results. The difference between the two jet scenarios appeared to be related to the size of drop structures: in the large drop structure, r of the free-falling jet was larger than that of the attached-falling jet; while in the small drop structure, r was almost the same. Finally, the mass transfer of O_2 in a prototype drop structure was estimated. If the drop height is < 3 m, almost all the mass transfer happens at the bottom pool of drop structure; if the drop height is > 6 m, falling droplets are the main (> 80%) contributor.

Field work was carried out in the west area of Edmonton, Alberta, Canada to investigate the wastewater quality and emission of H_2S in sewer network. The wastewater samples were collected and analyzed for sulfide and other relevant parameters (e.g., sulfate and COD). Empirical models can predict sulfide generation. The operation of the upstream pump station could cause the sudden increase of H_2S in the sewer air of the adjacent discharge manholes. Over 90% of H_2S stayed in the liquid phase when wastewater flowed by gravity in the sewer pipes. In the drop structure of 8 m, the H_2S concentration in the upstream was 2.6 times of that in downstream and r for H_2S was 2.0, which proves the enhancement to the emission of H_2S in drop structures.

This research provides new insights on the physical processes and modeling of H_2S emission in sewer drop structures. The research outcomes are useful for odor and corrosion control in municipal drainage systems.

Preface

This thesis is an original work by Letian Sun under the supervision from Dr. David Z. Zhu and Dr. Wenming Zhang. It is presented in a paper format and consists of six chapters.

Chapter 1 is a general introduction on the background and knowledge gap of this study.

Chapter 2 to 5 are the main contents of this thesis.

Chapter 2 was published as: Sun, L., Zhang, W., and Zhu, D. Z. (2020). "Emission of Hydrogen Sulfide from Falling Droplets in Sewage Drop Structures." *Journal of Environmental Engineering*, 146(12), 04020135. 10.1061/(ASCE)EE.1943-7870.0001819.

Chapter 3 was submitted to *Journal of Environmental Engineering* and under review.

Chapter 4 is currently being prepared as a journal manuscript and ready for submission.

Chapter 5 is currently being prepared as a journal manuscript.

Chapter 6 is a conclusion chapter. It contains the general conclusions of this thesis, and suggestions for the future research on this topic.

I was responsible for the experimental design, data collection and analysis as well as the manuscript composition. Dr. D. Zhu was the supervisory author and was directly involved with the concept formation and the manuscript composition. Dr. W. Zhang assisted with the experimental design and contributed to manuscript edits of the thesis. Dr. X. J. Shi assisted with the manuscript writing and Dr. T. Yu contributed to the manuscript edits of the chapter 5.

The author also contributed the following publications:

Sun, L, Zhang, W. and Zhu, D. Z. (2019). “Experimental Study of Mass Transfer in Single Falling Drops.” *Proceedings of the International Symposium on Sustainable Urban Drainage (SUD)*, Ningbo, China.

Sun, L, Zhang, W. and Zhu, D. Z. (2021). “Emission of Hydrogen Sulfide on the Turbulent Water Surface.” *Proceedings of the 2021 International Workshop on Sustainable Urban Drainage*, Ningbo, China.

Dedicated to:

My family

Thanks for your endless love and support

Acknowledgements

To Begin with, I want to sincerely thank my supervisor, Dr. David Z. Zhu, for offering me this great opportunity to pursue my doctoral degree and for kind support and guidance on my research. His enthusiasm for research is always inspiring me. From him I have learned how to think critically on the research. I would like to thank my co-supervisor, Dr. Wenming Zhang, for his valuable guidance and being patient with me for the research. I would also like to thank Dr. Tong Yu for his guidance and serving as my supervisory committee member, and support with his environmental laboratory. I am very grateful to Dr. Peter Steffler, Dr. Jes Vollertsen and Dr. Wei Victor Liu for serving on the PhD examining committee. Their insightful suggestions on this thesis are much appreciated.

I would like to thank my research partners, Xiao Jie Shi, Guijiao Zhang, Chenxi Wang, Hanyu Liu, Vivian Shao, and Pengcheng Li, for their help in the experiments and field work, and the general discussion with the research. Special thanks to Perry Fedun for his technical assistance with the setups of my lab experiments and field work. I would also like to thank Albert Kwan, Adam Shypanski, Brandy Mckay, Kerri Buck, Bappi Chowdhury, Scott Vatcher and Colin Bergsten at EPCOR.

Last but not the least, I gratefully acknowledge the support for the research project from the Natural Sciences and Engineering Research Council of Canada (NSERC) and EPCOR. I would like to express my gratitude to the group members. It is nice to meet you all. I would also like to express my gratitude my family and friends for their continuous support and encouragement, which gives me the courage to keep going. I cannot make this without them.

Table of Contents

List of Tables

List of Figures

1. General Introduction

1.1. Research Background

Mass transfer is the net movement of a species in a mixture from one phase to another in the presence of a difference in concentration (or partial pressure) (Seader et al. 2010; Mandal 2018). The mass transfer of a gas (oxygen, carbon dioxide, hydrogen sulfide, etc.) between gas phase and liquid phase are common in nature, for example, in open channels, oceans and sewers. In urban sanitary sewer system, one of the most concerned mass transfer processes is that of hydrogen sulfide (H_2S). H_2S is the primary cause for sewer odor and corrosion (Nielsen et al. 1992; Hvitved-Jacobsen et al. 2013). It is a colorless gas with a rotten egg smell and the odor threshold ranges 0.0005-0.3 ppm (USATSDR 2016). It is highly toxic, with the OSHA (Occupational Safety and Health Administration) ceiling of 20 ppm and NIOSH IDLH (National Institute for Occupational Safety and Health; immediately dangerous to life or health) of 100 ppm (USATSDR 2014). It is generated in the sewer biofilms under anaerobic condition by sulfate-reducing bacteria (SRB) (Hvitved-Jacobsen et al. 2013; Vollertsen et al. 2015). If dissolved oxygen (DO) concentration in the wastewater is high enough, the growth of the SRB is inhibited (Hao et al. 1996) and the generation of sulfide is reduced. H_2S can be oxidised to sulfuric acid at the sewer walls under aerobic conditions (Vollertsen et al. 2008; Jensen et al. 2009; Hvitved-Jacobsen et al. 2013), which causes the corrosion of concrete pipes or steel structures. Therefore, H_2S is of great interest to municipalities worldwide (US EPA 1974; Hvitved-Jacobsen et al. 2013; Carrera et al. 2016; Zhang et al. 2016; Jiang et al. 2017).

In the city of Edmonton, Alberta, Canada, residents in some neighbourhoods have been suffering from the problem of sewer odor for many years. H_2S can be emitted from liquid phase to the sewer

air space (Matias et al. 2014), move with the air (Zhang et al. 2016; Qian et al. 2018), release to the atmosphere at many parts of the sewer network such as manholes and pump stations (Pérez et al. 2013; Pan et al. 2018), and cause odor nuisances to the residents. From 2008 to 2017, 8,894 formal complaints in total were reported in the city area (Pan et al. 2018). One manhole in the west of the city even reached 400-500 ppm of H_2S (Yang et al. 2022). Besides of the odor problems, sewer pipe corrosion is a continuous issue in the city. In October 2020, a 23-meter deep sinkhole was discovered at the intersection of 61 Avenue and 109 Street in Edmonton because of the sanitary sewer corrosion and subsurface void, where the traffic was blocked for a few months (Shypanski 2020; Global NEWS 2021). Therefore, it is urgent to deal with the problems of H_2S in urban sewer systems in cities such as Edmonton.

In municipal sewer systems, sewer drop structures is a key location for the emission of H_2S (Yang et al. 2019; Zuo et al. 2019). Drop structures are common in Edmonton and worldwide for dropping sewage from a higher to a lower elevation. When wastewater falls down into the drop structure, the water breaks into water droplets if the falling height is large enough (Ma et al. 2016) or falls in the form of a jet if the height is small. When the drops or jet impinge on the bottom pool of the drop structure, sewer air is entrained into the pool, causing a large number of bubbles and strong turbulence there. These processes could enhance the mass transfer of H_2S and oxygen (O_2) in sewer drop structures. The mass-transfer could happen at jet surface, surface of falling droplets from jet breakup, bottom pool (turbulent water surface, bubbles, splashing droplets, etc.). However, the contribution of each mechanism to mass transfer is unclear.

1.1.1. Mass Transfer Coefficient (K_L)

For mass transfer of hydrogen sulfide (H_2S) and oxygen (O_2) in sewers between the liquid and the air, the driving force is the gas concentration difference in the two phases (Handlos and Baron 1957). Molecular diffusion controls the mass transfer process between the two phases, which is described by the Fick's First Law: the diffusion flux of a gas A in an isothermal, isobaric binary system is proportional to the concentration gradient in a particular direction (Mandal 2008):

$$N_A = -D\frac{\mathrm{d}C_A}{\mathrm{d}Z} \tag{1-1}$$

where N_A is the mass flux of the gas, D is the molecular diffusivity of the gas in the fluid, C_A is the gas concentration in the fluid.

The mass transfer coefficient, K_L, is defined as

$$K_L \equiv \frac{N_A}{\Delta C_A} \tag{1-2}$$

where ΔC_A is the gas concentration difference between liquid phase and air phase, $\Delta C_A = C_a/\mathrm{H}\text{-}C_L$, C_a is the gas concentration in the air, H is the Henry's Law constant = [equilibrium concentration in gas phase]/[equilibrium concentration in liquid phase], C_L is the gas concentration in the liquid. In Eq. (1-2), $N = dM/Adt = VdC_L/Adt = dC_L/adt$, where M is the gas mass, A is the mass transfer area between water and air, V is the volume of liquid, t is time, a is the specific area or the ratio between area and volume. Therefore, Eq. (1-2) becomes:

$$\frac{dC_L}{dt} = K_L a\left(C_a / H - C_L\right) \tag{1-3}$$

Eq. (1-3) can be integrated with the falling time of droplets as (Amokrane et al. 1994):

$$\ln\left(\frac{C_1 - C_a / H}{C_2 - C_a / H}\right) = K_L a \Delta t \tag{1-4}$$

where C_1 and C_2 = gas concentration in the liquid phase at two different times, respectively; and Δt = droplet falling time. If K_L is obtained at different temperatures, it is usually adjusted to standard temperature (20℃) (Elmore and West 1961):

$$K_{L,20} = K_{L,T}\left[1.0241^{(20-T)}\right] \tag{1-5}$$

where $K_{L,T}$ and $K_{L,20}$ = mass transfer coefficients determined under the test temperature T (℃) and 20℃, respectively.

1.1.2. Mass Transfer Theories

Two-film Theory

In Figure 1-1, $Z = 0$ is the interface (or boundary), and the film thickness is δ. In the thickness of ΔZ, the mass flux of input is $N_A|_Z$, the mass flux of output is $N_A|_{Z+\Delta Z}$, as the steady state, the rate of accumulation is 0, i.e. $N_A|_Z = N_A|_{Z+\Delta Z}$, that is

$$\lim_{\Delta Z \to 0} \frac{N_A|_Z - N_A|_{Z+\Delta Z}}{\Delta Z} = 0 \tag{1-6}$$

therefore,

$$\frac{dN_A}{dZ} = 0 \tag{1-7}$$

Substituting N_A with Fick's First Law [Eq. (1-1)],

$$\frac{d}{dZ}\left(-\frac{DdC_A}{dZ}\right)=0 \tag{1-8}$$

Since D is a constant,

$$\frac{d}{dZ}\left(\frac{dC_A}{dZ}\right)=0 \tag{1-9}$$

Integrating for the boundary conditions: $C_A = C_{Ai}$ when $Z = 0$, $C_A = C_{Ab}$ when $Z = \delta$,

$$C_A = C_{Ai} - \left(C_{Ai} - C_{Ab}\right)\frac{Z}{\delta} \tag{1-10}$$

That is,

$$\frac{dC_A}{dZ} = \frac{C_A - C_{Ai}}{Z} = -\frac{\left(C_{Ai} - C_{Ab}\right)}{\delta} \tag{1-11}$$

Hence, the concentration in the film is linear. Substituting to Eq. (1-1),

$$N_A = \frac{D}{\delta}\left(C_{Ai} - C_{Ab}\right) \tag{1-12}$$

This equation is the "two-film theory" of mass transfer, where δ is the film thickness. The two-film theory assumes that the fluid beyond the film is highly turbulent mixed (turbulent transport) and providing no resistance to mass transfer, and the resistance only exists in the hypothetical film where molecular transport exists and turbulence dies out. It also assumes a steady state. The final conceptional model (Lewis and Whitman 1924) is:

$$k_l = \frac{D}{\delta} \tag{1-13}$$

where k_l is the liquid mass transfer coefficient. $\delta \sim 0.1$ mm for liquid phase and $\delta \sim 1$ mm for gas phase (Mandal 2018). The theory suggests that k_l is proportional to D^1 in the film, and to D^0 at the outer boundary of the film. If a power function D^n is employed to represent the mass transfer coefficient k_l, n is expected to fall between 0 and 1 (Sherwood et al 1975). However, it cannot be used for calculating k_l because is usually unknown, but δ decreases with increasing turbulence (Skelland 1974).

In Figure 1-2, C_{sl} is called the interfacial concentration in liquid phase and often unknown. Since k_l is the liquid mass transfer coefficient, there should be a gas mass transfer coefficient, k_g. It follows that

$$N_A = k_l\left(C_{sl} - C_l\right) = k_g\left(C_g - C_{sg}\right) \tag{1-14}$$

Also, based on Henry's Law,

$$C_{sl} = \frac{C_{sg}}{H} \tag{1-15}$$

Eliminating C_{sg} and C_{sl} in the Eqs. (1-13) and (1-14),

$$N_A = \frac{1}{\dfrac{1}{k_l} + \dfrac{1}{Hk_g}}\left(\frac{C_g}{H} - C_l\right) \tag{1-16}$$

or

$$\frac{dC_l}{dt} = \frac{1}{\dfrac{1}{k_l} + \dfrac{1}{Hk_g}}a\left(\frac{C_g}{H} - C_l\right) \tag{1-17}$$

Comparing Eqs. (1-3) and (1-17), it is obtained

$$\frac{1}{K_L} = \frac{1}{k_l} + \frac{1}{Hk_g} \tag{1-18}$$

The resistance to mass transfer is defined as the inverse of the mass transfer coefficient, where $R_L = 1/K_L$, $R_l = 1/k_L$, $R_g = 1/Hk_g$. The relationship among the resistance is

$$R_L = R_l + R_g \tag{1-19}$$

For the gases with low solubility in water, such as O_2 and H_2S, $Hk_g >> k_l$ or $1/k_l >> 1/Hk_g$, i.e. the resistance in the liquid film is much larger than the gas film, therefore, $K_L \approx k_l$.

Penetration Theory and Surface Renewal Theory

The penetration theory for mass transfer was proposed by Higbie (1935). The fluids in turbulent flow contain "eddies". All eddies encounter the interface in direct contact for a time period, τ, in seconds. The contact time is too short to permit the attainment of a steady state. While in contact for this short time-period, diffusive mass transport "penetrates" from the surface into the adjoining fluid driven by the concentration differences. The entering chemical mass is viewed to be penetrating into the eddy, which is the origin of the term "penetration theory" for mass transfer. Depending on eddy size and its kinetic energy level, the contact time-periods are highly variable. Higbie assumed that one average contact time-period $\bar{\tau}$ was sufficient to characterize the eddy behavior (Thibodeaus 2011). The liquid mass transfer coefficient k_l is:

$$k_l = 2\sqrt{\frac{D}{\pi \bar{\tau}}} \tag{1-20}$$

Dankwerts (1951) proposed the surface renewal theory by extension of the penetration theory, which employs a wide spectrum of eddy contact times and averaged the varying degrees pf

penetration. It is assumed that the fluid on the surface is periodically renewed by the bulk fluid, i.e. eddies impinges on the water surface. He assumed a distribution function of eddy contact times, which yields liquid mass transfer coefficient k_l:

$$k_l = \sqrt{Ds} \tag{1-21}$$

where s is the fractional renewal rate. This value is a constant, no matter what the time of contact, all are renewed at the same rate. The films exist at the air-water interface, but the thickness varies over space and time. The surface-renewal theory states that the renewal rate is most important in air-water mass transfer, rather than the film thickness (Gulliver 1990).

The penetration theory and the surface renewal theory apply for the flow condition containing diffusion and convection. However, s for the surface renewal theory and $\bar{\tau}$ for the penetration model are generally unavailable which makes them not as widely used as two-film theory.

1.1.3. Previous study

There are previous studies on addressing the sewer odor and corrosion problems. Some of them concentrated on the biochemical reaction of H_2S generation and its control in sewers (Hvitved-Jacobsen et al. 2002; Nielsen et al. 2005; Jiang et al. 2013a b; Park et al. 2014; Zhang et al. 2022, etc.), and some studied the mass transfer of H_2S in a closed cylindrical rector or gravity sewer pipes (Jensen 1995; Yongsiri et al. 2003; Lahav et al. 2004, 2006; Carrera et al. 2017a b;). They provided a basic knowledge of the mass transfer of H_2S in sewers; however, the previous research can not be directly applied for sewer drop structures because of different mass-transfer mechanisms.

For mass transfer between air and a stagnant liquid droplet, the mass transfer is controlled by diffusion in the vicinity of the interface (Wylock et al. 2012). When a droplet is falling, there would be an internal flow field inside the drops (LeClair et al. 1972; Shao et al. 2012; Choi et al. 2016), which would enhance the mass transfer between air and water. There are some existing models of K_L for single droplets in air (Handlos and Baron 1957; Angelo et al. 1966; Ruckenstein 1967; Clift et al. 1978; Amokrane et al. 1994). In these models, K_L increases with droplet falling velocity and gas diffusivity in water but decreases with the droplet size; however, for a typical droplet size (1-9 mm), there can be up to 10 times difference in predicted values of K_L, which necessitates further research. To date, to the author's best knowledge, no direct experimental study has been reported on the mass transfer of H_2S from single falling droplets to air. A few experimental studies (Garner and Lane 1959; Altwicker and Lindhjem 1988) were conducted on the mass transfer of carbon dioxide (CO_2) between single falling droplets and air, but the applicability of CO_2 as a surrogate gas for H_2S need to be examined.

When falling sewer droplets or falling jet impinges the bottom pool of a drop structure, their energies cause cavities, drops and surface waves, which create a high level of turbulence on the pool surface (Banks et al. 1984). Previous research in this area focused on the mass transfer of O_2 and CO_2 between raindrops and natural water body (lakes, sea, etc.) (Banks et al. 1984; Belanger and Korzun 1990; Ho et al. 1997; Takagaki and Komori 2007; Harrison et al. 2012; Ashton et al. 2016; Jiang et al. 2018), where the turbulent water surface caused by the falling droplets had significant enhancement to K_L. Despite of recent progress, a systematic experimental study on the mass transfer of H_2S at the turbulent water surface under falling drops or single jet is missing. And the comparison between the two scenarios (falling drops vs. single jet) on the mass transfer is also missing. The applicability of O_2 as a surrogate gas for H_2S also need to be verified.

Mass transfer in drop structures of physical models or field prototypes has been studied (Pomeroy and Lofy 1977; Nakasone 1987; Pincince 1991; Labocha et al. 1996; Rahmé et al. 1997; Matias et al. 2014, 2017b), where jet drop height, discharge, and tail water depth are the key parameters affecting mass transfer. It is found that the mass transfer rate increases with drop height and tailwater depth, but the role of flow discharge has not been quantified. To the author's best knowledge, experimental study using H_2S directly (not via a surrogate gas like O_2) and examining K_L in drop structures, has not been revealed in the literature. The falling jet in sewer drop structures can exist as two forms: 1) free-falling jet; 2) attached-falling jet. Both forms of falling sewage jets substantially but differently affect the mass transfer of H_2S and O_2. The comparison of mass transfer between two sewage jet forms, free-falling and attached-falling, has not been reported.

Field studies of sewer odor were conducted in sewer pipes of Edmonton (Qian et al. 2021; Yang et al. 2022) and other locations in the world, such as USA (US EPA 1974), Denmark (Nielsen et al. 2008), Australia (Jiang et al. 2013a) and Portugal (Matias et al. 2017a). In Zhang et al. 2016, Guo et al. 2018 and Zhang et al. 2020, sewer air flow induced by drop structures was investigated. In Guo et al. 2018 and Yang et al. 2019, 2020, H_2S concentration in drop structures were measured, which shows that drop structures have big effect on emission of H_2S. However, the previous studies are not enough for quantifying the mass transfer of H_2S in field drop structures. Therefore, performing field work is necessary for estimating H_2S emission and addressing the sewer odor and corrosion issue.

1.2. Research Objectives

The research objectives are summarized herein:

1. To investigate the effect of droplet size and droplet falling velocity on K_L for H_2S from falling droplet to air.
2. To study K_L for H_2S at turbulent water surface under falling drops or single jet, and compare the effect of falling drops and single jet on K_L.
3. To experimentally examine r in drop structures using H_2S directly, and compare mass transfer between two sewage jet forms (free-falling and attached-falling).
4. To verify the applicability of CO_2 and O_2 as a surrogate gas for H_2S in sewer drop structure.
5. To estimate mass transfer in real-world or prototype sewer drop structures.

1.3. Thesis Outline

This thesis is composed of four research parts, and each of them is presented in a separate chapter. Chapters 2-4 are experimental results and Chapter 5 is the application in field drop structures. It is organized as follows:

Chapter 2 is an experimental study on emission of H_2S from falling droplets in sewer drop structures. The effects of droplet sizes and droplet falling velocity on the mass transfer were studied.

Chapter 3 is an experimental study on mass transfer of H_2S at turbulent water surface receiving falling drops or falling jet. The effect of water flow rate and falling velocity on K_L was invested. The effect of falling drops and single jet on K_L was compared.

Chapter 4 is an experimental study on mass transfer of H_2S in a drop structure. The effect of drop height, tail water depth and flow rate on the mass transfer rate was investigated. Two jet forms, free-falling and attached-falling, on mass transfer were compared. Finally, the mass transfer in drop structure prototypes was estimated.

Chapter 5 is a field work on the wastewater quality, sulfide generation and H_2S emission in a sewer network. The sulfide generation rate was estimated and the mass transfer of H_2S in a drop structure of 8 m was investigated.

Chapter 6 is the conclusions of the thesis and the future directions of this research.

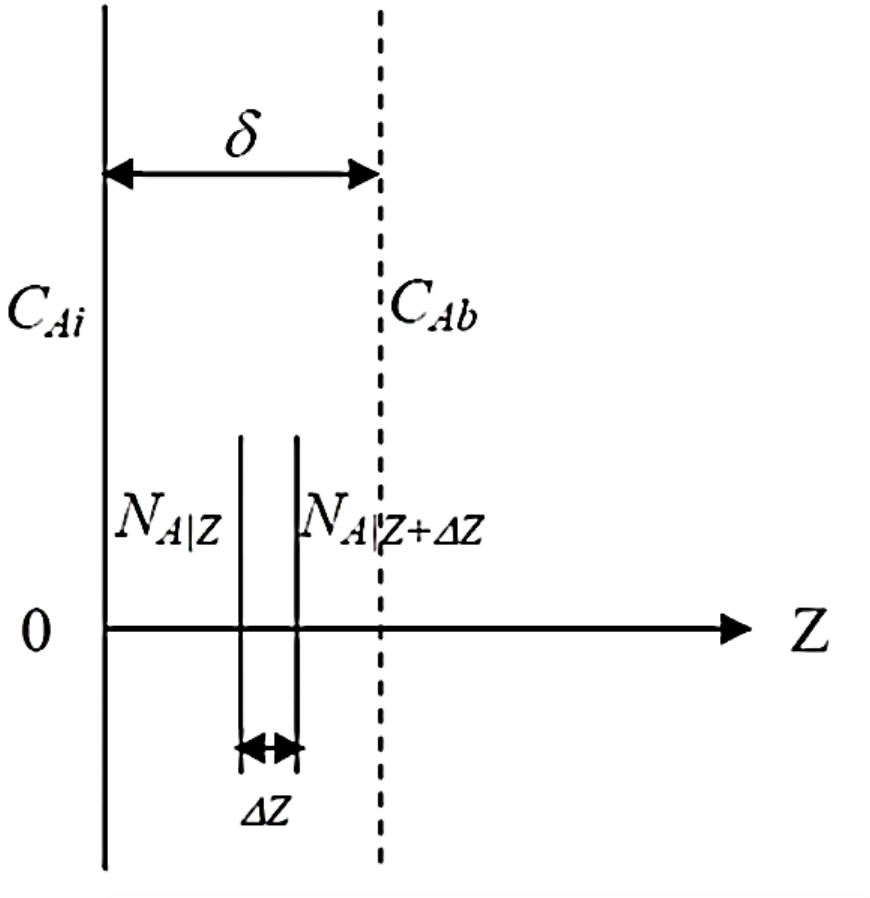

Figure 1-1 Mass flux in the film (Mandal 2008).

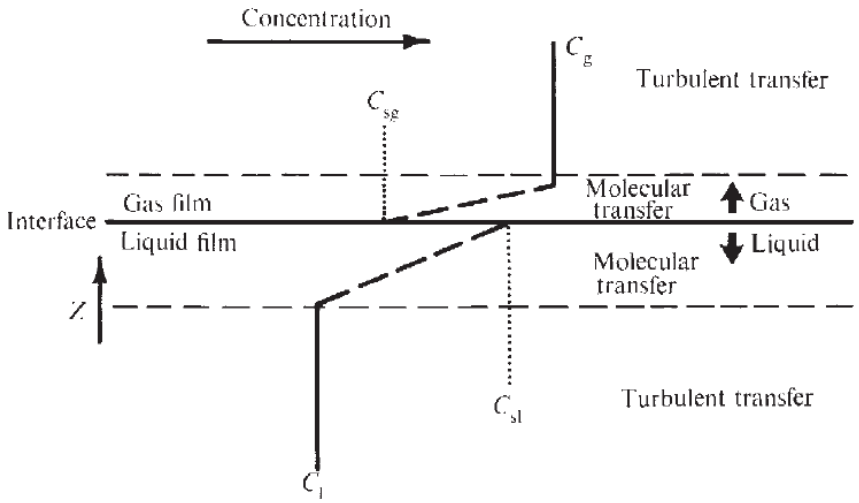

Figure 1-2 Two-film model of a gas-liquid interface (Liss and Slater 1974).

2. Emission of H_2S from Falling Droplets in Sewer Drop Structures*

2.1. Introduction

Hydrogen sulfide (H_2S) can be generated in sanitary or combined sewers under anaerobic conditions (Ganigué et al. 2016; Guo et al. 2018; Kaushal et al. 2020). H_2S is the primary cause of sewer odor and corrosion (Hvitved-Jacobsen et al. 2013; Zuo et al. 2019) and, thus, is of great interest to municipalities. When wastewater falls in the collection system, such as in a vertical drop structure, it breaks up into small water droplets with diameters of around 2 mm for a falling height of more than 6.32 m (Ma et al. 2016). Water droplets have much larger surface areas than the falling water jet and, thus, are expected to result in a much larger mass transfer of H_2S (Clift et al. 1978). The mass transfer of H_2S from single falling droplets to the sewer air is among a few important processes for sewer odor and corrosion control; however, relevant studies are limited, which trigged the current work.

For the mass transfer between a single water droplet and air, the driving force is the gas concentration difference between the liquid and the air (Handlos and Baron 1957). When a droplet is falling, an internal flow is generated inside the droplet, which enhances the mass transfer (Wylock et al. 2012). To better understand the mass transfer of a falling droplet in air, the two-film theory (Lewis and Whitman 1924) has been used. For H_2S and its potential surrogate gas CO_2 (due to the toxicity of H_2S) studied in this work, over 80% of the overall mass transfer resistance

* The content of this chapter has been published as: Sun, L., Zhang, W., and Zhu, D. Z. (2020). "Emission of Hydrogen Sulfide from Falling Droplets in Sewage Drop Structures." *Journal of Environmental Engineering*, 146(12), 04020135. 10.1061/(ASCE)EE.1943-7870.0001819.

lies in the liquid film (Matias et al. 2018) because of its low solubility in water (Amokrane et al. 1994), so their mass transfer is controlled by the liquid phase. The mass transfer process can be expressed as

$$\frac{dC}{dt} = K_L a\left(C_a / H - C\right) \tag{2-1}$$

where C = concentration of the dissolved gas in water; t = the time of mass transfer; K_L = the mass transfer coefficient; a = the surface-area-to-volume ratio of the droplet; C_a = the gas concentration in air; and H = Henry's law constant.

Models exist for the mass transfer coefficient K_L of single droplets in air that are provided in Table 2-1. Handlos and Baron (1957) theoretically and experimentally developed an equation for K_L by assuming turbulent conditions within a droplet (Altwicker and Lindhjem 1988) and did not consider the droplet size and diffusivity in their proposed equation. Angelo et al. (1966) generalized a theoretical model considering the oscillation of droplet shape and surface area with falling time. The mass transfer coefficient was correlated with the oscillation frequency and magnitude, where the frequency equation is provided in the notes of Table 2-1, but the magnitude was typically difficult to measure or predict (Yeh 2002). Ruckenstein (1967) also developed a model for K_L between a droplet and a continuous phase for small Reynolds numbers (Re) using a theoretical analysis of the convective-diffusion equation, and indicated that K_L was related to droplet velocity, droplet diameter and gas diffusivity. Clift et al. (1978) realized droplets were significantly non-spherical if their diameters were larger than 1 mm at terminal falling velocities; and therefore they increased K_L in their equation relative to that of Ruckenstein (1967). Despite this, the increase in K_L was less than 7.6% for the droplets with diameters smaller than 5 mm. By assuming that droplets were spheres, Amokrane et al. (1994) proposed an equation for K_L with the

interfacial liquid friction velocity between the droplet and the air based on their experiments on absorption of sulfur dioxide (SO_2). From the above equations listed in Table 2-1, it is not difficult to find that K_L increases with droplet falling velocity (U) and gas diffusivity in water (D) but decreases with the droplet size (d). When these equations are applied for a typical droplet size (1-9 mm), there are up to a ten times difference on K_L, which necessitates further research.

To date, to the authors' best knowledge, no direct experimental study has been reported on the mass transfer of H_2S from single falling droplets to air. Matias et al. (2014) conducted laboratory experiments on the mass transfer of H_2S from water to air but were under jet-induced turbulent conditions and did not evaluate single falling water droplets. A few experimental studies were conducted on the mass transfer of CO_2 between single falling droplets and air. Garner and Lane (1959) conducted experiments in a wind tunnel with droplets of d = 4.22 and 5.85 mm falling in an ambient of 50% air and 50% CO_2 at the terminal falling velocity of the droplets. The saturation percentage of CO_2 inside the droplets was presented at certain absorption time, but K_L was not calculated in their paper. Altwicker and Lindhjem (1988) experimentally studied the absorption of CO_2 by small droplets with d = 0.60 and 1.20 mm and droplet velocity of 1.2 and 1.4 m/s, and their $K_{L;20}$ was 9.4 and 5.5 × 10^{-4} m/s, respectively. However, no studies validated the use of CO_2 as a surrogate gas for H_2S mass transfer. According to the relationship of K_L between H_2S and oxygen (O_2) proposed by Yongsiri et al. (2004b), the relationship of K_L between H_2S and CO_2 under the same condition may be written as follows:

$$\frac{K_{L,H_2S}}{K_{L,CO_2}} = \left(\frac{D_{H_2S}}{D_{CO_2}} \right)^n \tag{2-2}$$

where the exponent $n = 1$ using the two-film theory (Lewis and Whitman 1924; Cussler 2009), and $n = 0.5$ using the penetration theory (Higbie 1935) or surface-renewal theory (Dankwerts 1951). At 20°C, D_{CO_2} is 1.76×10^{-9} m^2/s, and D_{H_2S} is 1.75×10^{-9} m^2/s (Tamimi et al. 1994), which are almost the same. Therefore, the two gases will have a similar mass transfer coefficient regardless of whether $n = 0.5$ or $n = 1$, making CO_2 a potentially suitable candidate for the surrogate gas of H_2S.

This paper mainly studied the effect of droplet size and droplet falling velocity on the mass transfer rates of H_2S and verified the applicability of CO_2 as a surrogate gas for H_2S. The research results were then applied to sewer drop structures to improve the understanding of H_2S mass transfer during the sewage falling process, which is useful for sewer odor and corrosion control.

2.2.Materials and Methods

2.2.1. Experimental Setup

The experimental setup is provided in Figure 2-1(a), with two gases: H_2S and its potential surrogate gas CO_2.

Experiments on H_2S Mass Transfer

Saturated H_2S solution of approximately 4 g/L (Ricca Chemical, USA) was pulled into a gastight syringe (Hamilton, Model 1025 TLL, USA), and then allowed to reach the room temperature (20 ± 1 ℃) before the experiments. A syringe pump (Chemyx, Fusion 100, USA) was used to expel the solution at a controlled speed into a needle (Hamilton, Luer Lock, USA) to generate single water droplets with negligible initial falling velocity.

The generated droplet size depended on the needle size and the pump speed used. The size was obtained by weighing a certain number of droplets on an analytical balance (APX-200, 0.1 mg resolution, Denver Instrument, Bohemia, New York). Droplet size was further confirmed by processing two-dimensional (2D) images from a high-speed camera (Phantom v211, Vision Research, Wayne, New Jersey) using Matlab and treating it as a circle. In addition to the careful control of droplet sizes, droplet falling height (h) was also varied from 0.1 to 1.5 m during the experiments to produce different droplet falling speed U. The speed was obtained from processing the 2D droplet images (Figure 2-1b).

The droplets were captured by a pool of sodium hydroxide (NaOH) solution (0.1 mol/L, 10 mL) in a vial. NaOH solution was used to quickly react with and, thus, fix H_2S when the droplets entered the pool. The vial was sealed immediately after receiving four droplets. Due to the toxicity of H_2S, the tests were conducted in a walk-in fume hood with a wind velocity of 0.1-0.3 m/s.

The concentrations of total sulfide in the vials were measured using a spectrophotometer (DR6000, Hach, Germany) using the methylene blue method (APHA, AWWA, and WEF 2017), which was sensitive to a low sulfide concentration. The mass of sulfide in each vial was then calculated. The average concentration of H_2S for each droplet was calculated based on the total sulfide mass and total droplet volume, where the volume was calculated from the weight (from the balance) and the density (0.998 g/mL). Note that the sulfide in the droplets only existed in its molecular form (H_2S) due to the low pH of the H_2S solution.

The first measurement height was selected at h = 0.1 m to avoid the complex mass transfer during the droplet formation at the tip of the syringe (approximately 3 s). Five falling heights were used: 0.1, 0.5, 0.75, 1.0, and 1.5 m. At each height, five parallel tests were conducted. Droplet

evaporation during falling was negligible (Walcek et al. 1984). The oxidation of sulfide by oxygen was also neglected because of the low oxidation rate (Luther et al. 2011), low solubility of oxygen in water, and short contact time between droplets and air.

Experiments on Surrogate Gas CO_2 for H_2S Mass Transfer

The basic experimental procedure for the surrogate gas CO_2 was the same as for H_2S. The main differences were as follows. First, the CO_2 solution was made by continuously blowing CO_2 gas into deionized (DI) water via a diffuser connected to a compressed cylinder of CO_2. This process took sufficient time until the solution was saturated with dissolved CO_2. Second, ten droplets (compared with four droplets in the H_2S experiments) were captured by each vial. Moreover, at each height, three parallel tests were conducted (compared with five in the H_2S experiments). In addition, the concentration of total carbon in the vials was measured using a total organic carbon (TOC) analyzer (Shimadzu, TOC-L, Japan).

Finally, a control group (only DI water in the syringe with no CO_2) was added for each experiment to remove potential errors. When a droplet impinges the pool (NaOH solution) in a vial, CO_2 from the ambient air could be entrained into the pool. Meanwhile, the surface of the NaOH solution absorbed some CO_2 from the air during the experiments despite the short experimental duration. These two processes could cause an increase in the carbon concentration in the pool. To account for this increase, the mass difference of carbon between the experimental and control groups was used as the total mass for the ten droplets. Note that no control groups were set up in the H_2S experiments because the concentration of H_2S in the air is negligible.

2.2.2. Method for Calculating K_L

For droplets falling in the air, Eq. (2-1) can be integrated with the falling time of droplets as (Amokrane et al. 1994):

$$\ln\left(\frac{C_1 - C_a / H}{C_2 - C_a / H}\right) = K_L a \Delta t \tag{2-3}$$

where C_1 and C_2 = gas concentration at the upper and lower height, respectively; and Δt = droplet falling time. By neglecting the shape deformation of droplets during the falling and assuming the droplet is a sphere, the specific area of the droplet is $a = 6/d$, where d = droplet diameter. To be noted is that this K_L is an average value between the two heights of the falling and corresponds to the average droplet falling velocity between the two heights. If K_L is obtained at different temperatures, it is usually adjusted to standard temperature (20℃) (Elmore and West 1961):

$$K_{L,20} = K_{L,T}\left[1.0241^{(20-T)}\right] \tag{2-4}$$

where $K_{L,T}$ and $K_{L,20}$ = mass transfer coefficients determined under the test temperature T (℃) and 20℃, respectively.

2.3. Results and Discussion

2.3.1. Droplet Size and Falling Velocity

In the experiments, four diameters of H_2S or CO_2 droplet solution were generated and studied: d = 3.02, 3.50, 3.78, and 4.68 mm, with a standard deviation of less than 0.01 mm for each size. An example of a falling droplet with d = 3.78 mm in air is provided in Figure 2-1(b). The droplet was observed to not be a perfect sphere and had shape oscillation even at a falling speed of

approximately 1.4 m/s. Further analysis of the 2D images indicated that the droplet oscillation frequency agreed with the frequency equation presented in the note for Table 2-1.

A comparison of droplet sizes from the 2D images with those from weighting the droplets is provided in Figure 2-2(a). The comparison indicates that the droplet sizes from the two methods were similar (<6% difference), revealing the reliability of the current weighting methods and the small oscillation of the droplet sizes. The droplet falling velocity (U) with respect to the falling height (h) is provided in Figure 2-2(b). The falling velocity did not reveal an evident difference with different droplet sizes at the same falling height, which is because the falling height was not large enough for the droplets to develop such a difference. With a sufficiently large falling distance, the terminal velocity of the falling water droplets will generally increase with droplet size (Clift et al. 1978; Zhang and Zhu 2015). Also indicated in Figure 2-2(b) is the simulated falling velocity for the droplet size d = 4.68 mm with consideration of the drag effect of the ambient air on the droplet [using Eq. (3) in Zhang and Zhu 2015], where the drag coefficient can be calculated as per the equation in Amokrane et al. (1994) (listed in the notes to Table 2-1). The measured and modeled droplet falling velocities were almost identical, suggesting the reliability of the velocity measurement using the 2D images from the high speed camera. The free-falling velocity without consideration of the drag effect of ambient air is also provided in Figure 2-2(b), which starts to overestimate the velocity at h = 0.75 m, at which the drag effect starts to play a role.

2.3.2. Mass Transfer of H_2S

The dimensionless form of the H_2S concentration in a falling droplet, C/C_0, is shown in Figure 2-3(a) with respect to the falling height, where C = gas (dissolved H_2S) concentration at a certain height and C_0 (1.8-2.2 g/L) = initial concentration at h = 0.1 m. The results indicate that C/C_0

declined up to 17% after a free-falling (h = 0.1-1.5 m) due to the gas mass transfer from the droplet to the air. A larger decline was observed with smaller droplet size, as expected. The error bars were small for the H_2S experiments, indicating the high repeatability of the experiment.

The mass transfer coefficient $K_{L,20}$ for H_2S in the experiments was calculated from Eq. (2-3) with C_a = 0 ppm, and the value ranged from 0.9-4.4 $\times 10^{-4}$ m/s (Figure 2-4) under the droplet Reynolds number 444 < Re < 1455 (the definition of Re is given in the notes of Table 2-1). The results clearly indicate that $K_{L,20}$ increased with the droplet falling velocity (U). For example, at d = 3.02 mm, $K_{L,20}$ increased from 1.0 to 4.4 $\times 10^{-4}$ m/s when the velocity increased from 2.2 to 3.9 m/s. The same trend can be observed with other droplet sizes (d = 3.50, 3.78 and 4.68 mm). The same experimental results of $K_{L,20}$ were also examined with droplet size (d), which shows that the $K_{L,20}$ value generally decreased with d. For instance, at U = 3.6-3.9 m/s, $K_{L,20}$ = 4.4, 2.5, 2.1 and 1.3 $\times 10^{-4}$ m/s for d = 3.02, 3.50, 3.78 and 4.68 mm, respectively. These general findings were in accordance with the existing predictive equations listed in Table 2-1.

As indicated in Figure 2-4, the predicted results of $K_{L,20}$ from the models in Table 2-1 were up to ten times different. The top two lines were the models of Ruckenstein (1967) and Clift et al. (1978), which had similar results because the Clift et al. (1978) model only made a small modification to that of Ruckenstein (1967). Both models overpredicted K_L, likely because the concentration in the droplet was assumed to be well mixed, and the entire resistance to mass transfer was restricted to a thin liquid film in their models (Altwicker and Lindhjem 1988). The remaining three models in Figure 2-4, that is, the models of Handlos and Baron (1957), Angelo et al. (1966), and Amokrane et al. (1994), predicted that they were much closer to the experimental results. However, the Handlos and Baron (1957) model did not include droplet size and gas characteristics (e.g.,

diffusivity). The Angelo et al. (1966) model only had reasonable predictions for droplets with large velocities, likely because the effect of the size oscillation is more important compared with that of small velocities. Therefore, in this study, the Amokrane et al. (1994) model was selected for further improvement.

2.3.3. Suitability of Using CO_2 as a Surrogate Gas for H_2S

The mass transfer coefficient $K_{L,20}$ for CO_2 was calculated to be 1.0-4.6 $\times 10^{-4}$ m/s (using CO_2 concentration in the air C_a = 300 ppm). The $K_{L,20}$ value range was almost identical to that of H_2S. The present results are comparable to $K_{L,20}$ = 2.6 and 2.2 $\times 10^{-4}$ m/s for the droplets with d = 4.22 and 5.85 mm, respectively, based on the raw data of Garner and Lane (1959). Moreover, the results are smaller than $K_{L,20}$ = 9.4 and 5.5×10^{-4} m/s for smaller droplets with d = 0.60 and 1.20 mm in Altwicker and Lindhjem (1988), which is expected as smaller droplets have larger specific surface area for mass transfer.

In the CO_2 experiments, the error bars of ± 1 standard deviation were larger than those for H_2S (Figure 2-3 and Figure 2-4), likely because the CO_2 in the ambient air still affected the measurements even though a control group was used in each experiment. As shown in Figure 2-4, most of the $K_{L,20}$ data points for H_2S and CO_2 were close to each other in the same experimental condition, which demonstrated the validity of Eq. (2-2) to a certain extent. This preliminary work indicates that CO_2 is likely a suitable surrogate gas for H_2S. To further confirm the conclusion, future work should focus on reducing the error level for the CO_2 experiments.

2.3.4. Modified Equations for H_2S Mass Transfer

As indicated in Figure 2-4, among these existing models listed in Table 2-1, the model of Amokrane et al. (1994) appeared to be the most reasonable in predicting K_L from single falling water droplets in the air. However, this model still had noticeable differences with the experimental results [e.g., when d = 3.02 mm and U = 3.89 m/s, $K_L = 1.8 \times 10^{-4}$ m/s from the Amokrane et al. (1994) model but was 4.4×10^{-4} m/s from the experiments]. In addition, the coefficient in the Amokrane et al. (1994) model, $\omega = 0.8$, was determined from the mass transfer experiment on SO_2, which may not be applicable to H_2S and CO_2. Therefore, a modified equation was proposed in this study with an adjustment to this coefficient to improve its prediction accuracy.

The modified equation is presented as Eq. (2-5) based on the experimental results for $3.0 < d < 4.7$ mm and $2.1 < U < 4.6$ m/s at 20 °C and the least square method:

$$K_{L,20} = 3.15 \times \left(\frac{U_* D}{d} \right)^{1/2} - 3.52 \times 10^{-4} \tag{2-5}$$

where the interfacial liquid friction velocity is defined as $U_* = U\sqrt{\frac{\rho_g}{\rho_L}\frac{c_D}{2}}$. A comparison of the predicted $K_{L,20}$ from Eq. (2-5) with the experimental values is presented in Figure 2-5. Reasonable agreement can be achieved: most of the predicted values are within a 30% difference from the experimental results. Potential factors for the differences in the measurements are the complex impinging process between the droplet and the receiving pool, the wind effect (0.1–0.3 m/s) in the fume hood, and the impact of the existence of CO_2 in the ambient air.

2.4. Applications in Sewer Drop Structures

2.4.1. Estimating H_2S Emission in Large Drop Structures

The modified equation [Eq. (2-5)] was applied in H_2S emission in large drop structure prototypes with falling height of up to 30 m to understand the role of falling water droplets in the emission. Based on typical field conditions in Edmonton, Alberta, Canada, the following parameters were used for the calculation: the sewer air pressure is 1 atm, the wastewater pH is 7.8, and the dissolved sulfide is 0.8 mg/L upstream of the drop structures (Yang et al. 2019). The assumption was that the sewer air temperature was the same as the sewage temperature, and the H_2S concentration in the sewer air (10 ppm) does not change in the drop structures due to their large volume of air inside.

Also assumed was that wastewater breaks up into uniform droplets when falling 6.3 m in the drop structures, as per the experiment in Ma et al. (2016), after which they fall at their terminal velocity (Zhang and Zhu 2015; Ma et al. 2016). Prior to the jet breakup into droplets, the jet itself and the ligaments contribute to the mass transfer but cannot make as great a contribution to mass transfer as droplets because of their smaller surface-area-to-volume ratio relative to droplets. Due to the current knowledge gap in accurately estimating the mass transfer prior to the jet breakup into droplets, it was simply assumed that the mass transfer rate of jet and ligaments is one-third that of water droplets—equivalent to the jet breaking up to droplets when falling 4.2 m and only water droplets contributing to H2S emission. Note that a rather complex droplet impingement to the bottom of the drop structures was not considered in this estimate.

The calculation procedure was as follows. First, the liquid phase (dissolved) molecular H_2S concentration in the sewage upstream of the drop structure, C_l, was calculated to be 0.13-0.17

mg/L at 10-20 ℃ from dissolved sulfide concentration (0.8 mg/L) and Eq. (2-6) because only the molecular H_2S can emit from wastewater to the sewer atmosphere (Zhang et al. 2008).

$$f_{H_2S} = \left(10^{pH-pk_a} + 1\right)^{-1} \tag{2-6}$$

where f_{H2S} = fraction of dissolved H_2S in all the forms of dissolved sulfide; k_a = equilibrium constant for $H_2S_{(aq)} \Leftrightarrow HS^- + H^+$ (mol/L) (Hvitved-Jacobsen et al. 2013); and $pk_a = -\log k_a = 6045.2/T - 106.67 + 37.744 \log T$, where the wastewater temperature T in K (Rao and Hepler 1977). Second, the dissolved H_2S concentration in the sewage downstream of the drop structure, C_2, was calculated to be 0.04-0.12 mg/L by using Eqs. (2-5), (2-4) and (2-3). Third, the H_2S emission fraction, F, was calculated as the ratio of the emitted H_2S to the maximum emitting potential (equilibrium),that is, $F = (C_1 - C_2)/(C_1 - C_a/H)$.

The calculation results are presented in Figure 2-6. The emission fraction F increases quickly when sewage falls within h = 15 m and approaches 100% (equilibrium) at h = 15–30 m depending on the droplet conditions (size and temperature). For instance, as indicated in Figure 2-6(a), for droplet sizes d = 2 and 3 mm, a fraction of more than 85% is achieved after falling 15 m. Therefore, the H_2S concentration difference between the droplet and the ambient air quickly approaches equilibrium in the first 15 m. At h = 25-30 m, the driving force of the concentration difference is so small that the mass transfer nearly stops, causing almost no increase in the emission fraction. This finding suggests the importance of the falling height of the drop structures in H_2S emission from sewage to sewer air. Figure 2-6(b) suggests that the emission ratio F is insensitive to the sewage/air temperature because temperature has a limited effect on K_L [Eq. (2-4)]. Generally, Figure 2-6(a) might be used to estimate H_2S emission in large drop structure prototypes, affected mainly by the falling height and droplet size. In the practice of sewer odor and corrosion control,

this suggests that the design or rehabilitation of drop structures should make the sewage falling height as small as possible and avoid the breakup of jets to reduce H_2S emission from sewage to sewer air. Of course, increasing the pH is also helpful in decreasing H_2S concentration in the sewage and, thus, reducing H_2S emission (Lahav et al. 2004; Carrera et al. 2016).

2.4.2. Modeling H_2S Emission in Small Drop Structures

In a small drop structure, the H_2S emission from the sewage is rather complex because it involves multiple physical processes, such as wastewater jet impingement on the side wall, jet falling in the air, and jet impingement into the water pool at the bottom of the drop structure, as well as the enhanced turbulence. Thus, modeling of H_2S emission in small drop structures is challenging but important for sewer odor and corrosion control. In this study, the hypothesis of modeling the complex H_2S emission in small drop structures using the simple model of falling droplets in air was tested against the laboratory results of Matias et al. (2014).

Matias et al. (2014) conducted experiments on H_2S emission of free-fall water jets in sealed small drop structures. In each experiment, a water jet from an inlet pipe (0.1 m in diameter) fell freely (0.3, 0.6, and 0.9 m) in a vertical pipe (0.2 m in diameter) and impinged into a water pool. The setup was sealed, and a recirculation pump (at a fixed flow rate Q = 0.18 L/s) was used to circulate water between the pool and the inlet. The volume of bulk water was approximately 18 L in the setup, and the air volume increased with different falling height (19.1, 27.8, and 36.5 L for falling height of 0.3, 0.6, and 0.9 m, respectively). Other experimental conditions were as follows: pH of the water = 7.0, total dissolved sulfide = 10.0 mg/L at the start of the experiments, and temperature = 24.2-24.3°C during the experiments. The H_2S gas concentration was measured continuously with a gas detector, which indicated that it increased from zero at the beginning to a peak of 195, 400,

and 500 ppm after 2.4, 2.4, and 2.9 min for the falling height of 0.3, 0.6, and 0.9 m, respectively, due to the emission of H_2S from the water to the air.

The modeling assumed that the jet breaks up into uniform water droplets of d = 2 mm immediately after exiting from the inlet pipe, which falls in the same closed drop structures. The continuous emission of H_2S from massive water droplets to air were modeled for a duration of 2-3 min, that is, from the start of the experiment until the H_2S concentration in the sewer air reached the peak in Matias et al. (2014). The modeling procedure is as follows. First, the number of droplets and their mass transfer coefficient K_L were calculated. Based on the simulation of a falling drop, the droplet falling time Δt for the 0.3–0.9 m falling height was 0.25-0.45 s. In this period, the volume of falling sewage jet was $Q\Delta t$, which corresponded to the following number of droplets: $Q\Delta t/V_{\text{droplet}}$ = 1.1-1.9 × 10^4, where V_{droplet} = volume of a single droplet of d = 2 mm. K_L was obtained with Eq. (2-5) and adjusted to the experimental temperature of Matias et al. (2014) with Eq. (2-4). Second, the initial dissolved H_2S concentration (C_1 = 5.4 mg/L) in the water was calculated using Eq. (2-6), and the H_2S concentration in the droplets at the bottom of the small drop structure C_2 was obtained using Eq. (2-3). Then, the sewer air H_2S concentration was calculated from dividing the emitted mass of H2S gas ($C_1 - C_2$) $Q\Delta t$ by the air volume in the sealed structures. Third, the process was repeated until the accumulated emission time was reached. For a more accurate calculation, in each time step Δt, the results were used from the preceding time step (H_2S concentration in the air and water, as well as pH in the water). As a result of H_2S emission, the H_2S concentration in the water was continuously decreasing, pH was increasing (impacting the transform between the ion HS^- and the molecular H_2S), and the H_2S concentration in the air was increasing. The modeling results are indicated in Figure 2-7 and Table 2-2.

The difference between the modeling condition of this work and the experimental condition of Matias et al. (2014) is that this work does not consider the effect of H_2S oxidation, whereas such an effect was important in their experiments as demonstrated by the gradual decrease of H_2S concentration in sewer air to zero after reaching the peak. The reason that such an oxidation effect is prominent in their experiments (but negligible in the experiments of this work) is that the sulfide concentration in their water jets was much lower (10 mg/L versus 2 g/L), and the reaction time in their experiments was much longer (2-3 min versus < 1 s). Therefore, to make the comparison more meaningful, the results of Matias et al. (2014) were adjusted to exclude the effect of H_2S oxidation. The adjusted results are also provided in Figure 2-7 and Table 2-2.

Table 2-2 indicates that the differences in the peak H_2S gas concentration between the modeling results (418, 519 and 581 ppm) and experimental results (287, 539 and 672 ppm) are less than 50% (46%, -4% and -14%). This preliminary comparison suggests that falling water droplets of d = 2 mm in air have a similar contribution to H_2S emission, as in small drop structures. Figure 2-7 provides the detailed comparison between the two cases in terms of the total mass of H_2S emitted [Figure 2-7(a)] and instantaneous H_2S concentration in sewer air [Figure 2-7(b)]. Interesting to observe is that the model of falling water droplets (Eq. 2-5) actually provided close estimates to the experimental results in small drop structures, which again indicates that the current simple model of H_2S emission from falling water droplets of d = 2 mm could be applied in small drop structures to approximately predict the H_2S emission from sewage jets. The limitation of this model is that it was only calibrated with Matias et al. (2014)'s experiment, which is currently the only one available in the literature. The hope is that this preliminary modeling work will stimulate more research in both the modeling and experimental work on H_2S mass transfer in sewer systems.

2.5. Conclusions

To reveal the role of free-falling water droplets in H_2S emission in sewer drop structures, two series of laboratory experiments were conducted on the mass transfer of single droplets using two gases: H_2S and its surrogate gas CO_2. The H_2S or CO_2 droplet concentrations (3.02–4.68 mm) at different falling heights (0.1-1.5 m) were measured based on the computed mass transfer coefficient K_L. The laboratory results were then applied to estimate H_2S emission in large and small drop structure prototypes. The main conclusions are as follows:

1. K_L increases with droplet falling height (or velocity) but decreases with droplet size. A modified equation was proposed to reasonably predict K_L with an error of within 30%.
2. CO_2 was found to be a suitable surrogate for H_2S, which provides a safer alternative for studying H_2S mass transfer in the lab.
3. In large drop structures, the emission of H_2S from sewage to air mainly depends on sewage falling height and droplet size. More than 70% of the equilibrium of H_2S emission can be achieved after falling 15 m.
4. In small drop structures, the results of free-falling water droplets can be used to approximately model the complex H_2S emission in small drop structures. Additional laboratory or field data are needed to further confirm this new concept.

Future research is suggested to better the understanding of H_2S emission during other physical processes in drop structures, including jet impingement to the side walls and bottom pools, droplet impingement to the pools, the effects of the pool's turbulence, and the impact of H_2S oxidation. Also recommended is that a non-contacting measurement technique be developed to measure H_2S or CO_2 concentration in a falling droplet to avoid the errors induced by the droplet impingement

into the receiving pool of a vial. All of these recommendations are useful for municipalities to address the challenging and critical issue of sewer odor and corrosion control.

Table 2-1 Summary of the existing models for estimating K_L for single falling droplets

Source	Equation
[a] Handlos and Baron (1957)	$K_L = \dfrac{0.00375U}{1+\mu_L/\mu_a}$
[b] Angelo et al. (1966)	$K_L = 1.13\left[fD\left(1+\varepsilon+\dfrac{3}{8}\varepsilon^2\right)\right]^{1/2}$
[c] Ruckenstein (1967)	$K_L = 1.13\left(\dfrac{UD}{d}\right)^{1/2}$
[d] Clift et al. (1978)	$K_L = 1.13\left(\dfrac{UD}{d}\right)^{1/2}\left[\dfrac{2e^3}{3E(\sin^{-1}e - eE)}\right]^{1/2}$
[e] Amokrane et al. (1994)	$K_L = \omega\left(\dfrac{U_* D}{d}\right)^{1/2}$ where $U_* = U\left(\dfrac{\rho_g}{\rho_L}\dfrac{c_d}{2}\right)^{1/2}$

[a] μ is the dynamic viscosity of fluid, the subscript a and L mean air phase and liquid phase respectively, same as follows.

[b] f is the frequency of oscillation = $(8/3\pi\times\sigma/m)^{0.5}$ (Garner et al. 1959), where σ = the surface tension of water in air = 0.0728 N/m at 20°C; m = the mass of droplet; ε = the magnitude of oscillation = $A_{max}/A_0 - 1$ (Brunson and Wellek 1970), where A_{max} = the maximum surface area of the droplet, and A_0 = the surface area of the spherical droplet. d_{max}, corresponding A_{max}, was determined by the high speed camera's 2D images in this paper.

[c] U = the droplet velocity, d = the droplet diameter, and D = the gas diffusivity in water, where D_{CO2} = 1.76 $\times$ 10^{-9} m^2/s and D_{H2S} = 1.75 $\times$ 10^{-9} m^2/s at 20°C (Tamimi et al. 1994).

[d] E = minor axis/major axis = 1.030–62d ($1 < d < 9$mm), d in m; $e = (1- E^2)^{0.5}$.

[e] U_* = the interfacial liquid friction velocity between the droplet and the air; ρ is density; ρ_a = 1.2 kg/m^3; ρ_L = 998 kg/m^3; c_d is the drag coefficient, where $\ln(R) = -3.12611+1.01338\times\ln(c_d Re^2)–0.0191182\times[\ln(c_d Re^2)]^2$; $Re = Ud/v_a$, where v_a = kinematic viscosity of air, 1.486×10^{-5} m^2/s (20°C); ω = 0.8 based on their experimental data.

Table 2-2 Comparison of the modeling results of free-falling droplets in air and experimental result of H_2S mass transfer in small sewer drop structures

Falling Height (m)	Oxidation rate of H_2S (ppm/min)	Emission time (min)	Peak H_2S in the air (ppm)		Difference (%)
			This work	Matias et al. (2014)[a]	
0.3	38	2.4	418	287	46
0.6	58	2.4	519	539	-4
0.9	60	2.9	581	672	-14

[a]: Peak values were adjusted to the condition that no oxidation of sulfide occurred.

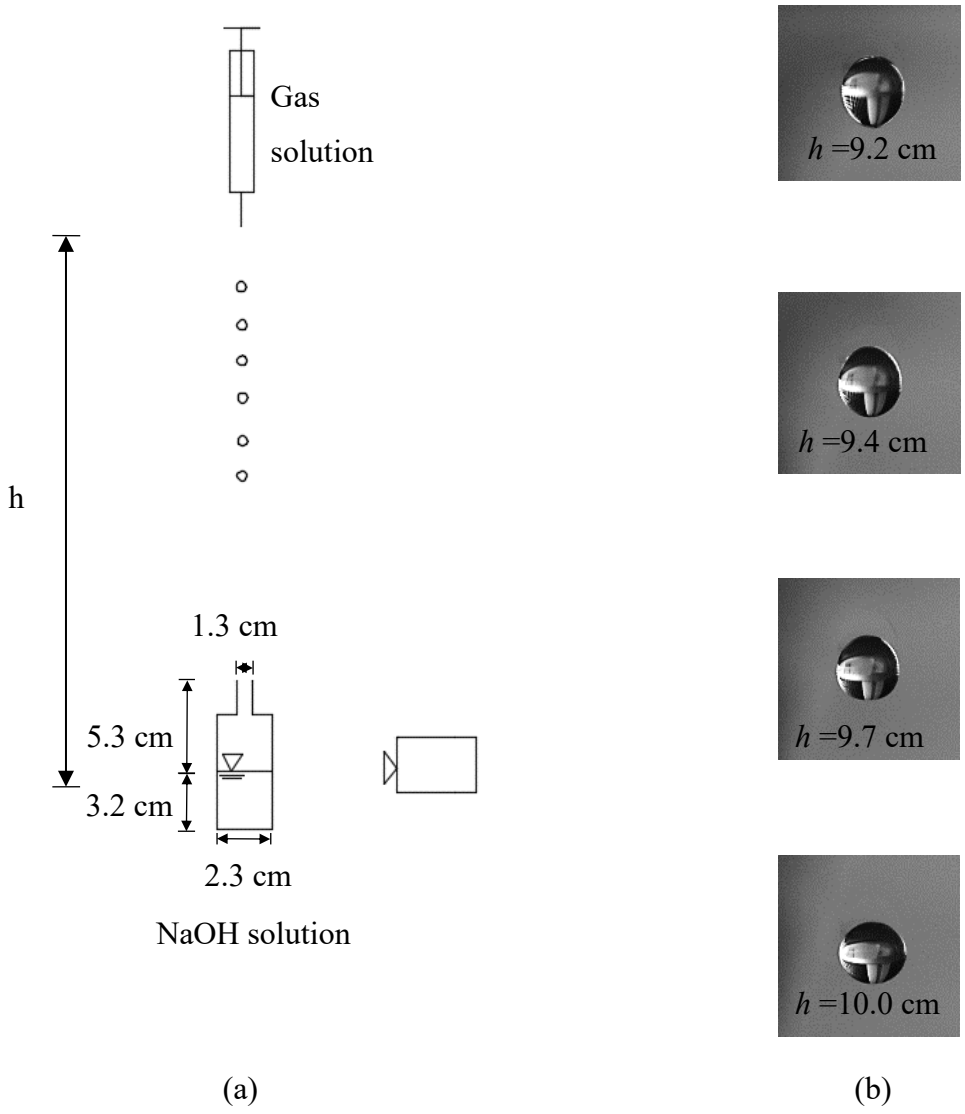

Figure 2-1 (a) Experimental setup for mass transfer of single falling droplets; falling height (h) varied from 0.1 to 1.5 m; and (b) deformation and oscillation of falling droplet after falling 10 cm (d = 3.78 mm and U = 1.4 m/s) from high-speed camera. Δt between two consecutive images is 0.002s. Size of each image is 1 × 1 cm^2.

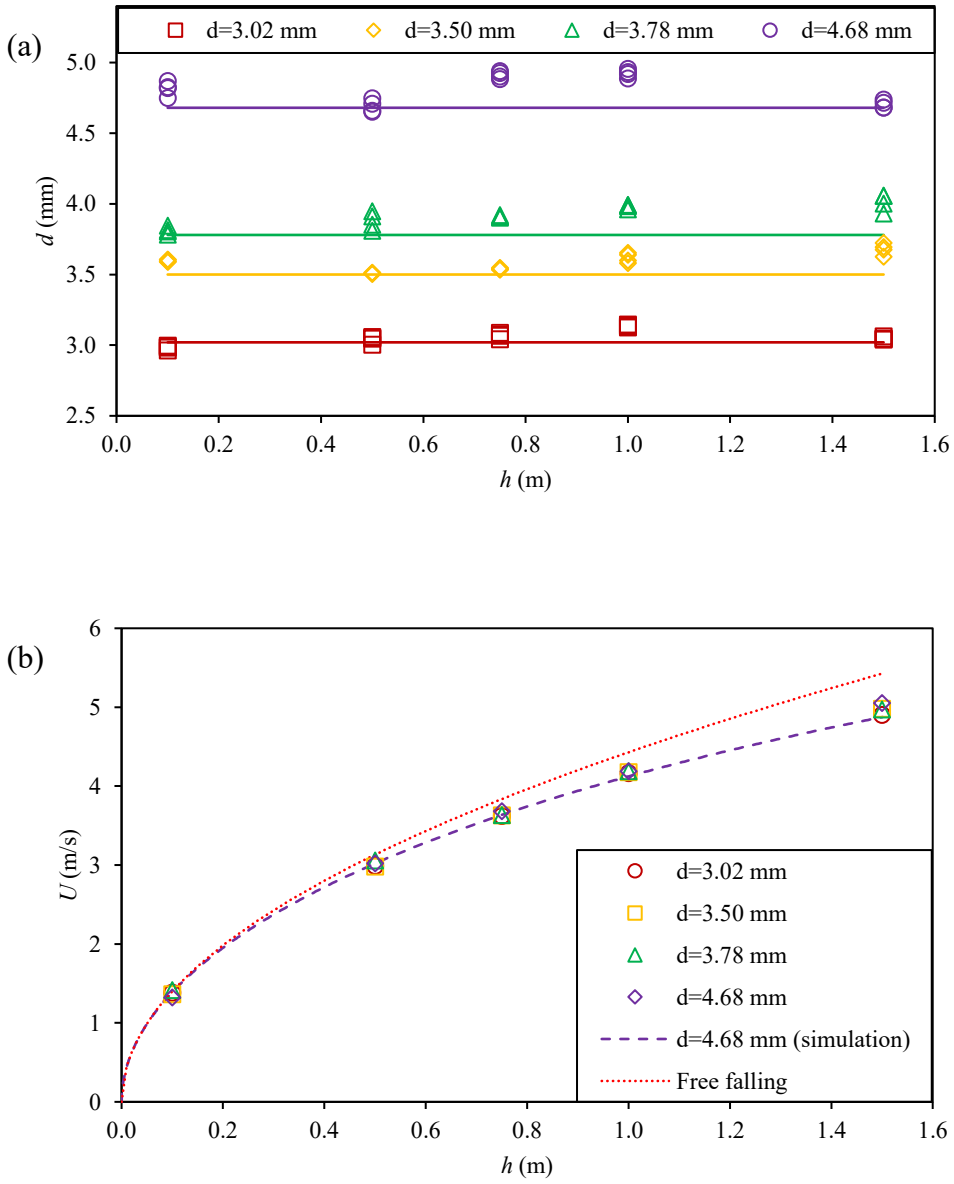

Figure 2-2 (a) Comparison of water droplet sizes at different heights between method using 2D images of high-speed camera (points) and method of weighting droplets on analytical balance (lines); and (b) comparison of water droplet velocities between measurements (points) and simulations with (dashed line) and without (dotted line) consideration of air dragging effect.

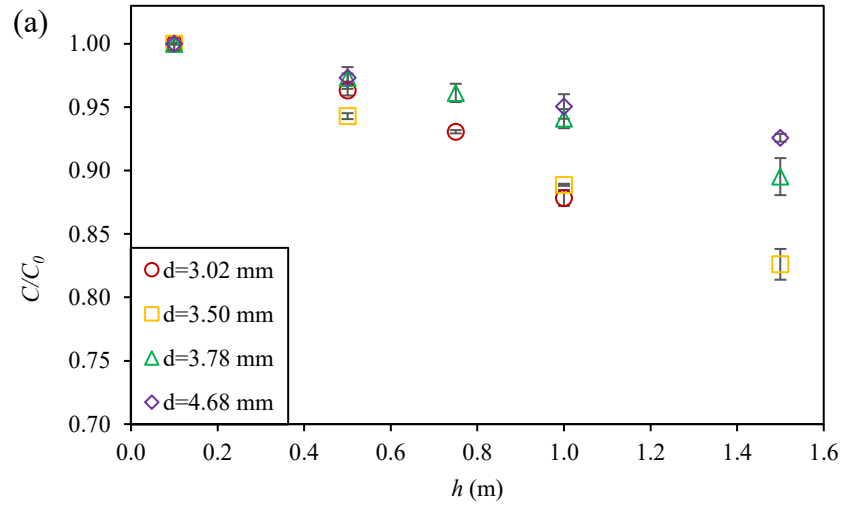

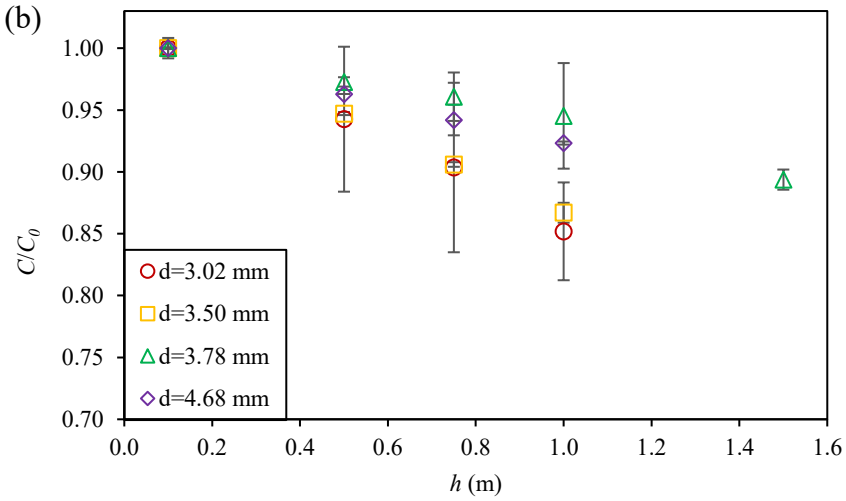

Figure 2-3 Variation of dimensionless gas concentration inside falling droplet with respect to falling height for all droplet sizes: (a) H_2S; and (b) CO_2. Error bars show ±1 standard deviation.

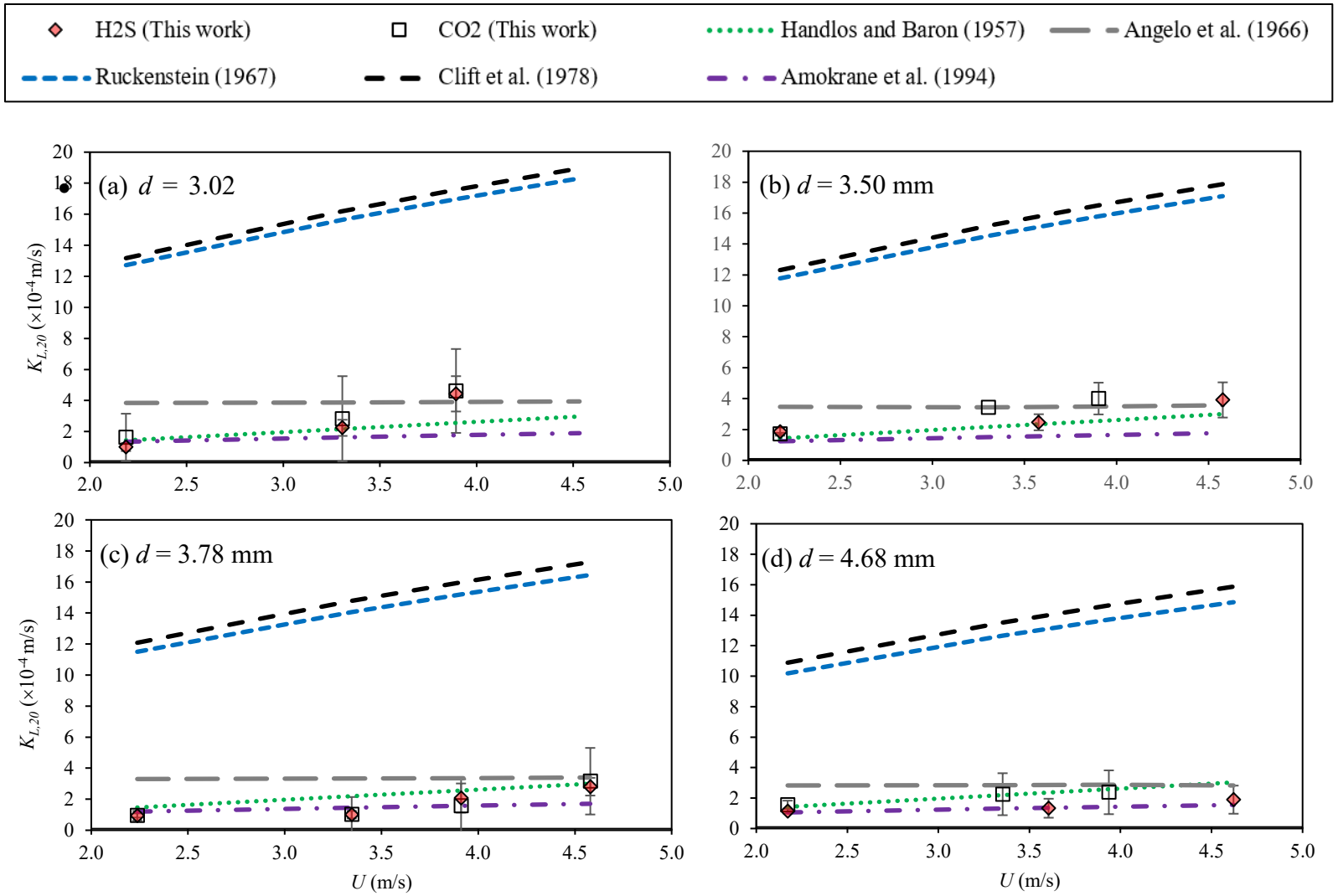

Figure 2-4 Variation of experimental and modeled $K_{L,20}$ with the droplet falling velocity U. Error bars of ±1 standard deviation are also shown.

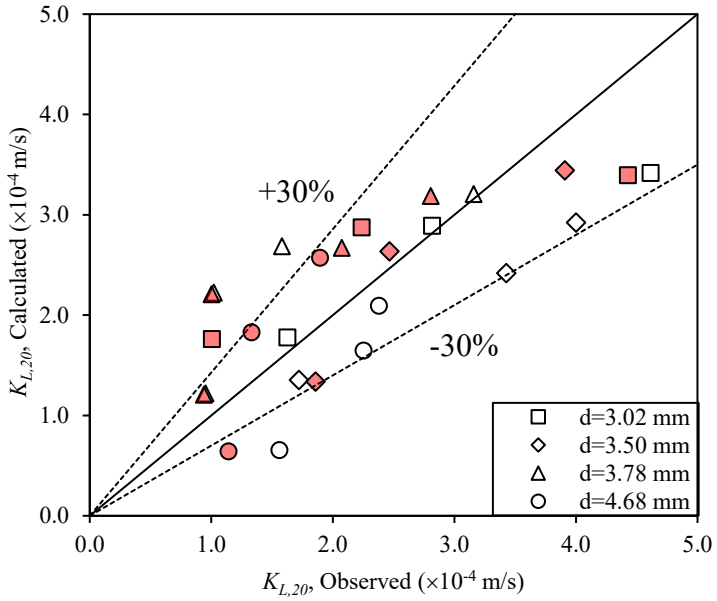

Figure 2-5 Comparison of observed $K_{L,20}$ with the proposed equation (filled symbols identify H_2S, and empty symbols identify CO_2).

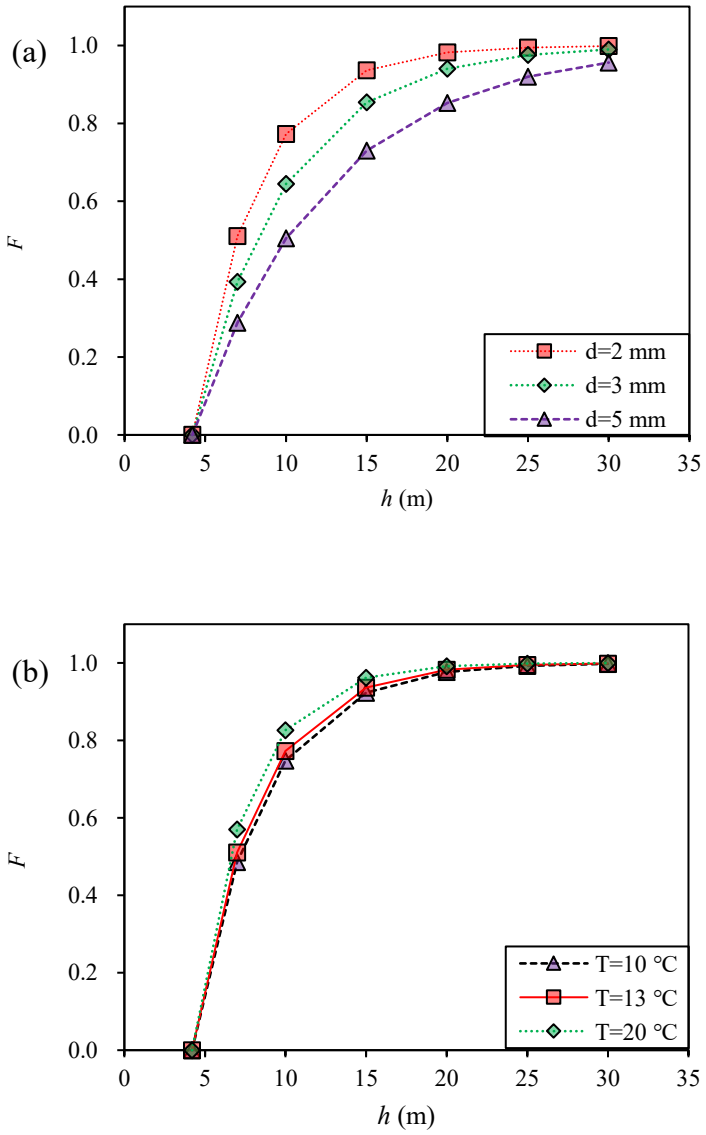

Figure 2-6 H_2S emission fraction, $F = (C_1 - C_2)/(C_1 - C_a/H)$, caused by free-falling water jet and droplets in large sewer drop structures under the conditions of (a) d = 2-5 mm and T = 13 °C; (b) d = 2 mm and T = 10-20 °C.

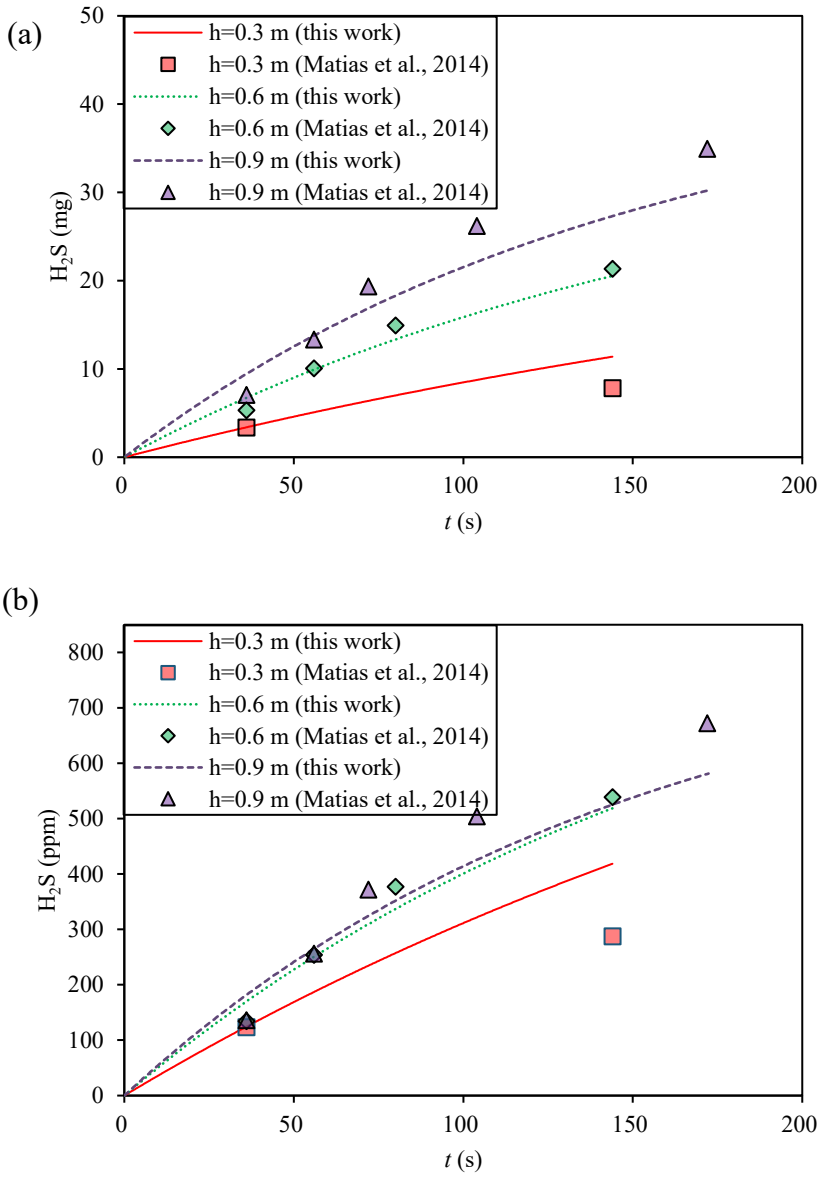

Figure 2-7 Comparison of H_2S emission in small sewer drop structures using the results of droplets in air (this work) with experimental results of falling jets by Matias et al. (2014): (a) emitted mass of H_2S gas and (b) sewer air H_2S concentration with time. Note that the results of Matias et al. (2014) were adjusted to the condition that no oxidation of sulfide had occurred.

3. Mass Transfer of H_2S at Turbulent Water Surface by Falling Drops and Single Jet

3.1. Introduction

Hydrogen sulfide (H_2S) can be generated in sanitary or combined sewers under anaerobic condition and cause wide-spread issues of sewer odor and sewer corrosion (Hvitved-Jacobsen et al. 2013; Zhang et al. 2016; Zuo et al. 2019). When wastewater falls in collection systems, for instance in a tall drop structure, it can break up into small water drops (Ma et al. 2016) and result in large mass transfer of H_2S in the falling process (Sun et al. 2020). The falling drops then impinge the bottom water pool of the drop structure, resulting in a high level of turbulence and splashing droplets at the pool surface. This is a key process of H_2S emission in drop structures. At the same time, sewer air containing O_2 is entrained into the wastewater, which mitigates the H_2S problems via alleviating anaerobic condition. If a drop structure is not tall enough for the jet to break up, the water would impinge into the bottom pool as a single jet. Therefore, it is imperative to study the mass transfer of H_2S and O_2 at the turbulence water surface generated by falling drops or single jet for better understanding of H_2S emission, control and mitigation in drop structures of urban drainage systems.

For mass transfer between a turbulent water surface and the atmosphere, the driving force is the gas concentration difference between the water and the air (Clift et al. 1978). In the two-film theory, the mass transfer process of H_2S and O_2 can be expressed as (Lewis and Whitman 1924):

$$\frac{dC}{dt} = K_L a\left(C_a/H - C\right) \tag{3-1}$$

where C is the concentration of the dissolved gas in water; t is time; K_L is the mass transfer coefficient; a is the surface-area-to-volume ratio of the collection pool; C_a is the gas concentration in air; and H is Henry's law constant.

In the previous relevant studies, oxygen (O_2), carbon dioxide (CO_2) and sulfur hexafluoride (SF_6) were used as the target gas for mass transfer (Banks et al. 1984; Ho et al. 1997; Takagaki and Komori 2007; Harrison et al. 2012; Jiang et al. 2018). In Banks et al. (1984), experiments were conducted to study O_2 transfer across water surface. A tank with nozzles generated drops on the top; and another tank with water collected the falling drops. To mix the water in the collection tank, an impeller was employed, which had an additional effect on the mass transfer. The K_L value of O_2 purely due to the turbulence caused falling drops (i.e., excluding the impeller's effect) was developed from numerical analysis. Kinetic energy flux (KEF) was employed to describe the turbulent level at the water surface, which is defined by the density of water ρ_w, flow rate R and the velocity of falling drops at the water surface U as Eq. (3-2). Ho et al. (1997) used SF_6 in a similar experimental setup as Banks et al. (1984)'s, and proposed 2nd order polynomial relationship between K_L and KEF. Takagaki and Komori (2007) conducted numerous experiments on CO_2 with flowing water in an open channel instead of a static tank, and the proposed a relationship between K_L and KEF based on the experimental data. In Harrison et al. (2012), the experiments setup was in a wind-wave-current flume and the gas was also SF_6, and a relationship was fitted with power law. These relationships showed the falling drops had significant enhancement to the mass transfer, as summarized in Table 3-1.

$$\mathrm{KEF} = \frac{1}{2}\rho_w R U^2 \tag{3-2}$$

More recently, Jiang et al. (2018) used a method called double parameters planar optode observation, to simulate the effect of raindrops on O_2 and pH distribution at the surface of the pool. Their experimental results showed that the raindrop could break the balance of water–gas interface and promote the dissolution of O_2 and CO_2 in water. The variation of gas concentration distribution in the vertical direction was shown; however, no quantitative analysis was given on K_L in their study.

According to Jähne et al. (1987), Ho et al. (1997) and Harrison et al. (2012), K_L is proportional to Sc^{-n}, where Sc is the Schmidt number, defined as the kinematic viscosity of water v divided by the molecular diffusivity of the gas in water D, and n is the exponent. In this paper it was assumed that v of the solutions was the same when containing low gas concentration, and therefore the relationship of K_L between Gas A and Gas B may be simplified as:

$$\frac{K_{L,\mathrm{A}}}{K_{L,\mathrm{B}}} = \left(\frac{D_{\mathrm{A}}}{D_{\mathrm{B}}} \right)^{n} \tag{3-3}$$

where the exponent n = ½ (Ho et al. 1997; Harrison et al. 2012). This equation was employed in this study to predict K_L of H_2S and O_2 from the equations in Table 3-1 if they were initially derived for other gases (e.g., SF_6 and CO_2). At 20 ℃, $D_{O2} = 2.0 \times 10^{-9}$ m/s (Ferrell and Himmelblau 1967; Haynes et al. 2014), $D_{H_2S} = 1.8 \times 10^{-9}$ m/s (Tamimi et al. 1994), and hence $D_{H_2S}/D_{O_2} = 0.90$. Therefore, based on Eq. (3-3), the theoretical mean value of $K_{L,H_2S}/K_{L,O_2} = (D_{H_2S}/D_{O_2})^{1/2} = 0.95$.

No direct experimental study has been reported so far on the mass transfer of H_2S at the turbulent water surface caused by falling drops or single jet. This paper mainly studied the effect of KEF on K_L of H_2S and O_2 under falling drops or single jet. The spatial variation of K_L in the collection water pond and the water depth's effect on K_L was also discussed. The research results are to

improve the understanding of mass transfer of H_2S and O_2 during sewage falling process, which plays an important role in odor management and corrosion control in sewer systems.

3.2. Materials and Methods

3.2.1. Experimental Setup and Procedures

The experimental setup for drops [Figure 3-1(a)] mainly included two parts: (1) a Perspex tank on the top, with a dimension of 25 × 40 × 5 cm^3; and (2) a collection tank on the floor, with a dimension of 35 × 35 × 25 cm^3. The initial water depth in the collection tank was 4 cm or 8 cm. The drop falling height (h) varied from 0.5 m to 1.5 m. Before the drops were generated, the dissolved oxygen (DO) concentration was almost saturated (~ 8.5 mg/L at 20 ± 1 ℃) in the upper tank, while the DO concentration in the collection tank was decreased to be around 2 mg/L via blowing nitrogen (N_2) gas into it (Chu and Jirka 2003; Carrera et al. 2017 b). Deionized (DI) water and tap water were both tested (seen in Table 3-2), as DI water stands for the ideal liquid phase condition and tap water is the source of real sewage. Two DO sensors (LDO101, Hach, USA), which were calibrated before the experiment according to the manual, were employed to measure the DO concentration. They were kept at the left and right bottom of the tank, with ~1.5 cm to the walls of the collection tank. The water in a basin was pumped into the upper tank by a peristatic pump (RK-77924-65, Masterflex, USA) and the drops fell freely through twenty-eight 1-mm holes (5 cm apart from each other) distributed evenly at the bottom of the upper tank. Only the right half part of the collection tank surface received the drops to stimulate the actual situation in drop structure.

Next, the mass transfer of H_2S and O_2 was tested simultaneously for H_2S solution under the scenarios of falling drops or single jet (see Table 3-2), where the oxidation of H_2S was negligible and discussed in the Appendix. The procedures for mass transfer of O_2 were kept same. By adding saturated H_2S solution (Ricca Chemical, Arlington, USA), the dissolved sulfide (DS) level in the collection tank was initially 3-6 mg/L. The water in the experiments was at the room temperature (20 ± 1 ℃). Due to the operability of the experiment, liquid samples (2.5 mL per sample) were obtained from the bottom pool in sequence at four locations (Top Right – TR, Bottom Right – BR, Top Left – TL and Bottom Left – BL) every 3 min. They were then measured in a spectrophotometer (DR6000, Hach, USA) by the methylene blue method (APHA at al. 2017) to obtain the dissolved H_2S level. pH value was measured before and after each test by a pH meter (AR15 accumet Fisherbrand, USA).

A single test lasted for 9 min. Before and after the test, the weight of the collection tank was measured in a scale (H1651, Uline, USA). The increase of total weight of the collection tank was the mass of the drops received, and based on it, the volume of water was obtained. The volume was then divided by the entire surface area of the collection tank and the time, the flow rate was obtained to be 62-223 mm/h. The mean diameter of water drops from 28 holes of the upper tank [Figure 3-1(a)] was 5.3 ± 0.2 mm, which was obtained by processing the two-dimensional (2D) images from a high-speed camera (Phantom v211, Vision Research, Wayne, USA) using Matlab and treating the drops as spheres (Zhang and Zhu 2015). The drops' falling velocity was calculated to be 3.1-5.2 m/s (shown in Table 3-2) as per Zhang and Zhu (2015) and Sun et al. (2020). The velocity calculation method has been proved reliable in Sun et al. (2020).

In addition to the cases of falling drops, single jet from a nozzle diameter of 6.4 mm with similar falling velocities and flow rates was studied [Figure 3-1(b)]. The jet impinged the center of the

right half surface of the pool. The experimental conditions were similar: the flow rate was 49-181 mm/h which was for comparison with drops scenario; the jet falling velocity was 3.1-5.1 m/s; the water was 20 ± 1 ℃ (Table 3-2). The other experimental procedures, e.g., deoxidation and measurement of gas concentration, were the same as those for the falling drops scenario.

3.2.2. Method for Calculating K_L for O_2

In each test, the DO concentration in the bottom pool increased due to two reasons: (1) the falling drops or jet had near-saturated DO concentration; and (2) oxygen transferred from the air to the water of bottom pool, which was the focus of this study. Based on the empirical equation of Sun et al. (2020), the mass transfer during drops falling was only 1% of that at the turbulent water surface. Because the falling jet had smaller surface-area-to-volume ratio than the drops, the mass transfer during the jet falling was smaller than that of the drops (1%) and thus neglected. In the collection tank, the total mass of DO was calculated by its concentration (average of the two DO sensors) and the total volume of the water; the mass of DO, directly from the falling drops or jet, was calculated based on its DO concentration and its volume, where the volume was calculated from the weight increase in the collection tank (from the scale) and the water density (0.998 kg/L). The mass difference between the total DO and the DO from the drops/jet was the mass transferred from the air to the collection pool. The mass of DO from the air divided by the initial water volume in the bottom pool was the amended C in Eq. (3-1).

After integration, Eq. (3-1) becomes:

$$K_{L,O_2} = \frac{\ln\left(\frac{C_1 - C_a/H}{C_2 - C_a/H}\right)}{a\Delta t} \tag{3-4}$$

where C_1 and C_2 are the amended DO concentration at two different times (mg/L), Δt = 3 min in the tests, and $a = 1/h_t$, where h_t is the mean water depth in the period of Δt in the bottom pool. This method was proven to have consistent results with the method proposed by Banks et al. (1997). If K_L was not obtained at standard temperature (20℃), it was adjusted to 20 ℃ (Elmore and West 1961):

$$K_{L,O_2(20)} = K_{L,O_2} 1.0241^{(20-T)} \tag{3-5}$$

where $K_{L,O_2(20)}$ and K_{L,O_2} are the mass transfer coefficients of O_2 determined under 20 ℃ and the test temperature T (℃), respectively. All the K_L valuo es in the following have been adjusted to 20℃.

3.2.3. Method for Calculating K_L for H_2S

In each test, the DS (dissolved sulfide) concentration in the bottom pool decreased due to two reasons: (1) dilution from the falling drops or jet; and (2) H_2S transferred from the water to the air, which was another focus of this study. The total mass of DS in the bottom pool was calculated by multiplying the concentration of DS (average of the four samples) and the volume of water in the bottom pool at the time of sampling. The total mass of DS at a certain time (e.g. t = 3 min) divided by the initial water volume in the bottom pool (i.e., the volume in the bottom pool before the drops or jet falling) was C at that time (e.g. t = 3 min) in Eq. (3-1). In this way, the effect of dilution from the falling water was eliminated.

In the experiments, the H_2S solution was obtained by diluting the saturated H_2S solution into the water of the collection tank, and therefore the solution in the collection tank follows the dynamic equilibrium (Yongsiri et al. 2004b):

$$H_2S \uparrow \rightleftharpoons HS^- + H^+ \quad pK_1 = 7.0 \qquad HS^- \rightleftharpoons S^{2-} + H^+ \quad pK_2 = 17.1 \quad (20\ ^\circ C)$$

Due to the large pK_2 value, the S^{2-} is found neglectable (Matias et al. 2017b). In our experiments, pH ≤ 8.0 in the collection tank, so sulfide exists in two forms: HS^- and H_2S. Note that only the molecular H_2S can emit from water to the atmosphere (Zhang et al. 2008). The percentage of H_2S, f, in total dissolved sulfide (H_2S and HS^-) is determined by pH and pK_1 as follows:

$$f = \frac{C_{H_2S}}{C_{DS}} = \left(10^{\mathrm{pH}-\mathrm{p}K_1} + 1\right)^{-1} \tag{3-6}$$

where C_{H_2S} is the concentration of molecular H_2S in water; C_{DS} is the concentration of total dissolved sulfide in water; pK_1 = 6045.2/T – 106.67 + 37.744log$T$, where the water temperature T was in K (Rao and Helper 1977).

Given that the change of the total mass of DS in the collection tank is caused by the H_2S mass transfer across the water surface, the mass transfer rate of H_2S is defined as (Yongsiri et al. 2005):

$$-\frac{dC_{DS}}{dt} = K_{L,H_2S}a\left(C_{H_2S} - C_{a,H_2S}/H_{H_2S}\right) = K_{L,H_2S}a\left(fC_{DS} - C_{a,H_2S}/H_{H_2S}\right) \tag{3-7}$$

where the H_2S concentration in the air $C_{a,\,H_2S}$ is 0 ppm in the tests. In the measurement duration of Δt = 3 min, f was assumed as a constant and taken as the mean value of the 3 min. By integration of Eq. (3-7) and adjusting to 20 ℃,

$$K_{L,H_2S(20)} = \frac{\ln\left(\dfrac{C_{DS,1}}{C_{DS,2}}\right)}{fa\Delta t} 1.0241^{20-T} \tag{3-8}$$

By comparing the equations for calculating K_L for H_2S and O_2 [Eqs. (3-8) and (3-5)], it can be found the numerators are both the natural logarithm (ln) of the deficit ratio at two different times. The difference is that there is a coefficient, f, in the denominator of Eq. (3-8), which represents the effect of pH on H_2S portion in the DS.

3.3. Results and Discussions

3.3.1. Fluid Phenomenon of Turbulent Water Surface

According to the videos from the high-speed camera, when a falling drop impinged the water surface of the pool, a hemisphere cavity formed and increased to a size of several times of the drop [Figure 3-2(a)]. Then the cavity shrank, and a thin water column rose above the water surface. The water column fell and caused cavity again. Sometimes the unstable water column broke into drops, and the drops fell to cause cavity and bubbles. It was observed that about 12% of the drops generated bubbles. In Kientzler et al. (1954), similar processes were also observed. Different from the drops, during the falling period, the jet impinged the water surface and caused cavities at the water surface. The cavities developed further until the deepest and then broke into bubbles [Figure 3-2(b)]. The bubbles' maximum penetration depth was 54 ± 3 mm.

Although falling drops could generate cavities and bubbles, the quantity and size of the bubbles were much less than those of single jet. The maximum depth of cavities (compared to the static water level) of drops or maximum penetration depth of jet Δh_{max} is shown in Figure 3-3. In Figure 3-3(a), under drops, Δh_{max} (10-17 mm) increased with the falling velocity (or height). However, it was interesting that Δh_{max} in medium flow rate (R = 122 mm/h) was even larger than those in the other two conditions, probably due to the interaction between the falling drops and the fluctuant

water surface. At the largest flow rate R = 184 mm/h, the drops fell at the most fluctuant water surface. This phenomenon was also evident with a falling jet where the jet hit the rising column frequently with this flow rate. In Figure 3-3 (b), under the jet, Δh_{max} was 29-54 mm, which was much larger than that of drops because the jet consequently impinged one point instead of multipoint. Only at R = 184 mm/h, Δh_{max} increased with the falling velocity. At the other two velocities, Δh_{max} even decreased with the velocity. Therefore, Δh_{max} did not increase with the falling velocity (or height) or flow rate under the jet scenario.

In general, the cavities generated by the drops were multiple but shallow, while the cavities by a jet was on a small area but deep. It is understood that cavities, bubbles, rising columns and turbulent water surface promoted the mass transfer at the water surface; however, it is difficult to quantify the individual contribution of them.

3.3.2. Comparison of K_L for H_2S and O_2

Under this section, the mass transfer of H_2S and O_2 took place simultaneously only in DI water. Figure 3-4 shows the change of DO concentration in the collection tank with falling drops at KEF = 0.51 J/(m^{2}s), where C_{DO} increased from 2.4 to 5.1 mg/L at the bottom left (BL) and to 5.5 mg/L at the bottom right (BR), while C_{DS} declined from 2.4 to 1.4 mg/L at all the four points in 9 mins. The increase of the DO concentration in the collection tank was more obvious in the right part of the tank where it received the drops than the left part; while for DS, the concentration difference cannot be recognized easily.

Figure 3-5 shows the comparison between K_L for H_2S and O_2 under the falling drops. At KEF = 0.43-0.72 J/(m^{2}s) and pH range of 5.86-7.44, K_L = 10.6-13.1 × 10^{-5} m/s for H_2S and 10.3-14.6 × 10^{-5} m/s for O_2. The results indicate that K_L values for H_2S and O_2 were similar under the same

experimental condition, with the average ratio of $K_{L,H_2S}/K_{L,O_2} = 0.98 \pm 0.05$. The ratio is almost the same as the theoretical ratio (0.95) from Eq. (3-3).

3.3.3. Mass Transfer of H_2S

Based on our experimental results, the results of oxygen mass transfer at the surface of tap water were not different from that of the DI water. Based on K_L for O_2 and the ratio of $K_{L,H_2S}/K_{L,O_2} = 0.98$, K_L for H_2S was calculated. The K_L value for H_2S calculated based on the concentration of DS directly was effected by the chemical constitution of the tap water, which will be discussed later.

Figure 3-6 shows the comparison of K_L between the left and right side of the collection pool. For the same KEF, K_L in the right ($K_{L,R}$) was larger than K_L in the left ($K_{L,L}$). For examples, when KEF = 0.20 J/(m^{2}s) under the drops scenario, $K_{L,L} = 5.4 \times 10^{-5}$ m/s, less than $K_{L,R} = 6.6 \times 10^{-5}$ m/s [Figure 3-6(a)]; when KEF = 0.24 J/(m^{2}s) under the jet scenario, $K_{L,L} = 4.0 \times 10^{-5}$ m/s, less than $K_{L,R} = 4.8 \times 10^{-5}$ m/s [Figure 3-6(b)]. On average, the ratio of $K_{L,L}/K_{L,R} = 0.79 \pm 0.18$ under the drops scenario and $K_{L,L}/K_{L,R} = 0.68 \pm 0.23$ under the jet scenario. These ratios are reasonable as the drops or jet fell in the right side of the colleting tank, causing more mass transfer at the surface there.

Figure 3-7 shows the effect of collection pool water depths on K_L. In the experiments, K_L of the water depth of 8 cm ($K_{L,8cm}$) was slightly larger than that of 4 cm ($K_{L,\ 4cm}$) under both droplet and jet scenarios. Specifically, $K_{L,8cm}/K_{L,4cm} = 1.15$ under drops scenario, and $K_{L,8cm}/K_{L,4cm} = 1.24$ under jet scenario. The reason for $K_{L,8cm}/K_{L,4cm} > 1$ could lie on the stronger turbulence at the water surface with 8 cm depth. In the jet scenario, the penetration depth of bubbles (Δh_{max}) could be over 5 cm (Figure 3-3) and the water depth of 4 cm limited the penetration of bubbles, and therefore the increase of water depth could promote the mass transfer rate under jet. For the drops, Δh_{max} was less than 2 cm, hence the depth's effect was not so much as jet.

In Figure 3-8(a), K_L was calculated based on the mean gas concentration of all the measurement locations in the collection tank with both water depths. K_L showed an increasing trend with KEF. KEF increased from 0.11 to 0.80 J/(m^{2}s), and the resulted K_L increased from 2.6 to 14.8 × 10^{-5} m/s. The relationship between K_L at 20 ℃ and KEF can be fitted by the following equations:

- For drops falling on a water surface,

$$K_L = 1.787 \times 10^{-4} \mathrm{KEF}^{0.738} \tag{3-9}$$

- For a jet falling on a water surface,

$$K_L = 9.005 \times 10^{-5} \mathrm{KEF}^{0.596} \tag{3-10}$$

Among the equations above, for the same KEF, K_L in Eq. (3-9) was larger than Eq. (3-10). In other words, at the same flow rate and falling velocity, the mass transfer rate at the turbulent water surface under falling drops was 76% larger than that under a falling jet. A comparison of the predicted K_L from Eqs. (3-9) and (3-10) against the experimental values is presented in Figure 3-8(b). Reasonable agreement can be achieved, demonstrated by that all the predicted K_L values are within 30% difference from the experimental results.

The present results were compared with existing studies of mass transfer at turbulent surfaces. The models of Banks et al. (1984), Ho et al. (1997), Takagaki and Komori (2007) and Harrison et al. (2012) in Table 3-1 were revised with Eq. (3-3) for H_2S and shown in Figure 3-8 (a) for comparison. They are all for falling drops. The predictions of Ho et al. (1997) and Harrison et al. (2012) were similar and closest to our results. The investigation range of KEF [< 1.23 J/(m^{2}s); see Table 3-1] in their studies was similar to the present study [0.11-0.80 J/(m^{2}s)], and their results were only 10% larger than our experimental results. In Banks et al. (1984), the KEF range [< 0.14 J/(m^{2}s)] was smaller than this study, and so their prediction generated most different results from ours. The

mass transfer experiment of Takagaki and Komori (2007) was in a turbulent flowing open-channel flow and their predicted K_L was on average 35% larger than our experimental results.

The present results were next compared with mass transfer at a quiescent water surface. In our experiments, if there are no falling drops hitting at the surface of the pool, i.e., KEF = 0, the mass transfer at the quiescent water surface still exists due to the gas concentration difference between the liquid and air phase. Chu and Jirka (2003) and Carrera et al. (2017 b) experimentally tested K_L of O_2, and Santos et al. (2012), Prata et al. (2016) and Carrera et al. (2017 b) tested K_L of H_2S at the quiescent water surfaces, and all these K_L values had an order of 10^{-6} m/s, ranging 2.2-8.7 × 10^{-6} m/s. K_L in this study was in the order of 10^{-5} m/s. Therefore, the turbulent surface due to impinging drops or single jet enhanced the mass transfer rate by over 10 times.

The present results were next compared with mass transfer of single falling drops or rising bubbles. In Sun et al. (2020), K_L of H_2S emission from single falling drops had a range of 0.9-4.4 × 10^{-4} m/s, where the diameter of the drops was 3.0-4.7 mm and the falling velocity was 1.3-5.1 m/s. In Jimenez et al. (2014), K_L of O_2 absorption from single rising bubbles in wastewater had a range of 0.3-4.0 × 10^{-4} m/s, where the diameter of the bubbles was 1.2 mm and the rising velocity was 0.1-0.3 m/s. Therefore, the range of mass transfer rate of single drops or bubbles is comparable with the present study. The present results were finally compared with mass transfer in sewers. In Carrera et al. (2017 a), laboratory experiments showed that K_L for O_2 varied between 6.0-6.9 × 10^{-5} m/s in gravity sewers with water velocity of 0.06-0.55 m/s. It was within the range of the results in the present study where K_L = 2.6-14.8 × 10^{-5} m/s.

3.4. Conclusions

Falling drops or jet on a pool water surface can significantly increase the mass transfer through the water surface. Understand the mass transfer of H_2S and O_2 in sewer drop structures is important for sewer odor management and corrosion control. Two series of laboratory experiments were conducted for falling drops or single jet, which impinged half of the collection water pool. The mass transfer coefficient K_L was examined for different gases, turbulent levels of the water surface (described by KEF), and depths and locations of the water pool.

The main conclusions are as follows:

1. With the impinging water flow rate of 49-223 mm/h and falling velocity of 3.1-5.2 m/s [KEF = 0.11-0.80 J/(m^2s)], K_L was found to be 2.6-14.8 × 10^{-5} m/s for H_2S and increased with KEF.
2. For the same KEF, K_L for O_2 and H_2S at the turbulent water surface due to falling drops was 76% larger than that of single falling jet.
3. K_L for O_2 and H_2S was larger in the half of the water surface directly receiving the drops or jet than the other half. The increase of pool water depth promotes the mass transfer, especially for the scenario of falling jet.
4. Two equations were proposed to reasonably predict K_L with an error level of < 30% for the two scenarios of turbulent water surfaces.
5. Compared to quiescent surface, the turbulent surface under impinging falling drops or single jet enhanced the mass transfer rate by over 10 times.
6. $K_{L,H_2S}/K_{L,O_2}$ = 0.98, which makes O_2 another safe surrogate gas for studying H_2S mass transfer in addition to carbon dioxide used in Sun et al. (2020).

It is important to point out that pH plays an important role in the mass transfer of H_2S. Besides, the abundant chemical constitutions in tap water (EPCOR 2022) significantly increases the complexity of this problem, let alone the wastewater in real sewer pipes. In future research it is suggested to test the experimental results in real sewers, which can enable researchers better predict H_2S emission in sewers and municipalities better deal with the problem of sewer odor and corrosion.

3.5.Notation

The following symbols are used in this paper:

a = surface-area-to-volume ratio of the collection tank (m^{-1});

C = amended concentration of the dissolved gas in water (mg/L or mol/L);

C_a = gas concentration in air (mg/L);

D = molecular diffusivity of the gas in water (m^2/s);

f = percentage of H_2S in total sulfide;

h = droplet or jet falling height (m);

H = Henry's law constant;

h_t = water depth at time t in the bottom pool (m);

h_{t0} = initial water depth in the bottom pool (m);

KEF = kinetic energy flux [$J/(m^2s)$];

K_L = mass transfer coefficient (m/s);

n = exponent;

pH = power of the hydrogen ion;

pK = equilibrium constant;

R = flow rate (m/s);

Sc = Schmidt number, v/D;

T = temperature (℃ or K);

t = time of mass transfer (s);

U = falling velocity of drops (m/s);

Δh_{max} = maximum depth of cavities of drops or maximum penetration depth of jet (mm);

v = kinematic viscosity of water (m^2/s);

ρ_w = density of water (kg/m^3).

Table 3-1 Summary of models for estimating $K_{L,20}$ with KEF on turbulent water surface under drops

Source	Equation	Conditions and Results
Banks et al. (1984)	$K_L = 3.62\times10^{-4}\mathrm{KEF}$	R = 5-25 mm/h, d = 3.31 and 4.73 mm, KEF = 0.02-0.14 J/(m^{2}s); K_L = 0.7-5.0 × 10^{-5} m/s.
Ho et al. (1997)	$K_L = -8.48\times10^{-5}\mathrm{KEF}^2$ $+2.55\times10^{-4}\mathrm{KEF}+9.65\times10^{-6}$	R = 7-110 mm/h, d = 2.8 and 4.2 mm, KEF = 0.06-1.23 J/(m^{2}s); K_L = 1.9-19.9 × 10^{-5} m/s.
Takagaki and Komori (2007)	$K_L = -1.32\times10^{-4}\mathrm{KEF}^2$ $+3.37\times10^{-4}\mathrm{KEF}+1.03\times10^{-5}$	2-435 mm/h, d = 2.1-5.7 mm, KEF = 0.01-1.24 J/(m^{2}s); K_L = 0.28-23.8 × 10^{-5} m/s.
Harrison et al. (2012)	$K_L = 1.75\times10^{-4}\mathrm{KEF}^{0.6242}$	R = 0-64 mm/h, d = 2.9 mm, KEF = 0-1.23 J/(m^{2}s); K_L = 1.4-19.4 × 10^{-5} m/s.
This work	$K_L = 1.787\times10^{-4}\mathrm{KEF}^{0.738}$	R = 62-223 mm/h d = 5.3 mm, KEF = 0.11 to 0.80 J/(m^{2}s); K_L = 2.6-14.8 × 10^{-5} m/s.

Note: In Banks et al. (1984), the original expression was $K_L = b_1 \times \mathrm{KEF}$, where $b_1 = 3.62 \times 10^{-5}$ cm^2/dyne. In Ho et al. (1997) and Harrison et al. (2012), the unit of K_L was cm/h. Here, all of them were changed to SI units. The equations of Ho et al. (1997) and Takagaki and Komori (2007) was fitted by us based on their raw experimental data. The temperature for K_L is 20 ℃.

Table 3-2 Summary of experimental conditions

Scenario	Water	Gas	h_{t0}* (cm)	R (mm/h)	h (m)	U (m/s)	KEF [J/(m^{2}s)]
Drops	DI	O_2 and H_2S	8	118-200	1.5	5.1	0.43-0.72
	Tap	O_2	8	80-223	0.5-1.5	3.1-5.1	0.11-0.80
		O_2 and H_2S	4-8	62-189	0.5-1.5	3.1-5.2	0.16-0.68
Jet	Tap	O_2	8	61-181	0.5-1.3	3.1-5.1	0.15-0.65
		O_2 and H_2S	4-8	49-178	0.5-1.3	3.1-5.1	0.12-0.50

*: h_{t0} is the initial water depth in the collection tank.

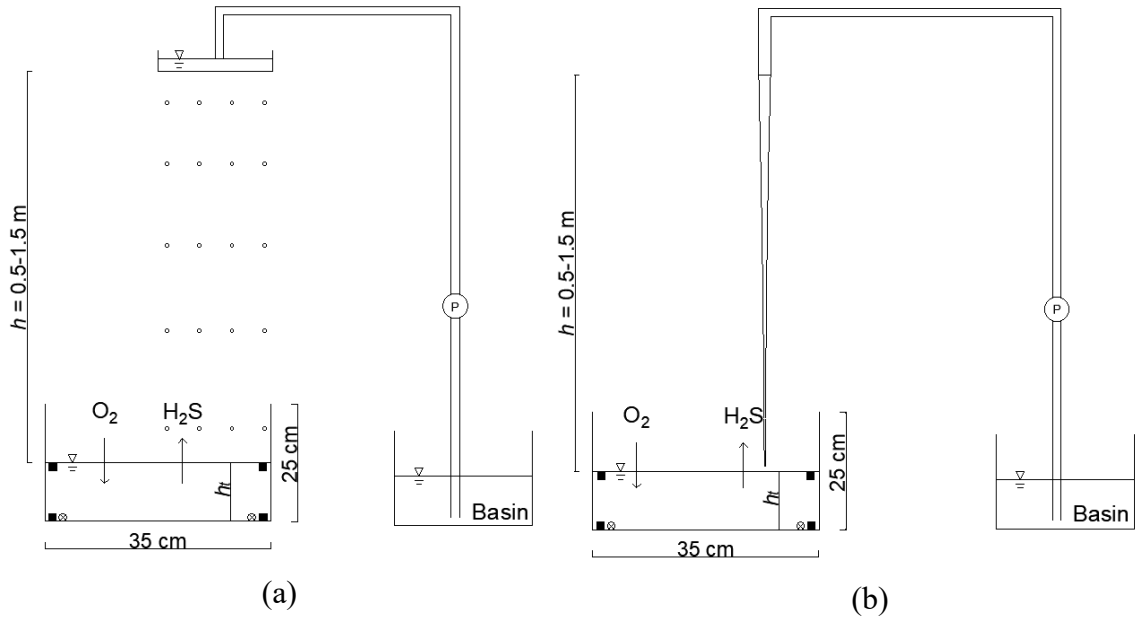

Figure 3-1 Experimental setup for mass transfer at the turbulent water surface: (a) falling drops at the right half part of surface; (b) falling single jet at the central point of the right half part of surface. Initial water depth h_{t0} = 4 or 8 cm. The squares are the sampling locations for H_2S concentration; the circles are the locations of DO sensors.

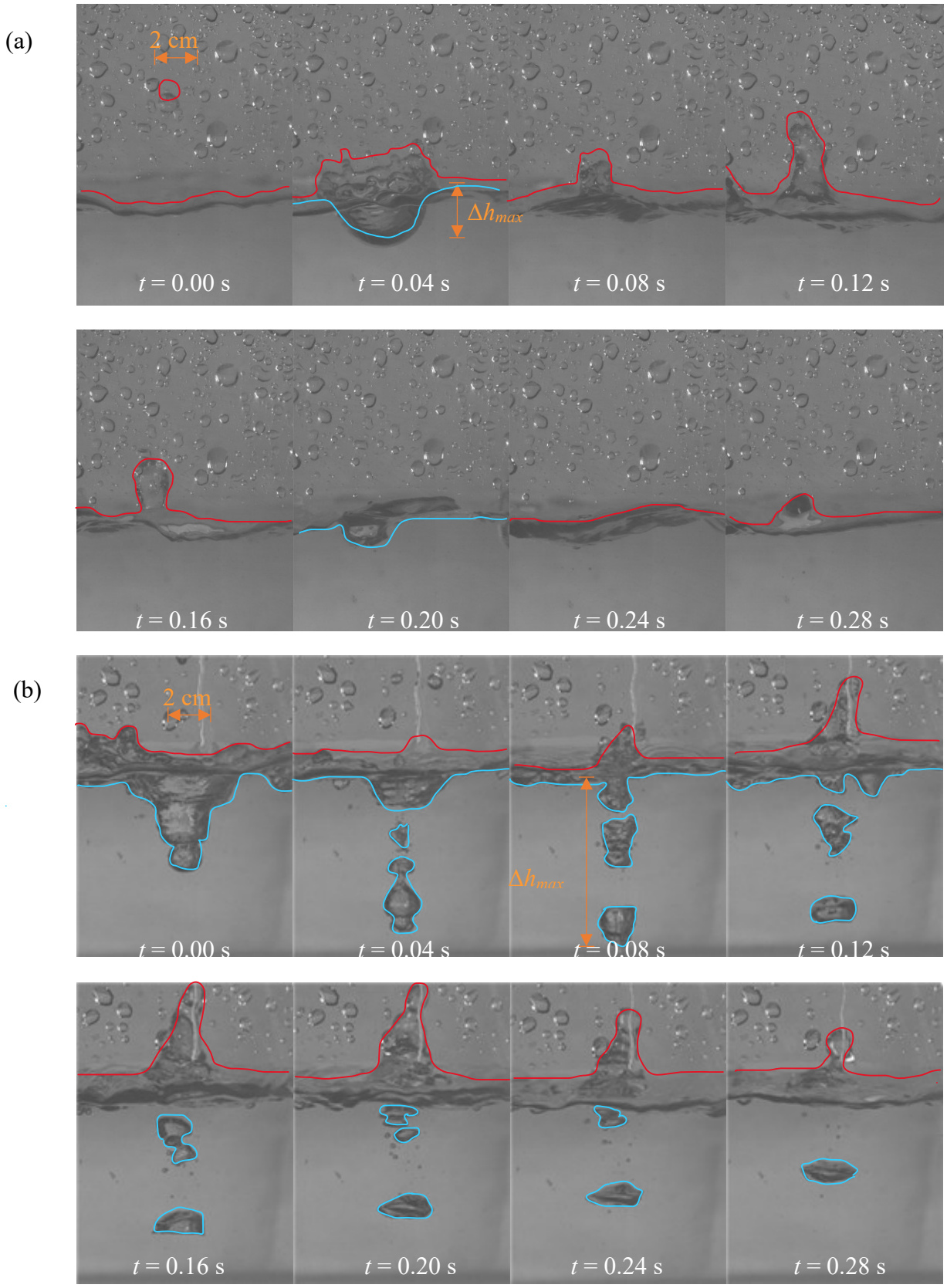

Figure 3-2 The cavity and bubbles caused by (a) a falling droplet and (b) a jet. Expt. condition: R = 61 mm/h, U = 2.9 m/s. Size of each image is 7.5 × 5.4 cm^2. The red and blue lines indicate the air-water interface.

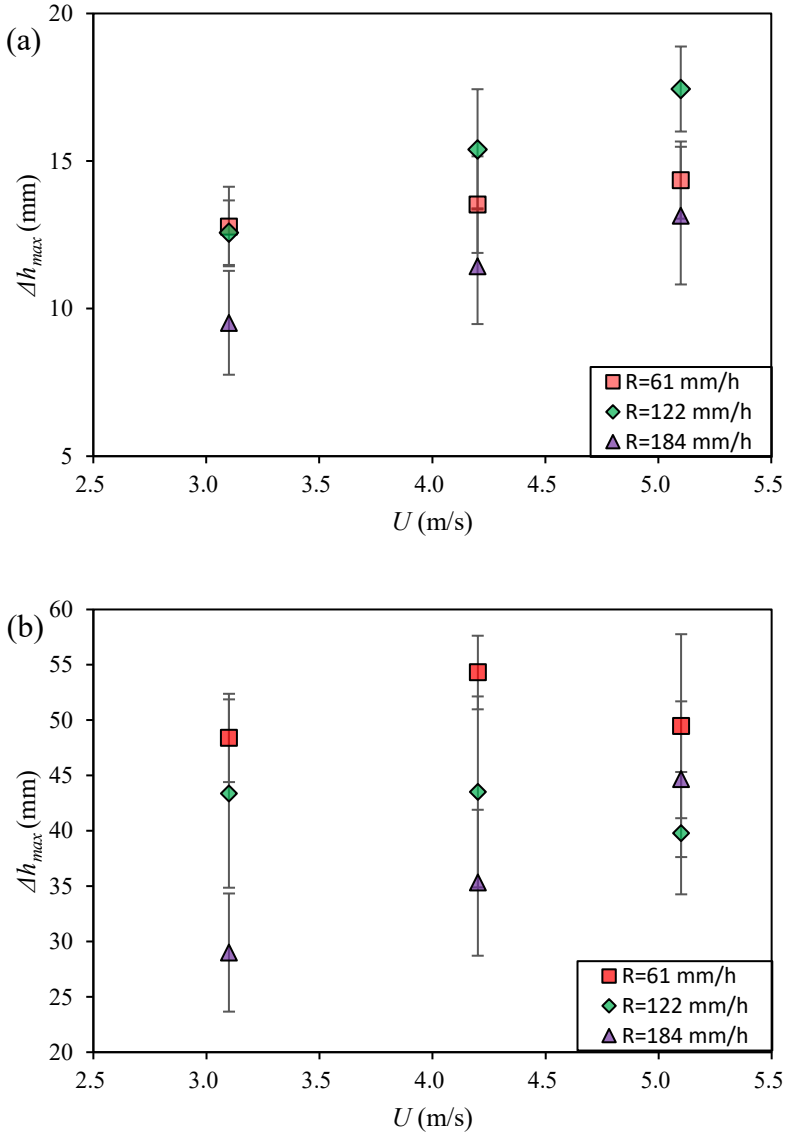

Figure 3-3 Changes of the maximum depth of cavity or penetration depth (Δh_{max}) with different falling velocity (3.1-5.1 m/s) and flow rate (61 – 184 mm/h) for (a) falling drops; (b) falling jet.

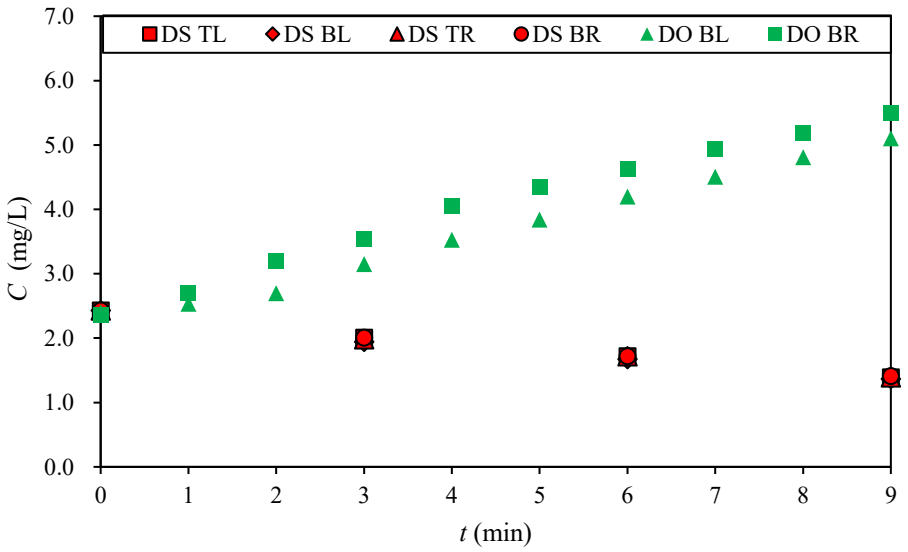

Figure 3-4 Variation of the concentrations (C) of DO and DS in the bottom pool with time at different locations. The turbulent water surface was caused by falling drops, with KEF = 0.51 J/(m^{2}s).

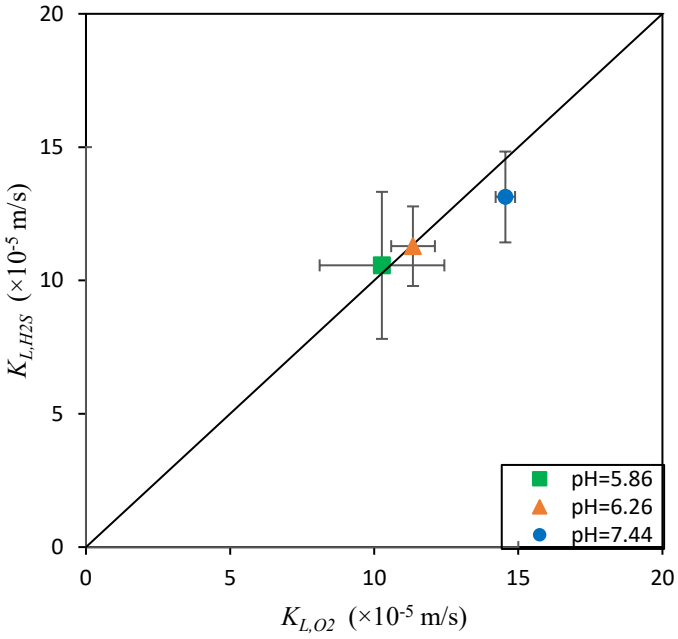

Figure 3-5 Comparison of K_L for H_2S and O_2 at the surface of DI water under falling drops. Error bars show ±1 standard deviation.

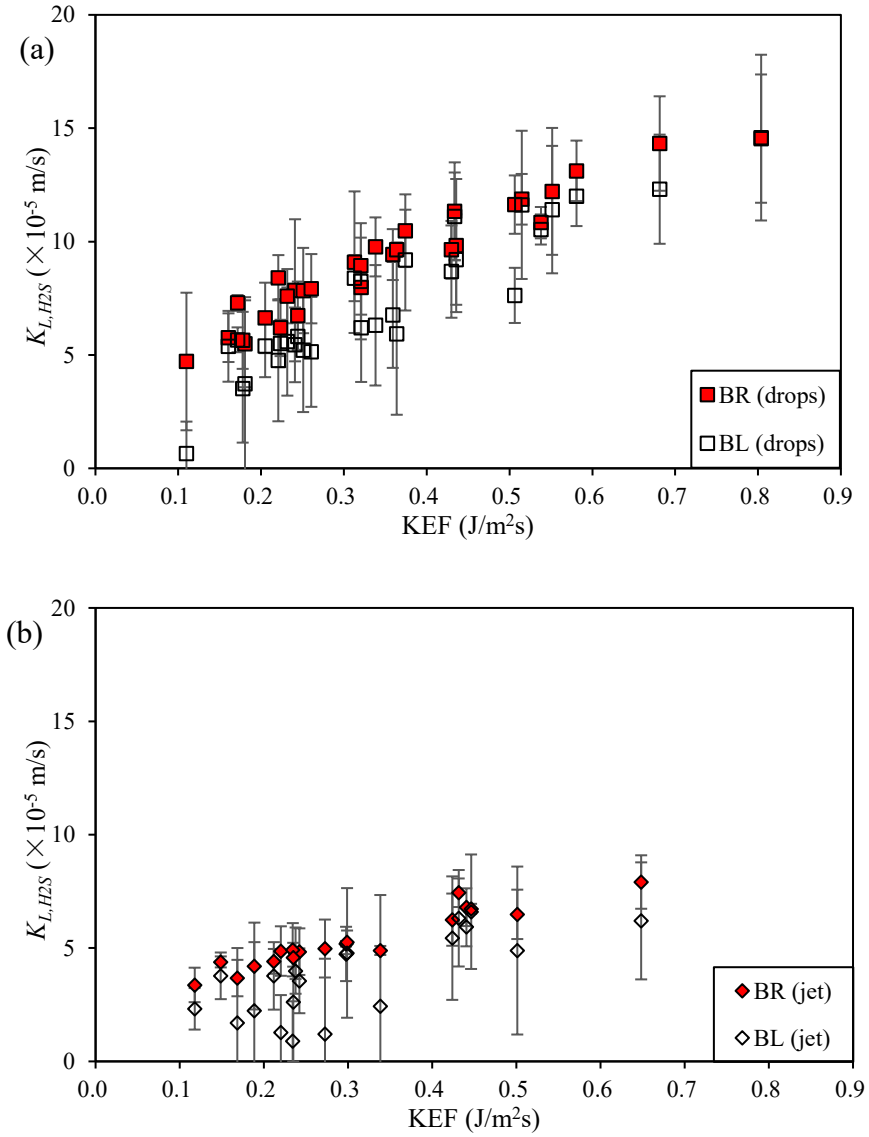

Figure 3-6 Comparison of K_L for H_2S between the left and right side of the collection pool: (a) under falling drops scenario; (b) under jet scenario. Error bars show ±1 standard deviation.

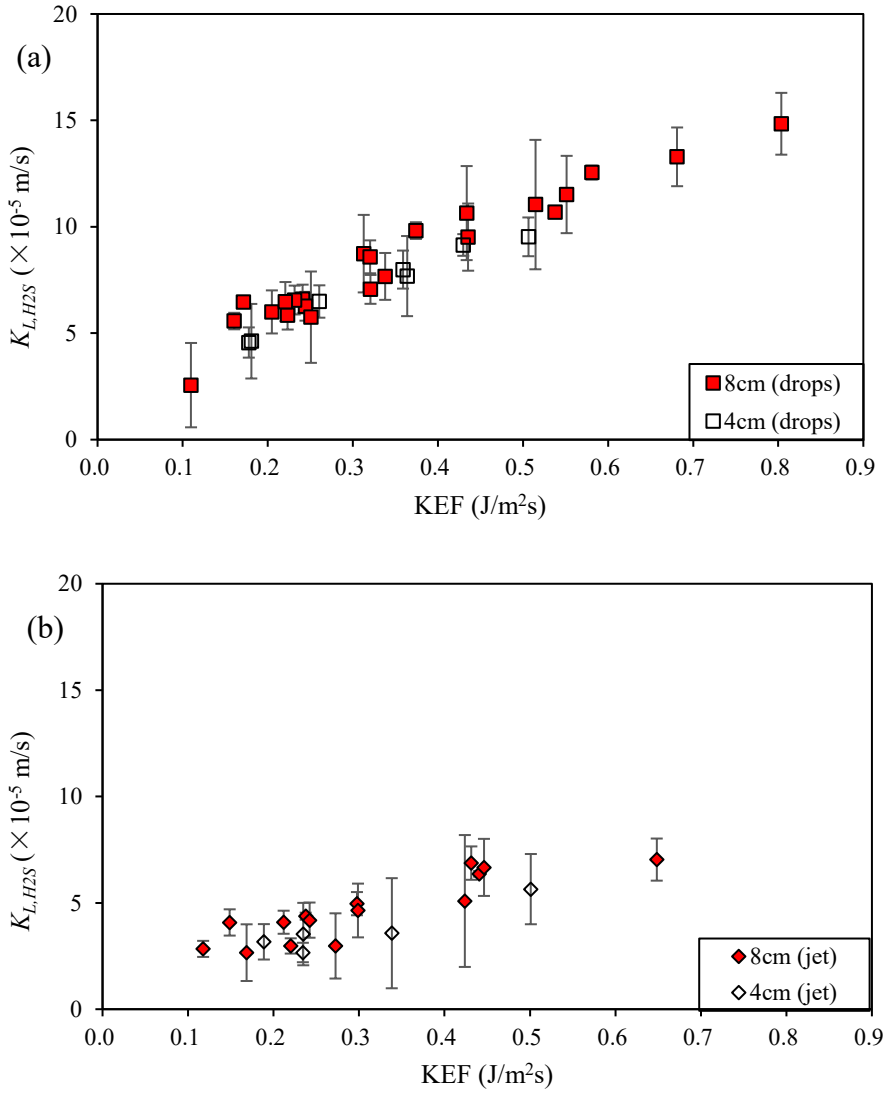

Figure 3-7 Comparison of K_L for H_2S between different water depths of the collection pool: (a) under falling drops scenario; (b) under jet scenario. Error bars show ±1 standard deviation.

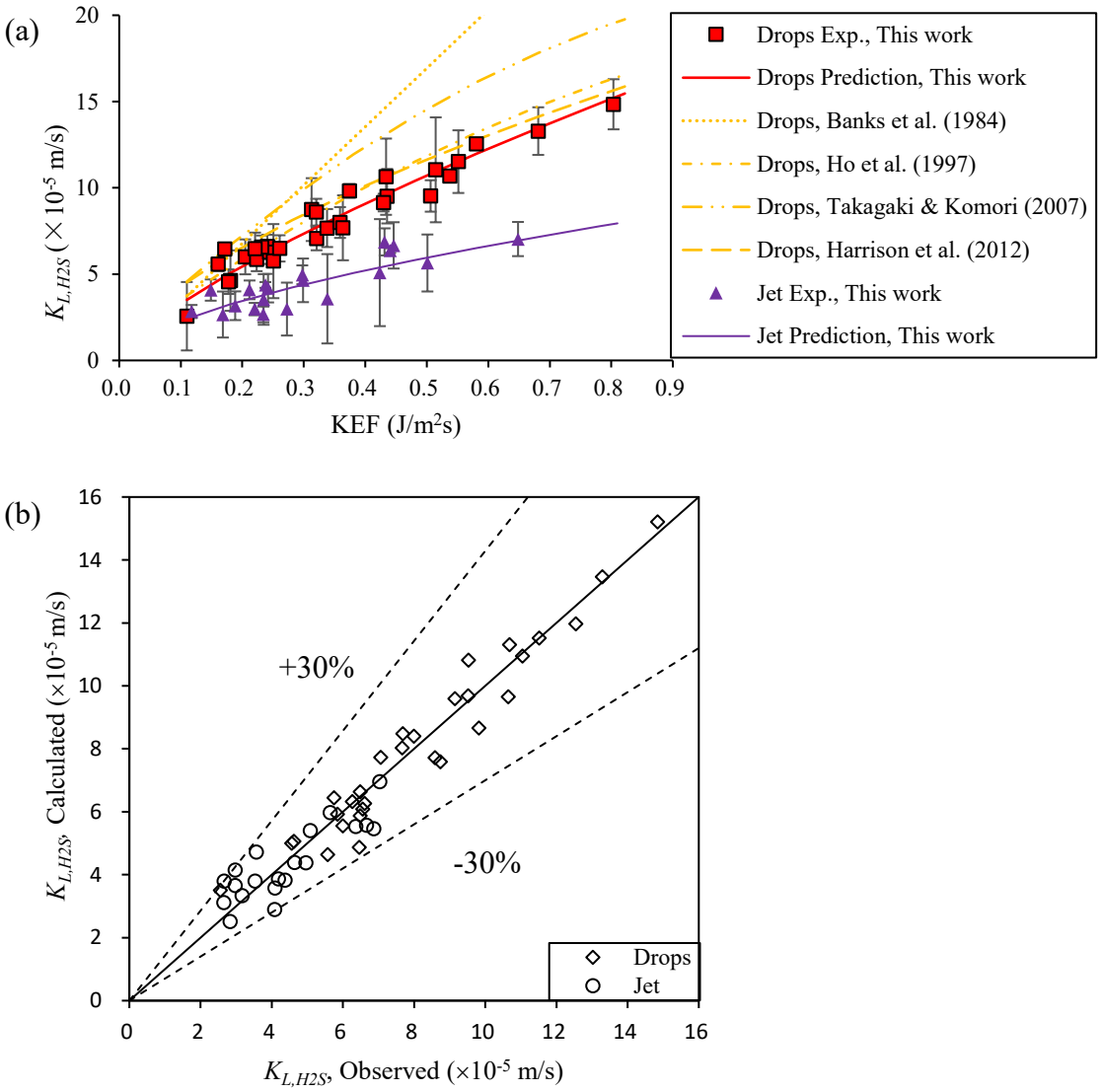

Figure 3-8 (a) Comparison of K_L for H_2S values from the experiments and models. Error bars show ±1 standard deviation. (b) Comparison of observed K_L with proposed models from this study.

4. Mass Transfer of Hydrogen Sulfide and Oxygen in Sewer Drop Structures

4.1. Introduction

Hydrogen sulfide (H_2S) is naturally generated in sanitary or combined sewers under anaerobic condition (Hvitved-Jacobsen et al. 2013). When wastewater falls in the sewage collection system, for instance in a drop structure, H_2S emits from sewage to air via the mass transfer. A sewage falling jet can induce a large amount of air into the headspace of the downstream sewer pipes, which pressurizes the sewer air, causes the release of sewer odor from the sewer system to the air above ground and generates the sewer odor issues (Zhang et al. 2016). H_2S is also the root-cause of sewer pipe corrosions (Hvitved-Jacobsen et al. 2013; Zuo et al. 2019). Meanwhile with the emission of H_2S from sewage to sewer air in drop structures, O_2 from sewer air is entrained into the sewage, which is another important mass transfer affecting the dissolved oxygen level and thus chemical and biological reactions in sewage (Lee et al. 1993; Yang et al. 2020).

The falling wastewater jet in a drop structure may exist in two forms: 1) free-falling jet, which falls freely without toughing the side wall and then impinges on the surface of the water pool at the bottom of the drop structure; and 2) attached-falling jet, which impinges on the side wall and falls along the wall as a thin attached film. Both forms of falling sewage jet substantially but differently affect the mass transfer of H_2S and O_2 in drop structures.

In sewer drop structures, the mass-transfer could occur at jet surface, falling droplet surface, and bottom pool (due to turbulent water surface, entrained bubbles, induced splashing droplets). The mass transfer triggers the gas concentration difference between the upstream and downstream of

drop structures: for H_2S, its emission makes the gas concentration in the downstream sewage C_d smaller than that in the upstream C_u; while for O_2, its absorption makes C_d larger than C_u. To quantify their relationship, the deficit ratio r is defined as follows (Pincince 1991):

$$r = \frac{C_s - C_u}{C_s - C_d} = \frac{C_a/H - C_u}{C_a/H - C_d} \tag{4-1}$$

where C_s is the saturation concentration of the gas (H_2S or O_2) in sewage, C_a is the gas concentration in air and H is the Henry's law constant.

So far, mass transfer of O_2 in laboratory or field drop structures has been studied. Nakasone (1987) experimentally found a distinct relation between r and three hydraulic parameters: drop height h_d, flow rate Q, and tailwater depth h_t. However, Pincince (1991) concluded that tailwater depth did not affect much on r in his experiments. Labocha et al. (1996) and Rahmé et al. (1997) also experimentally studied the reaeration process in drop structures, and the correlations of r were given as a function of drop height, flow rate, and tailwater depth, similarly as Nakasone (1987). More recently, Matias et al. (2017b) conducted lab experiments in a drop structure with tap water circulating inside, and proposed the correlation of r with the same three parameters. The existing correlations are summarized in Table 4-1. From the literature, h_d is probably the most important factor (Labocha et al. 1996), Q is related to the mass transfer efficiency (Nakasone 1987); and h_t affects the penetration depth of air bubbles (Nakasone 1987).

To the authors' best knowledge, experimental studies that directly use H_2S (not via a surrogate gas like O_2) and that examine r and K_L in drop structures, are missing in the literature. In addition, the comparison of mass transfer between the two sewage falling forms, free-falling and attached-falling jets, has not been reported. Moreover, the estimations of mass transfer in real-world or

prototype drop structures are limited. These knowledge gaps are explored in the current research, and the results will be useful in sewer odor and corrosion control and mitigation for municipal sewer systems.

4.2.Materials and Methods

4.2.1. Experimental Setup and Procedures

The experiments were conducted in two cylinders, to mimic drop structures in sewer systems (Figure 4-1). The sizes of the two cylinders were 20 cm (large drop structure) and 15 cm (small drop structure). Deionized (DI) water was circulated in the cylinder by a peristatic pump (RK-77924-65, Masterflex, USA). Two jet forms were used: free-falling and attached-falling jets. The drop height h_d ranged from 0.2-1.4 m from the jet outlet to the water surface of the receiving pool. The tailwater depth h_t was 0.1 (only for the large drop structure), 0.2 and 0.3 m. Flow rate Q had a range of 0.9-1.8 L/min. The outlet size of the jet was 6.4 mm and the initial jet velocity at the outlet was 0.5-1.0 m/s.

The mass transfer of O_2 for DI water was first tested, to examine the mass transfer of a single gas. Two DO sensors (LDO101, Hach, USA) were first calibrated as per the manual and used to measure the DO concentration every minute in the experiments. They were kept along two sides of the cylinder and in the middle of the water depth. The air concentration of O_2 was monitored by an oxygen detector (Pac 6000, Dräger, Germany). Their locations were schematically shown in . Before the test, the dissolved oxygen (DO) concentration in the water was decreased to be around 1 mg/L via blowing nitrogen (N_2) into it following Chu and Jirka (2003) and Carrera et al. (2017 b). The experiments were conducted at room temperature (19-22 ℃), and the temperatures were

recorded during each test so that the results were all adjusted to 20 ℃. A single test lasted for 10-25 minutes because DO level was close to saturation at the end. A high-speed camera (Phantom v211, Vision Research, Wayne, USA) was employed to capture the movement of bubbles and splashing droplets inside the drop structures.

Next, the mass transfer of H_2S and O_2 was tested simultaneously for H_2S solution, to compare the mass transfer rate of the two gases. The H_2S solution was made by adding saturated H_2S solution (Ricca Chemical, USA) into the DI water, and the initial concentration of dissolved sulfide (DS) in the tailwater was 5-10 mg/L. Because of the toxicity of H_2S, the experiments were conducted in a walk-in fume hood. pH was 5.4-6.4 in the cylinder, which was measured before and after each test by a pH meter (AR15 accumet Fisherbrand, USA). Two samples of 2.5 mL H_2S solution were taken at the locations of the DO sensors every five minutes, and their DS levels were measured in a spectrophotometer (DR6000, Hach, USA) by the methylene blue method (APHA at al. 2017). The air concentration of H_2S was monitored by a H_2S data logger (App-Tek, Queensland, Australia). The procedures for the O_2 mass transfer were the same as in the previous paragraph.

4.2.2. Method for Calculating K_L for O_2

The driving force of mass transfer is the gas concentration difference between the water and the air (Clift et al. 1978). In the two-film theory (Lewis and Whitman 1924), the mass transfer process of O_2 can be expressed as:

$$\frac{dC_{DO}}{dt} = K_{L,O_2} a \left(C_{a,O_2} / H_{O_2} - C_{DO} \right) \tag{4-2}$$

where C_{DO} is the DO concentration in water; t is the time of mass transfer; K_{L,O_2} is the mass transfer coefficient for O_2; a is the surface-area-to-volume ratio of the collecting tank; C_{a,O_2} is the O_2

concentration in air; and H_{O_2} is Henry's law constant for O_2. In the current setup, $a = A/V = 1/h_t$, where A is the surface area of the tailwater, V is the total water volume in the cylinder and h_t is the tailwater depth.

After integration, Eq. (4-2) becomes:

$$\ln\left(\frac{C_{a,O_2}/H_{O_2} - C_{DO,1}}{C_{a,O_2}/H_{O_2} - C_{DO,2}}\right) = K_{L,O_2} a \Delta t \tag{4-3}$$

where the subscripts 1 and 2 mean two different times. If K_{L,O_2} was not obtained at the standard temperature (20℃), it was adjusted to that at 20 ℃ (Elmore and West 1961):

$$K_{L,O_2(20)} = \frac{\ln\left(\frac{C_{a,O_2}/H_{O_2} - C_{DO,1}}{C_{a,O_2}/H_{O_2} - C_{DO,2}}\right)}{a\Delta t} 1.0241^{20-T} \tag{4-4}$$

where T is the experimental temperature in Celsius, and $K_{L,O_2(20)}$ is the mass transfer coefficient at 20℃. All the K_L values in the following results have been adjusted to 20℃.

4.2.3. Method for Calculating K_L for H_2S

In the experiments, the H_2S solution in the cylinder followed the dynamic equilibrium (Yongsiri et al. 2004):

$$H_2S \uparrow \rightleftharpoons HS^- + H^+ \quad pK_1 = 7.0 \qquad HS^- \rightleftharpoons S^{2-} + H^+ \quad pK_2 = 17.1 \quad (20\ ^\circ C)$$

Due to the large pK_2 value, the S^{2-} is negligible (Matias et al. 2017a). In the experiments, pH = 5.4-6.4 in the cylinder, sulfide existed in two forms: HS^- and H_2S. Note that only the molecular H_2S

can emit from water to atmosphere (Zhang et al. 2008). The percentage of H_2S in total dissolved sulfide (H_2S and HS^-), f, is determined by pH and pK_1 as follows:

$$f = \frac{C_{H_2S}}{C_{DS}} = \left(10^{\mathrm{pH}-\mathrm{p}K_1} + 1\right)^{-1} \tag{4-5}$$

where C_{H_2S} is the concentration of molecular H_2S in water; C_{DS} is the concentration of total dissolved sulfide in water; and pK_1 = 6045.2/T – 106.67 + 37.744log$T$, where T is the water temperature in Kelvin (Rao and Helper 1977).

The mass transfer rate of H_2S is (Yongsiri et al. 2005):

$$-\frac{dC_{DS}}{dt} = K_{L,H_2S}a\left(C_{H_2S} - C_{a,H_2S}/H_{H_2S}\right) = K_{L,H_2S}a\left(fC_{DS} - C_{a,H_2S}/H_{H_2S}\right) \tag{4-6}$$

where C_{a,H_2S} is the H_2S concentration in air; and H_{H_2S} is Henry's law constant for H_2S. In each measurement duration Δt (5 min), f was assumed to be a constant. By integration of Eq. (4-6) and adjusting to 20 °C,

$$K_{L,H_2S(20)} = \frac{\ln\left(\dfrac{C_{a,H_2S}/H_{H_2S} - fC_{DS,1}}{C_{a,H_2S}/H_{H_2S} - fC_{DS,2}}\right)}{fa\Delta t} 1.0241^{20-T} \tag{4-7}$$

By comparing the equations for calculating K_L for H_2S and O_2 (Eqs. 4-7 and 4-4), it can be found that the numerators are both the natural logarithm (ln) of the deficit ratio at two different times. The difference is that there is a coefficient, f, in the denominator of Eq. (4-7), which represents the effect of pH.

If we need to convert K_L from Gas A to Gas B, e.g., from O_2 to H_2S, the following equation can be used (Jähne et al. 1987; Ho et al. 1997; Harrison et al. 2012):

$$\frac{K_{L,\mathrm{A}}}{K_{L,\mathrm{B}}}=\left(\frac{D_{\mathrm{A}}}{D_{\mathrm{B}}}\right)^{1/2} \tag{4-8}$$

where D is the molecular diffusivity of the gas in water. At 20 °C, $D_{O_2} = 2.0 \times 10^{-9}$ m/s (Ferrell and Himmelblau 1967), and $D_{H_2S} = 1.8 \times 10^{-9}$ m/s (Tamimi et al. 1994). Therefore, $K_{L,H_2S}/K_{L,O_2} = (D_{H_2S}/D_{O_2})^{1/2} = 0.95$.

4.2.4. Method for Calculating Deficit Ratio *r*

By assuming a complete mixture in the tailwater (Matias et al. 2017b), the mass balance for O_2 is described by:

$$C_{t+\Delta t}V = C_t V + \left(C_d - C_u\right)Q\Delta t \tag{4-9}$$

where C_t is the DO concentration at time t. By substituting Eq. (4-1) into Eq. (4-9),

$$\frac{C_{t+\Delta t}-C_t}{\Delta t}=\left(C_d-C_u\right)\frac{Q}{V}=\left(C_a/H-C_u\right)\left(1-\frac{1}{r_{O_2}}\right)\frac{Q}{V} \tag{4-10}$$

When $\Delta t \rightarrow 0$, Eq. (4-10) becomes:

$$\frac{dC}{dt}=\left(C_a/H-C_u\right)\left(1-\frac{1}{r_{O_2}}\right)\frac{Q}{V} \tag{4-11}$$

In Eq. (4-11), C_u is equal to C_{DO} in Eq. (4-2). Therefore, by combining Eqs. (4-2) and (4-11), it is obtained:

$$\frac{1}{r_{O_2}}=1-\frac{K_{L,O_2}aV}{Q}=1-\frac{K_{L,O_2}A}{Q} \tag{4-12}$$

By monitoring the O_2 concentrations in liquid and air continuously, K_La was obtained with Eq. (4-3), and r_{O_2} was calculated with Eq. (4-12).

Similar analysis was conducted for H_2S: $\frac{1}{r_{H_2S}} = 1 - \frac{fK_{L,H_2S}A}{Q}$, where $r_{H_2S} = \frac{C_{a,H_2S}/H_{H_2S} - fC_{DS,1}}{C_{a,H_2S}/H_{H_2S} - fC_{DS,2}}$.

4.3. Results and Discussion

4.3.1. Mass Transfer of O_2 for DI Water

The free-falling jets in drop structures

An example of the variation of DO concentration with time for free-falling jet in drop structures is shown in Figure 4-2, where C_{DO} was the mean concentration of DO in the tailwater and the experimental conditions were similar: h_t = 0.2 m and Q = 1.7 L/min. For the large drop structure, in the mass transfer time of 15 min, C_{DO} increased from 1.3 to 4.4 mg/L with the drop height h_d of 0.3 m, from 1.8 to 6.4 mg/L with h_d of 0.8 m, and from 1.7 to 7.0 mg/L with h_d of 1.2 m [Figure 4-2(a)]. In Figure 4-2(b) for the small drop structure, in the same mass transfer time, C_{DO} increased from 1.1 to 4.0 mg/L with h_d of 0.3 m, from 1.3 to 5.1 mg/L with h_d of 0.8 m, and from 1.0 to 5.9 mg/L with h_d of 1.2 m. The results suggest that the increase of the DO concentration in the tailwater was more substantial with larger h_d for the two sized drop structures. This can be explained by that, an increase of h_d means a larger surface area of the jet, more splashing droplets generated at the tailwater surface, more turbulent tailwater surface and more air bubbles entrained in the tailwater. The results also suggest that, under the same hydraulic conditions, DO increased faster (by ~ 50%) in the large drop structure, meaning larger K_L there.

Based on the DO concentration in Figure 4-2, K_L was calculated with Eqs. (4-3) and (4-4) and the results are shown in Figure 4-3 (a). Under the same experimental conditions as in Figure 4-2, K_L increased from 1.3 to 3.9×10^{-4} m/s when h_d = 0.3-1.3 m in the large drop structure; while in the small drop structure, it increased from 1.3 to 2.6×10^{-4} m/s. In Figure 4-3 (b), all the K_L values from this study are compared between the two sized drop structures. In the large drop structure, K_L was from 1.0 to 5.4×10^{-4} m/s; while in the small drop structure, K_L was from 1.0 to 4.4×10^{-4} m/s. Most (~80%) of K_L values in the large drop structure were larger than those in the smaller drop structure under the same experimental condition, with the average ratio of 1.2 ± 0.3. In the free-falling jet scenario, large amounts of splashing droplets impinged on the cylinder wall, and the droplets have larger travelling time before they impinged on the cylinder wall in the large drop structure than the smaller drop structure, which may be the reason for the larger K_L in the large drop structure.

Based on K_L, r was calculated with Eq. (4-12) and the results are shown in Figure 4-4. Under the same experimental conditions as in Figure 4-2 and Figure 4-3 (a), r increased from 1.2 to 1.9 in the large drop structure and from 1.1 to 1.2 in the small drop structure. The increase was almost linear with an increase of h_d [Figure 4-4(a)]. The r value in the large drop structure was larger than that in the small drop structure, because both K_L and A in Eq. (4-12) were larger in the large drop structure. Figure 4-4(b) shows the caparison of r between the large and small drop structures. The ratio of r from the large drop structure to the small drop structure ranged 1.0-2.2, with the mean value of 1.4 ± 0.3. Figure 4-4(b) also suggests that the ratio of r increased with an increase of h_d: r was 1.1 on average for h_d = 0.2-0.3 m;, r was 1.4 for h_d = 0.7-0.8 m; and r was 1.8 when h_d = 1.2-1.3 m.

Figure 4-5 shows the effect of the flow rate Q on r. In the large drop structure [Figure 4-5(a)], r decreased with an increase of Q as clearly shown by the trendlines. From the low flow rate (0.9-1.0 L/min) to the high flow rate (1.8-2.0 L/min), r decreased by 10-16% for h_d = 0.4 -1.4 m. In the small drop structure, similarly, r decreased with an increase of Q [Figure 4-5(b)], and from the same low to high flow rate, r decreased by 5-17% for h_d = 0.2-1.3 m. This demonstrates that the aeration efficiency decreased with an increase of discharge, which agrees with Nakasone (1987).

For the large drop structure, the predicted r values using Labocha et al. (1996)'s equation (Table 4-1) is 0.88 ± 0.15 times of our experimental values, and the ratio is 1.6 ± 0.4 using Rahmé et al. (1997)'s equation [Figure 4-6(a)]. For the small drop structure, both Labocha et al. (1996) and Rahmé et al. (1997)'s equations overestimate our experimental data [Figure 4-6(b)], with the ratios of 1.2 ± 0.2 and 2.1 ± 0.6 times, respectively. The experiments of the two previous studies were conducted in drop structures where the water was not circulating, which is different from this study. Besides, their maximum water flow rate Q was about 20-150 times of ours (see the impact of Q in the equations listed in Table 4-1). Those reasons might cause the several times difference in predicted r than observed r.

Since the existing equations cannot predict the results well, efforts were made to propose new equations for r. Based on our experimental results, h_d (m), Q (L/min) and h_t (m) are all controlling parameters of r. The correlation between ln r and the three parameters was optimized by nonlinear regression in Matlab for free-falling jet:

$$\ln\ r = a h_d^{\ b} Q^c h_t^{\ d} \tag{4-13}$$

where a = 1.25, b = 0.783, c = -0.430, and d = 0.347 for the large drop structure, with R^2 = 0.80; and a = 0.97, b = 0.876, c = -0.645, and d = 0.827 for the small drop structure, with R^2 = 0.82.

Figure 4-7 (a) shows the comparison of the predicted r from Eq. (4-13) and with the experimental data. Reasonable agreement could be achieved: 98% of the predicted r values are within 20% difference from the experimental results. In Eq. (4-13), h_d is the most important parameter as its exponent is larger than those of the other two parameters, and similar conclusion can be also made from the correlations of Labocha et al. (1996) and Rahmé et al. (1997) listed in Table 4-1.

The limitation of Eq. (4-13) is that the three parameters on the right hand side are dimensional, meaning that they might be only valid for specific experimental setup. Therefore, dimensionless correlation was proposed in this study for wider applications in engineering:

$$\ln\ r = 1.13\times10^{-4}\left(\frac{h_t}{h_d}\right)^{-0.00917}\left(\frac{Q/A}{\sqrt{gh_d}}\right)^{-0.998} \tag{4-14}$$

for which $R^2 = 0.67$. Figure 4-7(b) shows the comparison of the predicted r from Eq. (4-14) with the experimental results, where 96% of the predicted r values are within 25% difference from the experimental results. In Eq. (4-14), the role of h_t/h_d is limited because of its small exponent, so this term might be ignored to obtain:

$$\ln\ r = 4.61\times10^{-5}\left(\frac{Q/A}{\sqrt{gh_d}}\right)^{-1.101} \tag{4-15}$$

for which $R^2 = 0.66$. Figure 4-7(c) shows the comparison of the predicted r from Eq. (4-15) with the experimental values, where 95% of the predicted r values are within 25% of error level.

In Sun et al. (2022), the mass transfer of O_2 was investigated at turbulent water surface induced by single jet. The correlation between K_L and KEF (kinetic energy flux, defined as $\mathrm{KEF} = 0.5\times Q/A\times v_j^2$, where v_j is the jet falling velocity at the pool surface) was built as $K_L = 9.234\times10^{-5}\mathrm{KEF}^{0.596}$. With

that correlation, K_L predicted with KEF was compared with the experimental values of this work in Figure 4-8. For the large drop structure, nearly all the predictions are within ±25 % error level and the ratio of the predicted to experimental K_L is 0.97 ± 0.16; for the small drop structure, nearly 78% of the predictions are within ±25 % error level and the ratio of the predicted to experimental K_L is 1.17 ± 0.27. For the two drop structures, the averaged ratio of the predicted to experimental K_L is 1.04 ± 0.23. Therefore, the mass transfer of free-falling jet mainly occurs at the tailwater surface, including turbulent tailwater surface, splashing droplets and air bubbles, i.e., the mass transfer at the surface of falling jet in air could be neglected.

Chu and Jirka (2003) and Carrera et al. (2017 b) conducted experiments on the mass transfer of O_2 at flowing water surface in gravity sewers. In Chu and Jirka (2003), water flow velocity was 0.20-0.62 m/s and water depth was 0.10-0.20 m, and K_L was found to be 1.9 $\times 10^{-5}$ m/s on average. In Carrera et al. (2017 b), water flow velocity was 0.27-0.61 m/s and water depth was 0.015-0.075 m, and K_L was 0.8 $\times 10^{-4}$ m/s on average. In our experiment [Figure 4-3 (b)], K_L was averaged to be 2.4 $\times$ 10^{-4} m/s, which shows that the mass transfer rate in drop structures was 3-13 times of that in gravity sewers.

The attached-falling jets in drop structures

In the attached-falling jet scenario, the corresponding K_L and r were calculated with the same method presented above. In the large drop structure when h_t = 0.2 m and Q = 1.7 L/min, K_L = 0.9, 1.8 and 2.0 $\times$ 10^{-4} m/s for h_d = 0.3, 0.8 and 1.3 m, respectively, which are all smaller than those of small drop structure, where K_L values were 1.8, 2.3 and 3.0 $\times$ 10^{-4} m/s, respectively (Figure 4-9). Under other experimental conditions of h_t and Q, K_L in the large drop structure was also less than that in the smaller drop structure, with an overall ratio of 0.6 ± 0.2. In the attached-falling jet

scenario, the number of bubbles entrained into the tailwater was much less than that in the free-falling jet scenario as per the images of the high-speed camera. Also, splashing droplets due to impingement were rarely found in this scenario. Therefore, the reason for the smaller K_L values in the large drop structure could be the lower turbulence level at its tailwater surface because of the larger volume and surface area of water under the same experimental conditions.

Despite of the smaller K_L in the large drop structure, it has larger A and therefore r calculated from Eq. (4-12) was similar between the large and small drop structures [Figure 4-10(a)]. Under all the experimental conditions, the range of r with the attached-falling jet in both large and small drop structures was 1.1-1.8, and the r ratio of the large to small drop structure was 1.0 ± 0.1 [Figure 4-10(b)].

The correlation between ln r at 20 ℃ and the experimental conditions in the scenario of attached-falling jet, was fitted by nonlinear regression in MATLAB as:

$$\ln\ r = 0.124 h_d^{\,0.561} Q^{-0.393} h_t^{\,-0.498} \tag{4-16}$$

for which $R^2 = 0.82$. The dimensionless correlation was fitted as:

$$\ln\ r = 4.92\times10^{-3}\left(\frac{h_t}{h_d}\right)^{-0.360}\left(\frac{Q/A}{\sqrt{g h_d}}\right)^{-0.407} \tag{4-17}$$

for which $R^2 = 0.85$. Figure 4-11(a) and (b) shows a comparison of the predicted r values from Eqs. (4-16) and (4-17) with the experimental values. Good agreement was achieved: all the predicted r values are within 10% difference from the experimental results.

Comparison between the two jet scenarios

Comparison of mass transfer rate between the two jet scenarios was conducted in both drop structures. In the large drop structure, under experimental condition of h_t = 0.2 m, Q = 1.7 L/min, K_L ranged from 1.3 to 3.9 × 10^{-4} m/s in the scenario of free-falling jet [Figure 4-3 (a)]; while in the scenario of attached-falling jet, K_L ranged from 0.9 to 2.0 × 10^{-4} m/s (Figure 4-9), which shows that free-falling jet could increase the mass transfer efficiency. The r ratio of free-falling to attached-falling jet was all above 1 [Figure 4-12(a)], with the mean of 1.4 ± 0.8, i.e., the r values of the free-falling jet were larger than those of the attached-falling jet. As stated earlier, that could also be related to 1) bubble entrainment: more bubbles were entrained into the tailwater by the free-falling jet than by the attached-falling jet; and 2) splashing droplets: large number of splashing droplets in the free-falling jet while rare splashing droplets in the attached-falling jet. Furthermore, the r ratio generally increased with an increase of the tailwater h_t, e.g., the ratios were 1.05-1.22, 1.13-1.54 and 1.40-2.01, respectively, with h_t = 0.1, 0.2 and 0.3 m. At the same h_t, the ratio of r increased with the drop height h_d, e.g., at h_t = 0.2 m, the r ratios were 1.1, 1.3 and 1.5, respectively, when h_d = 0.3, 0.8 and 1.3 m. Moreover, the r ratio slightly decreased with an increase of Q as shown in Figure 4-12(a). These phenomena were affected by the bubble entrainment, splashing droplet movement and turbulent water surface.

In the small drop structure, r was almost same between the two jet scenarios [shown in Figure 4-12(b)], where 80% of r ratio data points were between 0.9 and 1.1, and its mean value was 1.0 ± 0.1. In both jet scenarios, air bubbles, turbulence on the tailwater surface and splashing droplets contributed the mass transfer. More air bubbles and splashing droplets took place in the scenario of free-falling jet, while in the scenario of attached-falling jet, stronger turbulence on the tailwater surface could happen. The result of r ratio shows that different mechanisms contributed to a similar

magnitude of mass transfer under the two jet scenarios. Similarly, in the large drop structure, the r ratio also increased with an increase of h_t and h_d and a decrease of Q.

4.3.1. Simultaneous Mass Transfer of O_2 and H_2S for H_2S Solution

The experimental results for the simultaneous mass transfer of O_2 and H_2S for H_2S solution is shown in Figure 4-13. Based on the pH values of 5.4-6.4, f was calculated to be 0.81-0.98 with Eq. (4-5). C_{a,H_2S} was 11 to 318 ppm. The oxidation of sulfide by O_2 could be ignored, which is proved in the Appendix. K_L for H_2S was then calculated with Eq. (4-7).

In Figure 4-13, five experiments were performed in the large drop structure with free-falling jet under the conditions of h_d = 0.2-1.4 m, Q = 0.9-1.7 L/min and h_t = 0.1-0.3 m, and K_{L,H_2S} was found to be 1.4-3.5 × 10^{-4} m/s and K_{L,O_2} was 1.5-4.1 × 10^{-4} m/s. Two experiments were performed in the small drop structure with free-falling jet under the conditions of h_d = 0.2-0.7 m, Q = 1.0 L/min and h_t = 0.3 m, and K_{L,H_2S} was 1.3-2.2 × 10^{-4} m/s and K_{L,O_2} was 1.3-2.6 × 10^{-4} m/s. And one test was performed in the small drop structure with attached-falling jet under the conditions of h_d = 1.2 m, Q = 0.9 L/min and h_t = 0.3 m, and K_{L,H_2S} was 1.9 × 10^{-4} m/s and K_{L,O_2} was 2.1 × 10^{-4} m/s. In these experiments, K_{L,O_2} for H_2S solution was similar to that for DI water. Also, the ratios of K_L between the two gases, $K_{L,H_2S}/K_{L,O_2}$ = 0.85-0.99, with the mean of 0.90 ± 0.05. The mean value was almost the same as the theoretical value of 0.95 from Eq. (4-8). As O_2 is non-toxic and easier for measurement, it is a good surrogate gas for studying the mass transfer of H_2S in municipal drainage systems.

4.3.2. Estimating Mass Transfer in Prototype Drop Structure

In Sun et al. (2020), H_2S emission in prototype drop structure was estimated due to the mass transfer in falling droplets. However, the mass transfer between the air and bottom pool was not considered, which triggered the following predictions. Herein, O_2 was used as the mass transfer gas because reliable field monitoring data are available. It is assumed that the sewage jet breaks up to droplets of 2 mm when it falls 4.2 m and after that the water droplets fall at the terminal velocity of 6.5 m/s (Sun et al. 2020). When h_d is smaller than 4.2 m, the mass transfer occurred at the surface of falling jet (0 - bottom pool) and bottom pool can be calculated from Eq. (4-15). When h_d is larger than 4.2 m, the mass transfer at the surface of falling jet (0-4.2 m) and falling droplets (4.2 m-bottom pool) can be calculated with empirical equation of Sun et al. (2020), shown in Eq. (4-18); and the mass transfer at the bottom pool is calculated with Eq. (4-15) and then multiplied by a coefficient of 1.76. The multiplier of 1.76 is because from the experimental results of Sun et al. (2022), K_L and ln r under droplets increased by 76% than that under free-falling jet. The calculation flow chat is shown in Figure 4-14.

$$K_{L,20} = 3.15 \times \left(U \sqrt{\frac{\rho_g}{\rho_L} \frac{c_D}{2}} \frac{D}{d} \right)^{1/2} - 3.52 \times 10^{-4} \tag{4-18}$$

where U is the droplet velocity, d is the droplet diameter, c_d is the drag coefficient of falling drop lets, and ρ is density, ρ_a = 1.2 kg/m^3, ρ_L = 998 kg/m^3.

Next, an example is provided to estimate mass transfer in a prototype drop structure. DO concentration in the upstream, $C_{DO,u}$, is assumed to be 2 mg/L, the sewer air pressure is 1 atm, the temperature of the sewer air and wastewater T is 13 ℃, the diameter of the drop structure is 1.2 m, Q ranges 10 – 1000 L/s, and h_d is up to 20 m. The oxygen level in the sewer air is 98% of the

normal air (from our field work measurement), and the saturation concentration of the gas C_s in wastewater is 97% of that in water (Tewari and Bewtra 1982). K_L in wastewater was found to be 0.67-0.93 of K_L in water (Tewari and Bewtra 1982), and based on Eqs. (4-1) and (4-3), the ratio of ln r in wastewater and water is the same as that of K_L, which is assumed to be 0.80 (mean value of 0.670-0.925).

Figure 4-15 (a) shows the calculation results of DO concentration in the downstream, $C_{DO,d}$, of a prototype drop structure using the conditions specified above. When $h_d \leq 3$ m, $C_{DO,d}$ only changes slightly compared with the upstream DO level ($C_{DO,u}$ = 2mg/L). When h_d = 3 m, $C_{DO,d}$ = 2.30 and 2.02 mg/L for Q = 10 L/s and 100 L/s, respectively. When $3 \leq h_d \leq 5$ m, $C_{DO,d}$ increased with h_d. When $h_d \geq 5$ m, the mass transfer rate increases quickly, and $C_{DO,d}$ (> 9 mg/L) is over 90% of the saturation level when h_d = 14 m. The reason for the quick increase is that the droplets contributed substantially to the mass transfer [Figure 4-15 (b) and (c)]. When Q = 10 L/s, h_d = 5 and 10 m, the fraction of the droplets' contribution to total mass transfer was 69% and 95%, respectively; When Q = 10 L/s and h_d > 10 m, the droplets' contribution is close to 100%, which means the jet and pool surface' contribution could be neglected. With the same h_d, the droplets' contribution increases with an increase of flow rate. For instance, with h_d = 5 m, the droplets' contribution was 0.69, 0.96 and 1.00 (to be more precisely, 0.997) when Q = 10 L/s [Figure 4-15 (b)], Q = 100 L/s [Figure 4-15 (c)] and 1000 L/s, respectively. Since the mass transfer efficiency at the bottom pool decreases with an increase of discharge (see Figure 4-5), the percentage of droplets' contribution increases with an increase of discharge.

The prediction model was then compared with field monitoring results conducted by Yang et al. (2020) in Edmonton, AB, Canada. In their study, Q was 1.26 m^3/s, T was 12.9 °C, the diameter of the drop structure was 1.2 m, and the two consecutive drop structures had h_d = 2.7 m and 5.2 m.

Their field results showed that C_{DO} increased from 1.2 to 3.2 mg/L after the two drop structures. Based on our simulation method presented above, by calculating separately for the two drop structures and add them together, $C_{DO,d}$ = 2.9 mg/L, which was 9% smaller than their field data. This demonstrates the reliability of the simulation method.

4.4. Conclusions

To the authors' best knowledge, the effects of falling jet forms on mass transfer have not been reported, and experimental studies of directly using H_2S in drop structures are limited. In this study, laboratory experiments on the mass transfer of O_2 and H_2S in sewage drop structures were conducted with two forms of falling sewage jet (free-falling and attached-falling) and in two sized drop structures (large and small). The mass transfer coefficient K_L and deficit ratio r were examined under different hydraulic conditions, i.e., with different drop height h_d, sewage flow rate Q and tailwater depth h_t. Based on laboratory results, mass transfer in drop structure prototypes was estimated. The main conclusions are as follows:

1. Nonlinear correlations between r and the hydraulic parameters (h_d, Q and h_t) were proposed for both falling jet scenarios, with good agreement (R^2 = 0.7 - 0.9) between the experimental and predicted results.
2. The drop height h_d is the key factor for the mass transfer in drop structures. r increased with an increase of h_d and a decrease of Q.
3. Bubbles, splashing droplets and turbulence at the tailwater surface are the main contributor to mass transfer. In the large drop structure, r of free-falling jet was 40% larger than that of the attached-falling jet; while in the small drop structure, r was almost the same.

4. $K_{L,H_2S}/K_{L,O_2} = 0.90 \pm 0.05$, suggesting that O_2 is another safe surrogate gas for studying H_2S mass transfer.
5. A flow chart and method for modeling mass transfer in drop structure prototypes was proposed. When $h_d < 3$ m, the pool surface makes the main contribution to the mass transfer; When $h_d > 6$ m, the falling droplets contributed for over 80% to the mass transfer. The jet surface's contribution is negligible. Furthermore, the mass transfer in drop structures is 3-13 times compared with that in gravity pipes.

For future research, it is suggested to further explore the effect of drop structure size on mass transfer and validate the experimental conclusions in real sewer drop structures. The ultimate goal is to better predict H_2S emission and O_2 mass transfer for the challenging issue of sewer odor and corrosion control faced by many municipalities on the globe.

4.5. Notation

The following symbols are used in this paper:

a = surface-area-to-volume ratio of the tailwater (m^{-1});

A = the surface area of the tailwater (m^2);

C = concentration of the dissolved gas in water (mg/L);

C_a = gas concentration in air (ppm);

c_d = drag coefficient of falling droplets;

C_d = gas concentration in the downstream sewage of the drop structure (mg/L);

$C_{DO,d}$ = DO centration in the downstream sewage of the drop structure (mg/L);

$C_{DO,u}$ = DO centration in the upstream sewage of the drop structure (mg/L);

C_s = saturation concentration of gas in the sewage (mg/L);

C_t = DO concentration at some time (mg/L);

C_u = gas concentration in the upstream sewage of the drop structure (mg/L);

d = droplet diameter (m);

D = molecular diffusivity of the gas in water (m^2/s);

f = percentage of H_2S in total sulfide;

H = Henry's Law constant;

h_d = jet falling height (m);

h_t = tailwater depth (m);

K_L = mass transfer coefficient (m/s);

pH = power of the hydrogen ion;

pK = equilibrium constant;

Q = flow rate (L/min);

r = deficit ratio;

Sc = Schmidt number, v/D;

T = temperature (℃ or K);

t = time of mass transfer (s);

U = droplet velocity (m/s);

V = the total water volume in the cylinder (m^3);

v_j = jet falling velocity at the pool surface;

v = kinematic viscosity of water (m^2/s);

ρ = density (kg/m^3), ρ_a = 1.2 kg/m^3, ρ_L = 998 kg/m^3.

Table 4-1 Summary of existing models for estimating deficit ratio of O_2 in drop structures with free-falling jet

Source	**Equation**	**Conditions**
Labocha et al. (1996)	$\ln r = 0.0030 h_d^{1.08} Q^{0.22}$	h_d < 50 cm Q < 37 L/min
Rahmé et al. (1997)	$\ln r = 1.048 h_d^{0.765} Q^{-0.140} h_t^{-0.071}$	h_d < 1.67 m, Q < 267 L/min
Matias et al. (2017b)	$\ln r = 0.525 h_d^{0.756} Q^{-0.796} h_t^{0.360}$	h_d < 1.2 m, Q = 0.09, 0.18 L/s
This work	$\ln r = (0.97 \sim 1.25) h_d^{0.783 \sim 0.876} Q^{-0.430 \sim -0.645} h_t^{0.347 \sim 0.827}$ $\ln r = 4.61 \times 10^{-5} \left(\frac{Q/A}{\sqrt{g h_d}} \right)^{-1.101}$	h_d < 1.5 m, Q = 0.9-1.8 L/min

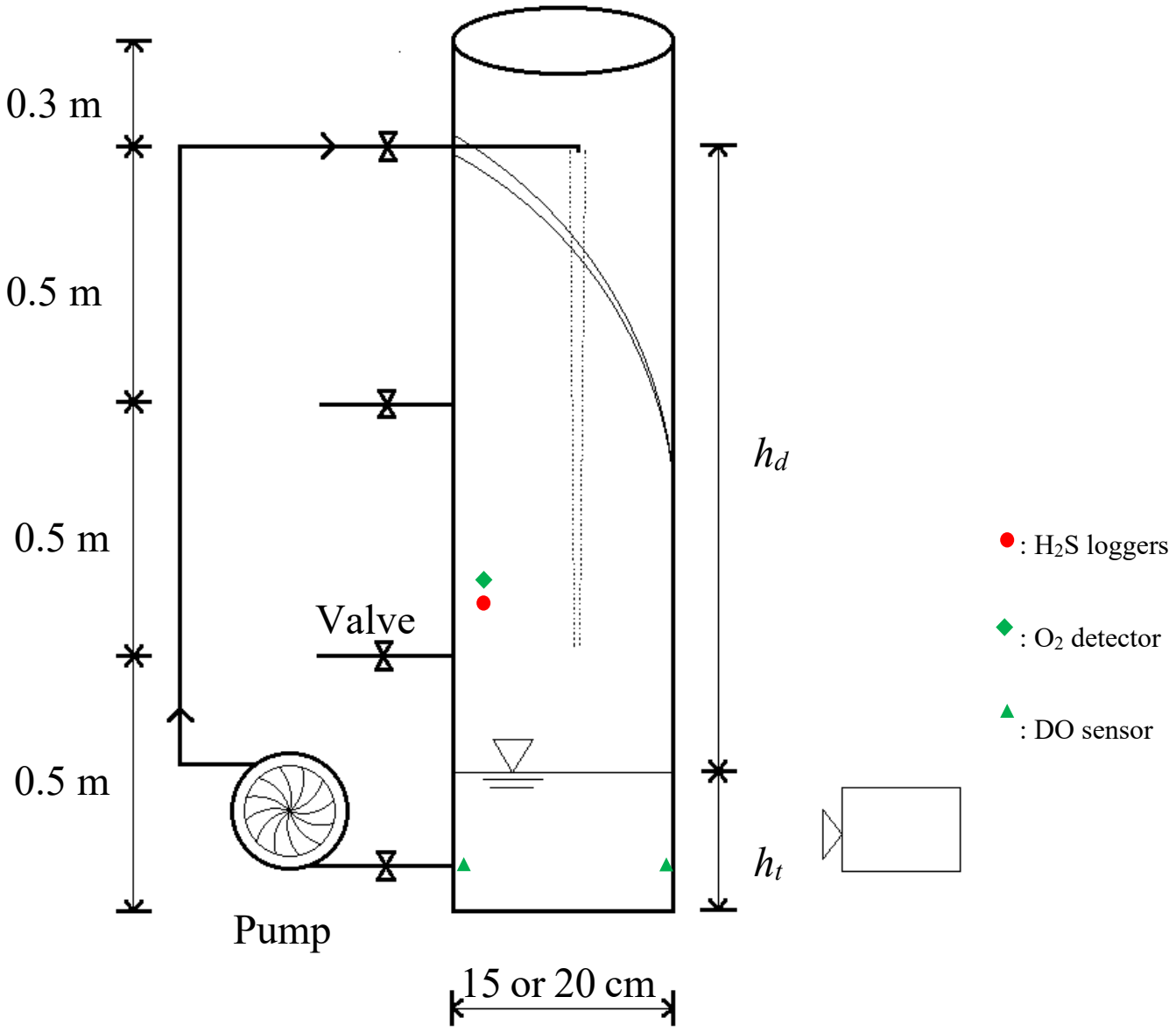

Figure 4-1 Schematic of the experimental setup.

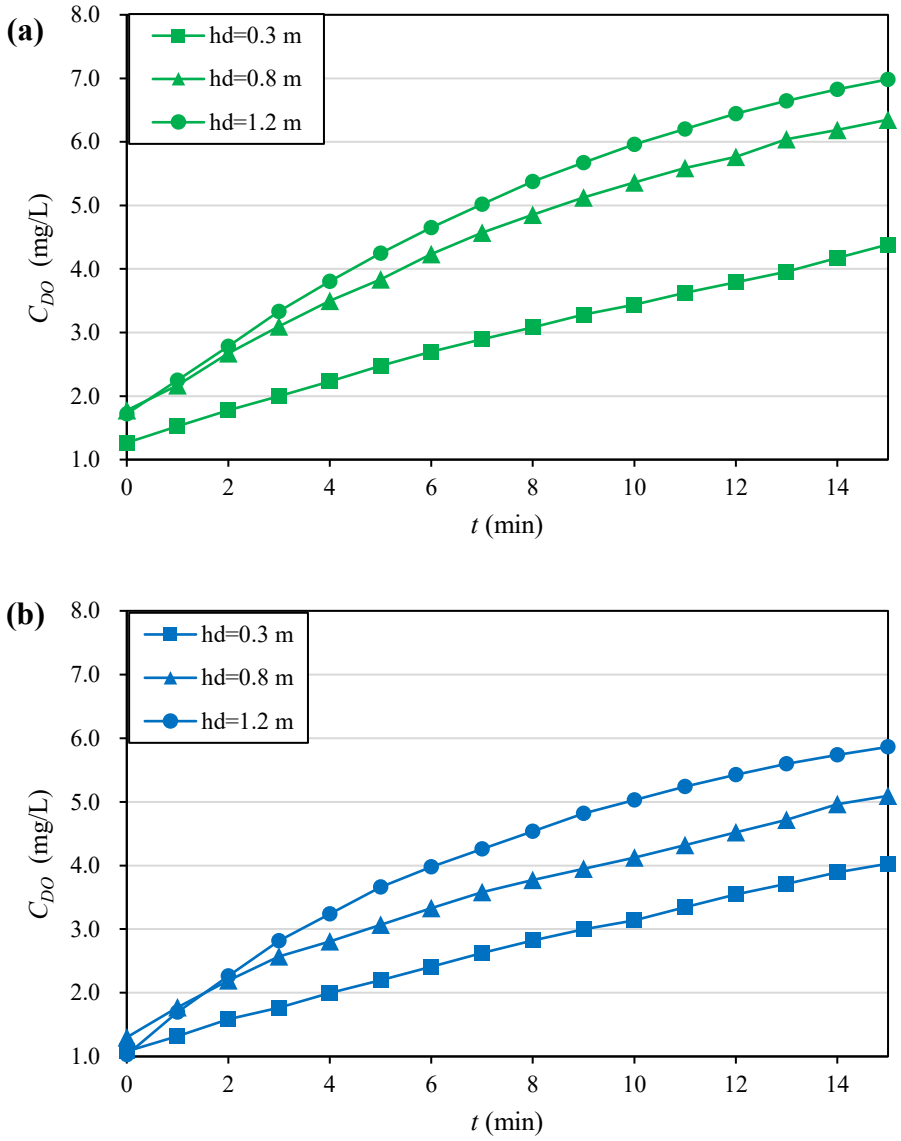

Figure 4-2 An example of variation of the DO concentration (C_{DO}) with time for free-falling jet in the (a) large and (b) drop structures. Experimental condition: h_t = 0.2 m; Q = 1.7 L/min

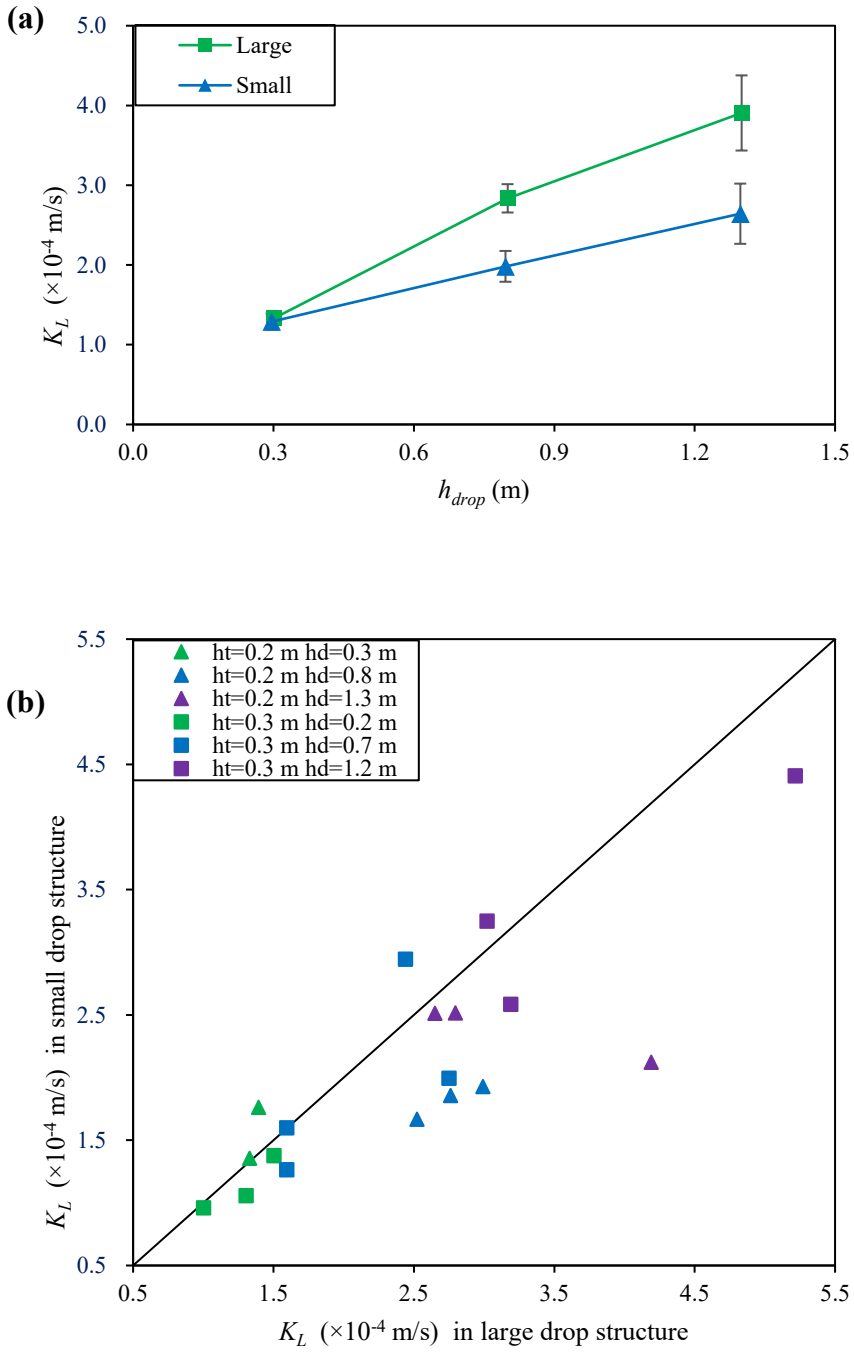

Figure 4-3 (a) An example of K_L of O_2 with free-falling jet in drop structures. Experimental condition: h_t = 0.2 m, Q = 1.7 L/min. In the legend, "large" means large drop structure, and "small" means small drop structure. (b) Comparison of K_L values between the large and small drop structures. Q = 0.9-1.8 L/min.

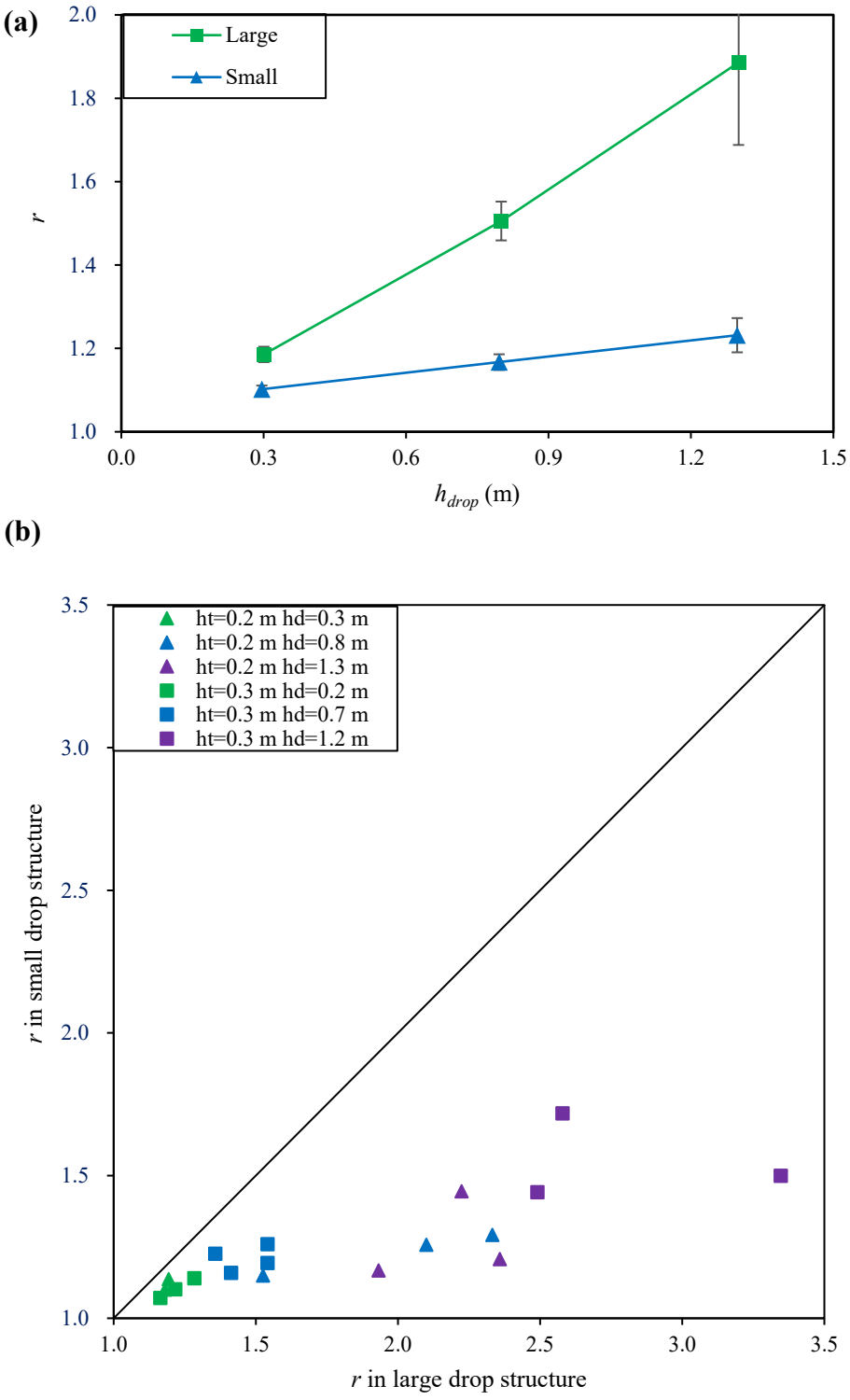

Figure 4-4 (a) An example of r for O_2 mass transfer with free-falling jet in drop structures. Experimental condition: h_t = 0.2 m, Q = 1.7 L/min. (b) The comparison of r values between the large and small drop structures. Q = 0.9-1.8 L/min.

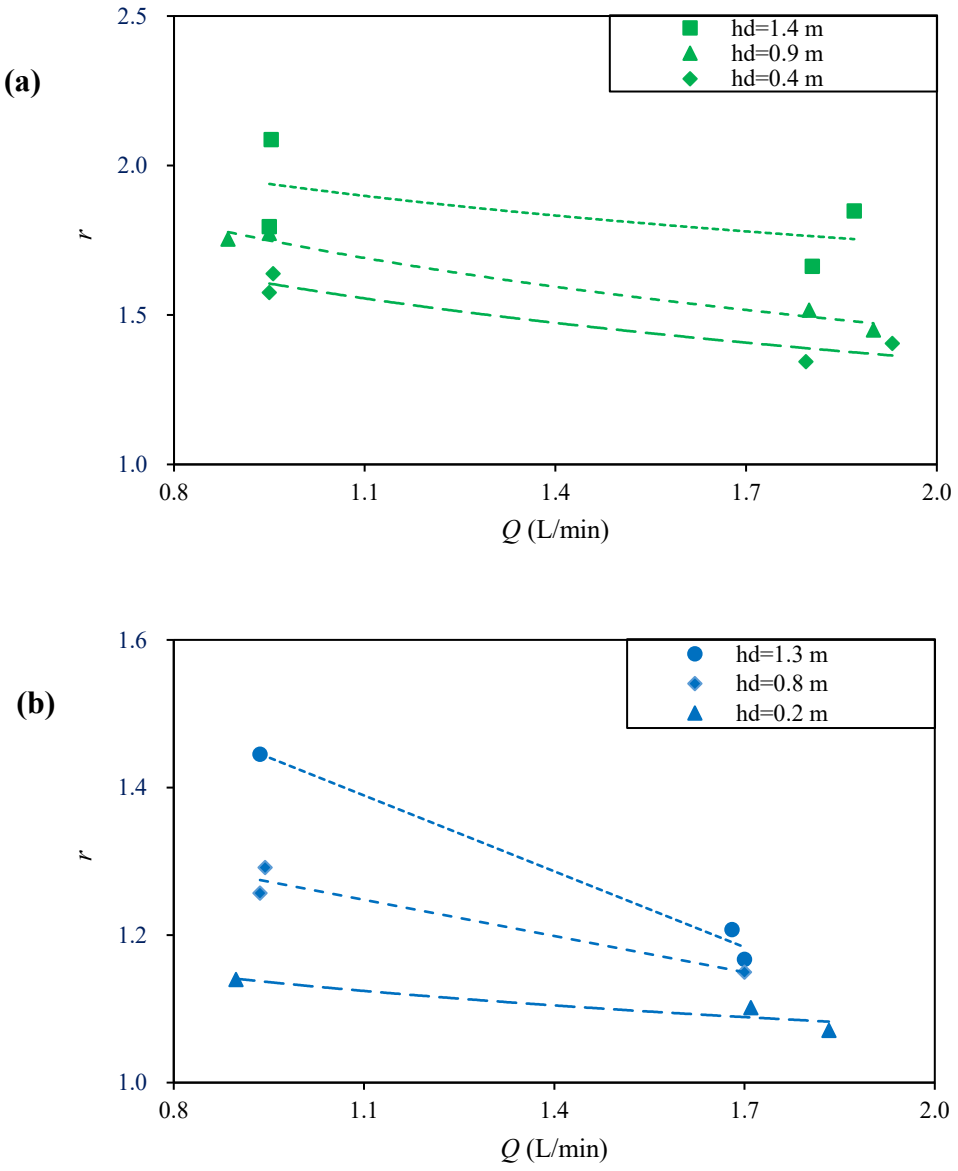

Figure 4-5 An example of variation of r with Q for free-falling jet in the (a) large and (b) small drop structures. In the large drop structure, h_t =0.1-0.3 m; in the small drop structure, h_t =0.2-0.3 m. The trend lines were logarithmically fitted.

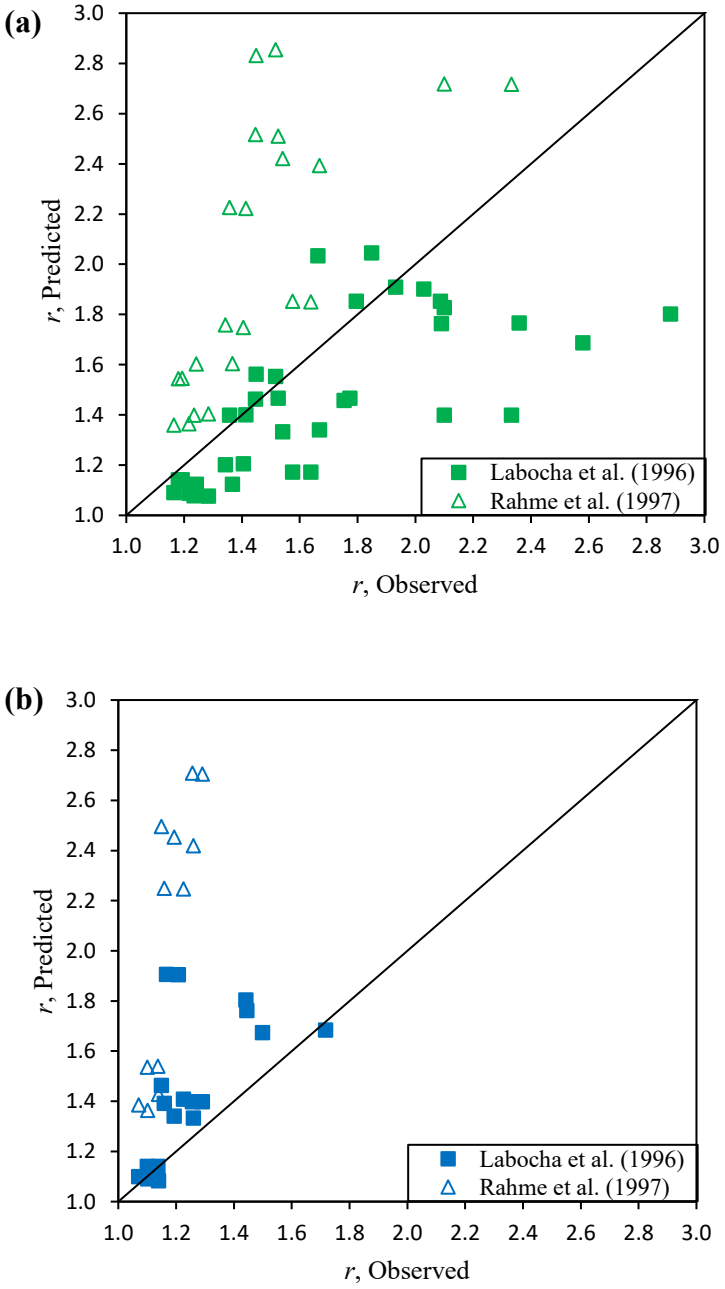

Figure 4-6 Comparison of observed r values in this work with the predicted values from the equations of Labocha et al. (1996) and Rahmé et al. (1997) for (a) large and (b) small drop structures.

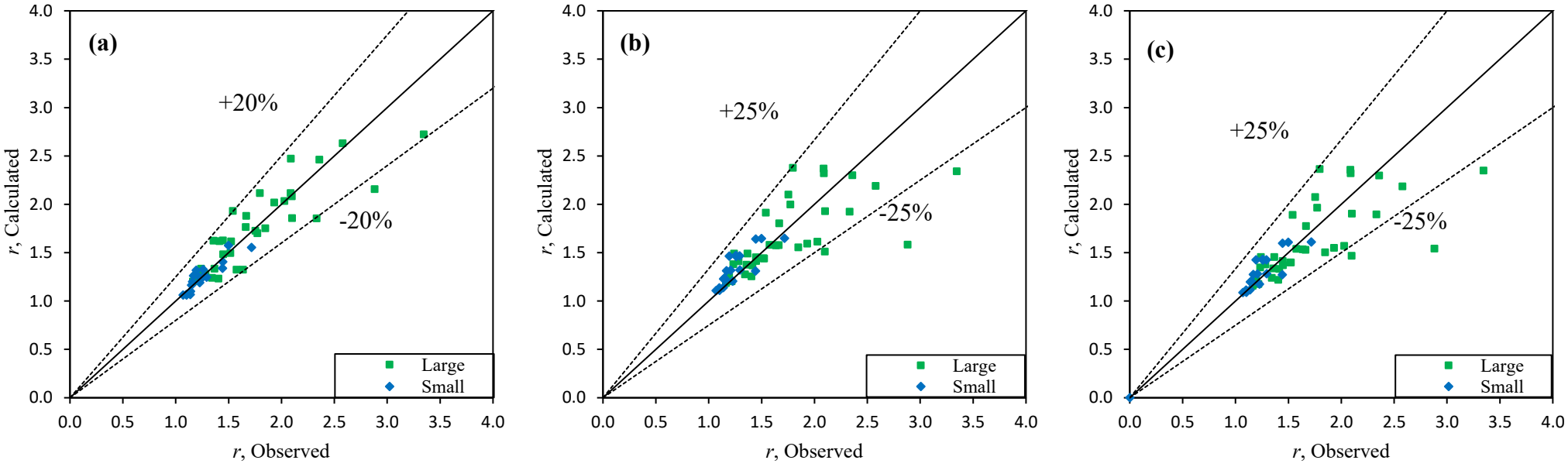

Figure 4-7 Comparison of observed and predicted *r* values for free-falling jet in drop structures. The predictions use (a) Eq. (4-13); (b) Eq. (4-14); and (c) Eq. (4-15).

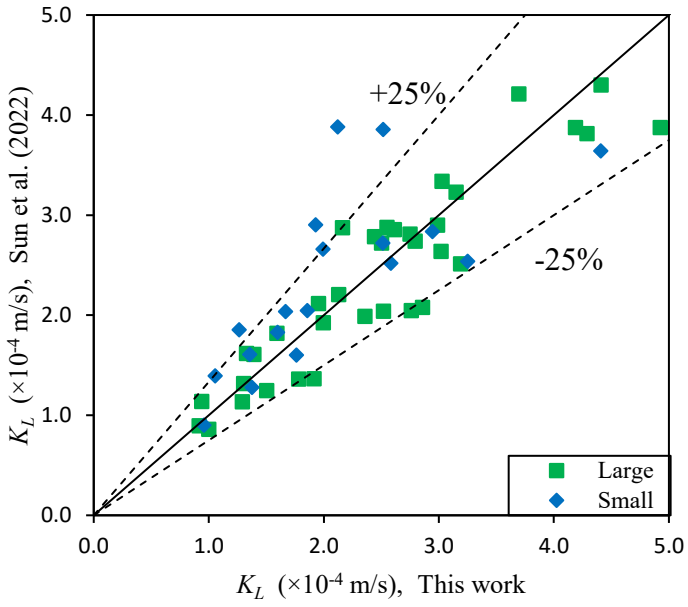

Figure 4-8 Comparison of K_L for O_2 between the experiment results of this work and the prediction of Sun et al. (2022).

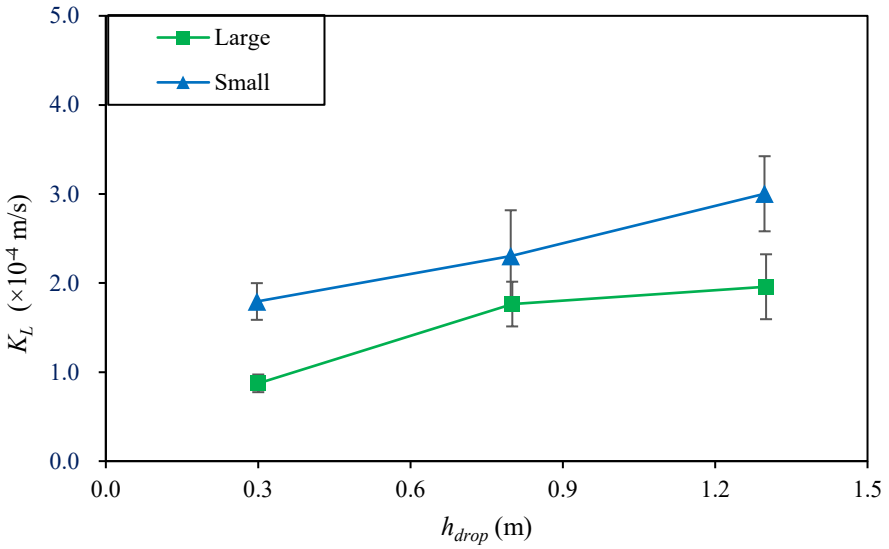

Figure 4-9 An example of K_L for O_2 for the attached-falling jet in drop structures. Experimental condition: h_t = 0.2 m, Q = 1.7 L/min.

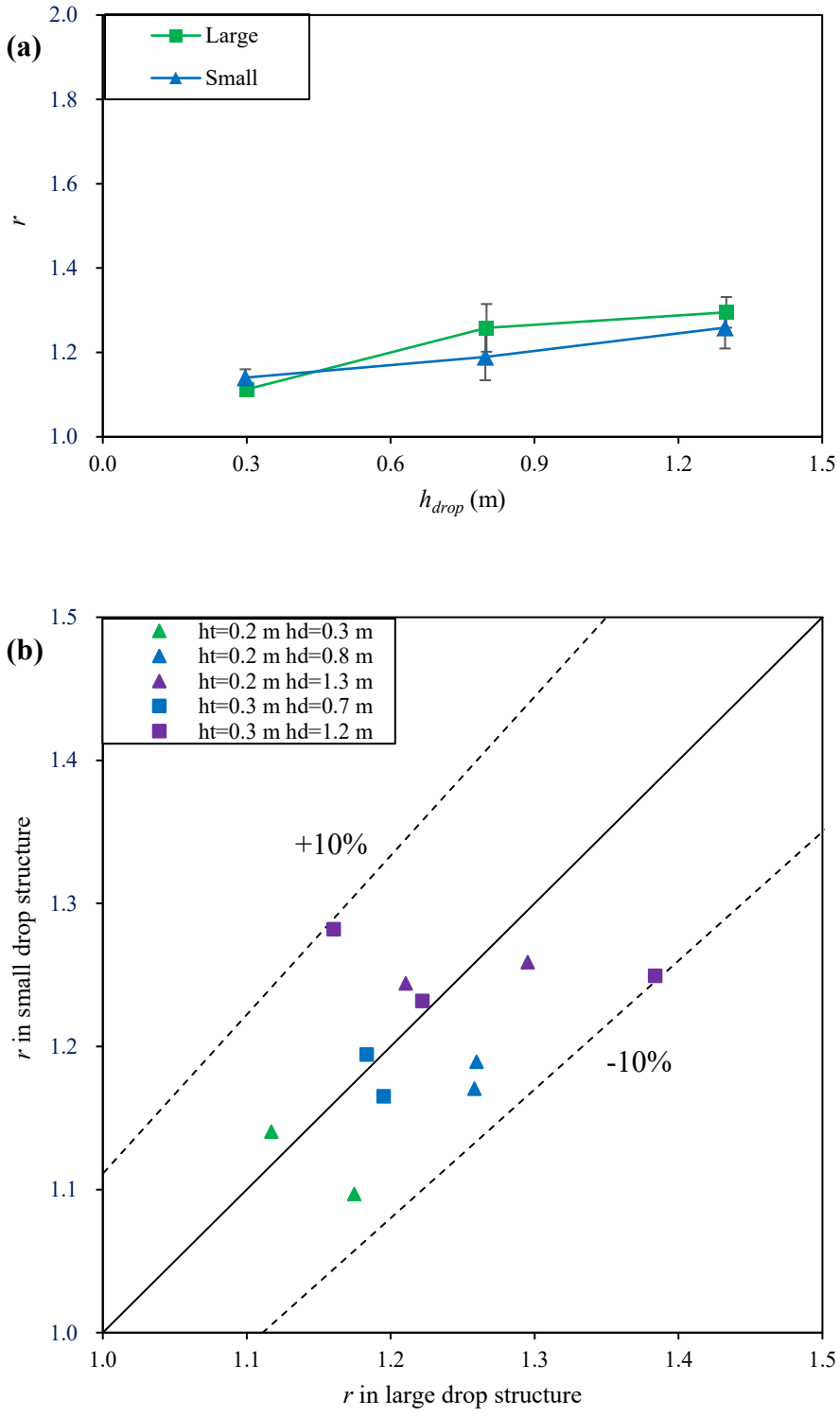

Figure 4-10 (a) An example of r of O_2 with the attached-falling jet under the experimental conditions: h_t = 0.2 m, Q = 1.7 L/min. (b) The comparison of r values between the large and small drop structures.

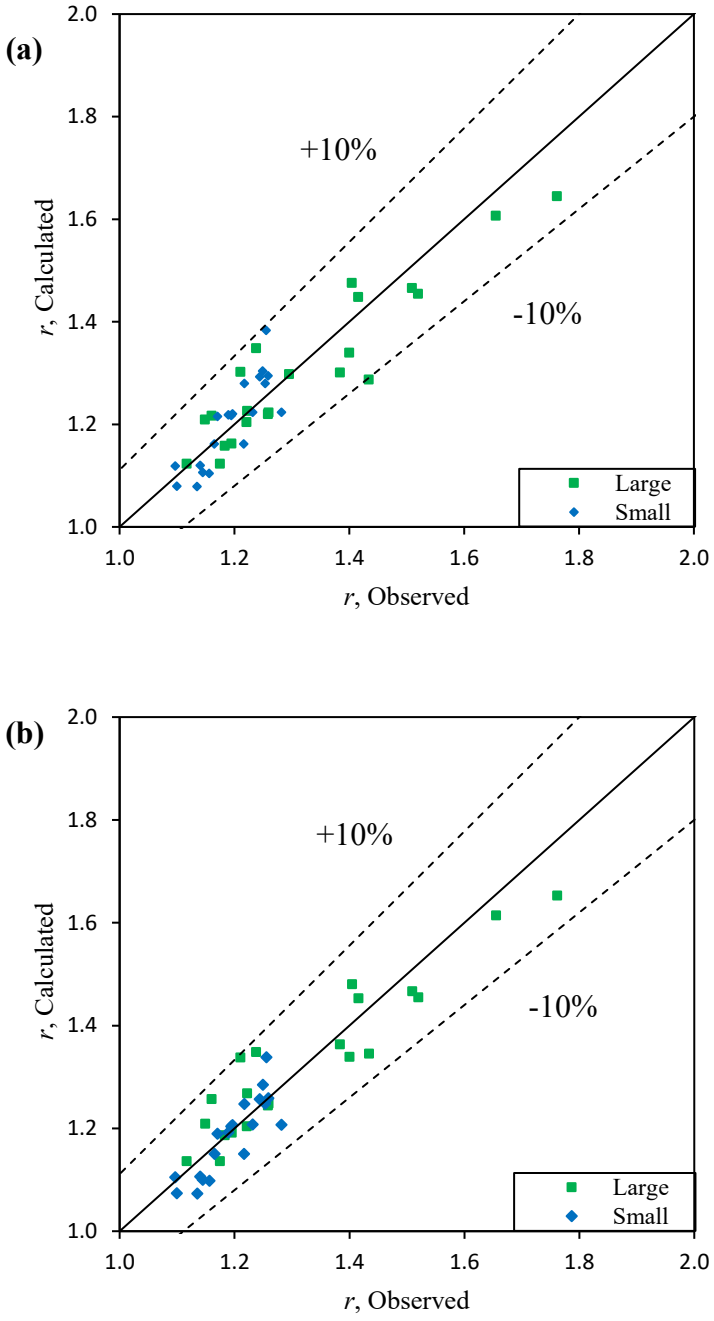

Figure 4-11 Comparison of observed and predicted r values for the attached-falling jet in drop structures. The predictions use (a) Eq. (4-16); and (b) Eq. (4-17).

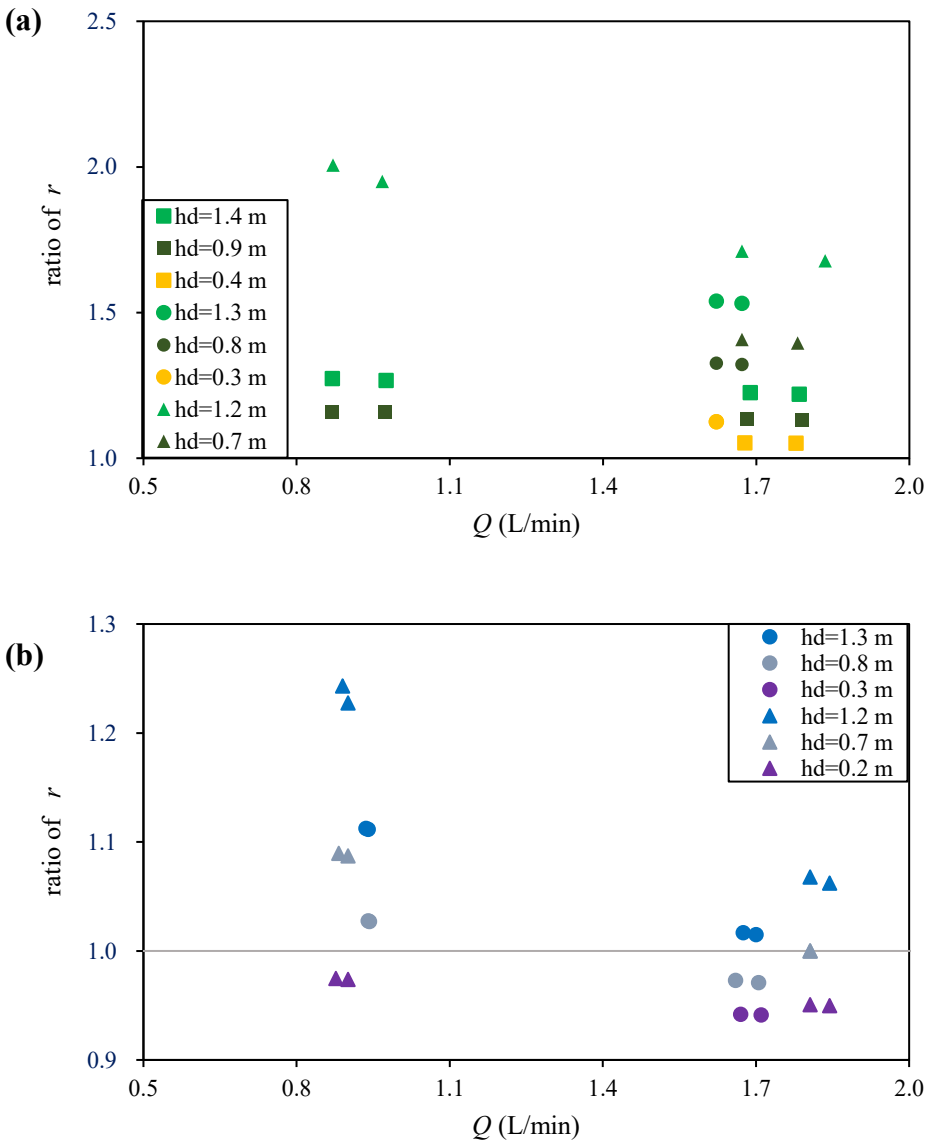

Figure 4-12 The r ratios of the free-falling to attached-falling jet in (a) large and (b) small drop structures. Squares are the data with h_t = 0.1 m, circles with h_t = 0.2 m and triangles with h_t = 0.3 m.

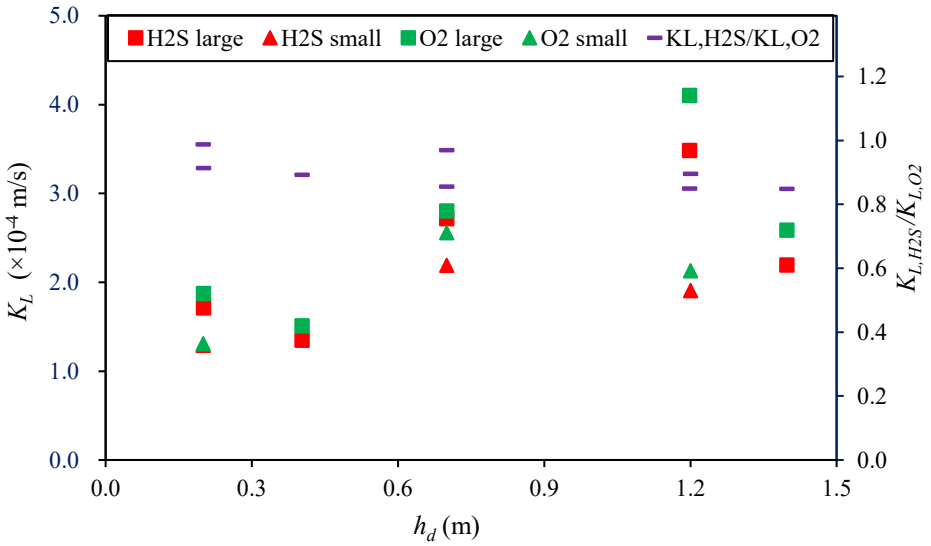

Figure 4-13 Comparison of K_L for H_2S and O_2 in drop structures. In the legend, "large" means large drop structure, and "small" means small drop structure.

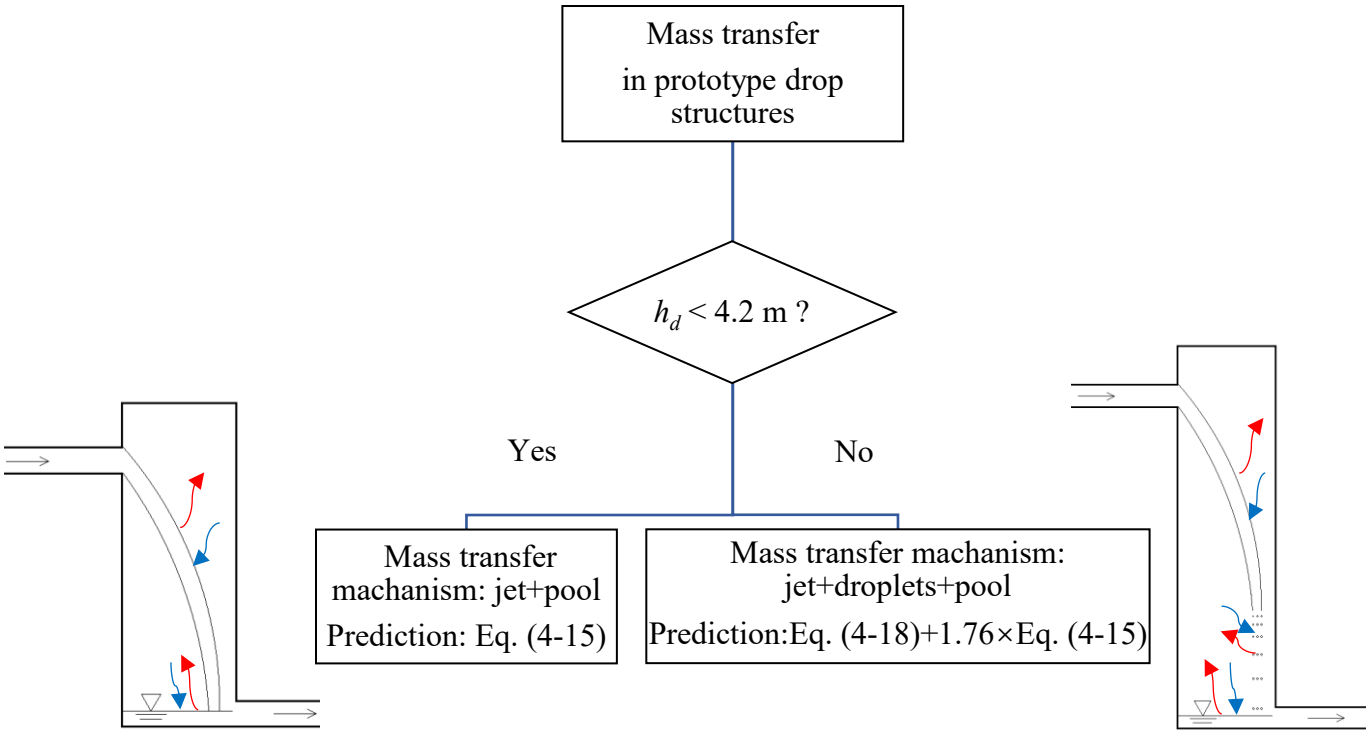

Figure 4-14 Calculation of mass transfer in drop structure prototypes. Red arrows mean H_2S emission, and blue arrows mean O_2 absorption.

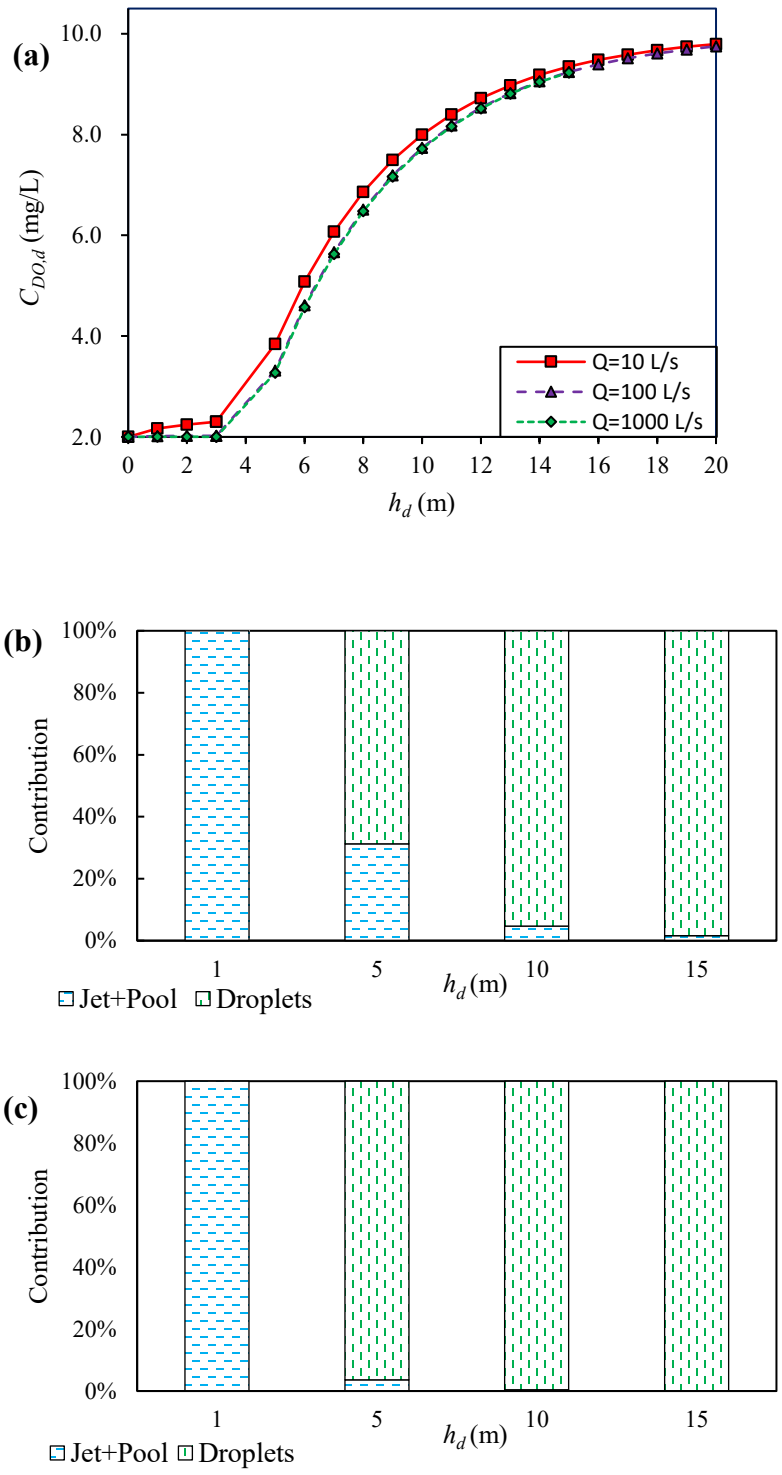

Figure 4-15 (a) Predicted DO concentration in the downstream of a prototype drop structure; Contribution of different mechanisms when (b) Q = 10 L/s and (c) Q = 100 L/s.

5. Field Study of Wastewater Quality and Emission of H_2S in a Sanitary Sewer Network

5.1. Introduction

Hydrogen sulfide (H_2S) is the primary cause for sewer odor and can be oxidised to sulfuric acid (H_2SO_4) which corrodes sewer pipes (Hvitved-Jacobsen et al. 2013). Understanding the generation and transport of H_2S in sewer networks is of great concerns to worldwide municipalities. The study has been carried out in countries like USA (US EPA 1974), Denmark (Nielsen et al. 2008), Australia (Jiang et al. 2013a) and Portugal (Matias et al. 2017a).

H_2S was generated under the anaerobic condition by sulfate-reducing bacteria (SRB) in sewer pipes facilitates (Hvitved-Jacobsen et al. 2013). SRB growth relies on the organic matter in the wastewater. A model, named WATS (Wastewater Aerobic/anaerobic Transformations in Sewers) was developed at Aalborg University, Denmark to analysis the sulfide generation rate based on relative wastewater characters, such as organic matters, biofilm, dissolved oxygen (DO), temperature (Hvitved-Jacobsen et al. 2013). After sulfide is generated and dissolved in wastewater, pH affects its chemical equilibrium form. At 20 ℃, the molecular form of sulfide, H_2S, accounted for 92% and 11% of total sulfide when pH = 6 and 8, respectively. Only the molecular form of sulfide could emits from wastewater to air (Zhang et al. 2008). There are several chemical and physical factors affecting its emission rate, like pH, temperature, turbulence intensity, wastewater constituents and characteristics of the sewer air (Yongsiri et al. 2004a). Drop structures in sewer systems are hot spots of H_2S emissions as the wastewater is under highly turbulent conditions (Matias et al. 2017b). The H_2S emission could occur at jet surface, falling droplet surface, and

bottom pool (due to turbulent water surface, entrained bubbles, induced splashing droplets). Moreover, drop structures have been identified as an important factor in ventilation, which brings H_2S from sewers to the atmosphere above ground to cause sewer odor (Guo et al. 2018).

In Edmonton, Alberta, Canada, the sewer odor problem is a city-wide concern. In Zhang et al. 2016, Guo et al. 2018 and Zhang et al. 2020, sewer air flow induced by drop structures was investigated. In Guo et al. 2018 and Yang et al. 2019, 2020, H_2S concentration in drop structures were measured, which shows that drop structures have big effect on emission of H_2S. However, the previous studies are not enough for quantifying the mass transfer of H_2S in field drop structures. Therefore, performing field work is necessary for estimating H_2S emission and addressing the sewer odor and corrosion issue.

The density map of complaints in Edmonton is shown in Figure 5-1. In the residential neighbourhood of the Glenora area (blue circle in Figure 5-1), the complaint density is high. The sewer trunk in Glenora area is in the downstream of the west area of the city, therefore it collects the wastewater from the west neighborhoods. Based on the previous field measurement data, the gaseous H_2S concentration had reached 400 - 500 ppm in the first discharge manhole of the Big Lake Pump Station (Yang et al. 2022). This manhole is in the upstream of the sewer system and the distance to Glenora is over 10 km. Its H_2S contribution to Glenora was unknown. Also, there are some drop structures in the sewers from the Big Lake Pump Station to Glenora, which could be hot spots of H_2S emission. Additionally, a number of pump stations in the area contribute to the trunk sewer leading to the Glenora area. Therefore, the west area of Edmonton from the Big Lake Pump Station to Glenora was chosen as the study area to examine the generation (sources) and transport of H_2S in the area.

The purposes of this study are: 1) to analyze the general wastewater qualities and H_2S generation in the sewers; 2) to determine the H_2S distribution of liquid and air phases in the trunk and laterals; 3) to identify the H_2S contribution to the Glenora area from the Big Lake Pump Station and the main laterals; 4) to investigate H_2S emission in sewer drop structures.

5.2. Methodology

5.2.1. The study area

The field work was conducted along the trunk and its laterals from the Big Lake to Glenora area, which covers about 1/6 of the city area (Figure 5-2). The upstream of the trunk is the Big Lake Pump Station. A 5.6 km-long pressurized force main connects the pump station and its first discharge manhole (T1, MH 461065). Because of the long retention time (~32 h) and the anaerobic condition, significant amount of H_2S was generated in the force main and gaseous H_2S concentration reached 400-500 ppm in T1 (Yang et al. 2022). The total distance of the trunk from T1 to T13 is 10.1 km, with sizes varying from 525 to 1950 mm and slope varying from 0.1-10%. T4, T5, and T7 are the three drop structures with a drop height of 1.9, 1.0, and 8.1 m, respectively. T5 is a connective junction which is not accessible. Another drop structure of 3.1 m is located between T9 and T10, which is also not accessible. There are 7 main laterals chosen for the study for their potential of large discharge or high H_2S. L3-1 and L3-2 are the manholes on the laterals connecting to T3. L5, L8, L9, L10 and L13 are the MHs on the laterals connecting to T5, T8, T9, T10 and T13, respectively, and in the upstream of these laterals there are a number of pump stations. The mean flow rate from upstream to downstream is from 0.008 - 0.570 m^3/s, which was obtained from the simulation of Mike Urban. The details are shown in Table 5-1 and Figure 5-3.

5.2.2. Field measurements

Two rounds of field measurements were conducted in this area on October 4 - 19 and November 5 - 23, 2021. In the first round, wastewater samples were collected from manholes with bucket in the trunk (T2, T3, T4, T6, T7, T11 and T12) from 11:10 to 15:27 on Oct. 4th, 2021 (Table 5-2). In the second round, water samples were obtained in the laterals from 10:42 to 14:48 on Nov. 5 for L3-1, L3-2, L9, L10 and L13, and from 13:52 to 14:39 on Nov. 10 for L5 and L8 (Table 5-3). H_2S concentration at the sewer headspace of the trunk and laterals were monitored continuously by Odalog (App-Tek, Queensland, Australia) for around two weeks after sampling wastewater. DO, pH and temperature (*T*) of the water samples were measured on site by portable pH sensor (EC500, Extech) and DO sensor (LDO 101, Hach).

All the field water samples were stored in coolers with ice bags, transported back to the laboratory within the same day, and kept refrigerated until analysis was done. Water qualities were analyzed with the following parameters: the total sulfide (TS) and dissolved sulfide (DS), sulfate (SO_4^{2-}), total nitrogen (TN), ammonia (NH_4^+), nitrate (NO_3^-), total phosphorus (TP), total suspended solid (TSS) and volatile suspended solid (VSS), total COD (TCOD) and dissolved COD (DCOD), and volatile fatty acid (VFA).

TS and DS were analyzed according to the methylene blue method (APHA et al. 2017). First, suspended sulfide was separated by adding aluminum chloride to the sample. The reaction will form aluminum hydroxide flocs that trap floated sulfide. After the flocs settle down, the dissolved sulfide in the solution can be measured in the supernatant. Total sulfide of the sample was preserved by adding 2M zinc acetate and 6N sodium hydroxide. SO_4^{2-}, TN, NH_4^+, NO_3^-, TP, TCOD and DCOD in wastewater samples were analyzed according to Standard Methods (APHA et al.

2017) in our lab. Samples were also sent to a commercial lab (Caro Analysis) for analysis of TSS, VSS and VFA.

5.3. Field Work Results

5.3.1. Wastewater qualities

Nitrogen (N) can be measured in terms of total nitrogen (TN), ammonia (NH_4^+) and nitrate (NO_3^-). Phosphorus (P) can be determined by the concentration of total phosphorus (TP). High TSS and VSS indicate high solids contents in the wastewater. COD reflects the oxygen demand of organic content and represents the carbon source for microbes in wastewater, which is incorporated into the empirical formula of sewer biofilm and discussed in Section 5.3.2.

In the trunk, the wastewater quality parameters was stable (Table 5-2). TN, NH_4^+, and NO_3^- ranged 67.4 - 97.3 mg N/L, 39.4 - 58.1 mg N/L and 0.82 - 1.05 mg N/L. TP was 22.4 - 30.0 mg/L. TSS, VSS, TCOD and DCOD were 195 - 336 mg/L, 168 - 212 mg/L, 611 - 895mg/L and 234 - 320 mg/L. pH remained mostly neutral. The measured water qualities from the trunk were close to the previous fieldwork results in Edmonton reported by Yang et al. (2019), showing typical common values of municipal wastewater.

In the laterals, the range of wastewater quality parameters were larger than those in the trunk (Table 5-3). TN, NH_4^+ and NO_3^- ranged 49.5 - 163.3 mg N/L, 20.2 - 74.2 mg N/L and 0.68 - 2.64 mg N/L. The nitrogen concentration in the laterals peaked at the location L5. TP was 12.7 - 59.4 mg/L. TSS, VSS and COD peaked at location L5 with maximum values of 3510, 2950 and 5225 mg/L, respectively. It seems that all physical and chemical parameters of water qualities peaked at this location. Moreover, TCOD and DCOD also showed spikes at L9 and L8. The high COD

concentration at these locations implicated that higher microbial growth could be happening within the pipeline that connects L5, L8, and L9.

Because this field work focused on the domestic wastewater, taking the ratios of NH_4^+/TN, VSS/TSS, and DCOD/TCOD would simplify the data presentation and show differences across the locations in relation to the wastewater quality parameters. In the first round of fieldwork, NH_4^+/TN suddenly increased at T4-T6, and VSS/TSS decreased from T4-T6 [Figure 5-4(a)]. This might be due to the flow of wastewater along the three kilometers pipe and additional laterals attached. All of which could dilute the total nitrogen content in the wastewater and wash the bacteria slimes off the pipes. NH_4^+/TN decreased at T6-T7 is due to the increase of total nitrogen content. T6 and T7 were the upstream and downstream of a drop structure, VSS/TSS and DCOD/TCOD were slightly increased. The reason could be the drop structure, where additional biofilms/biosolid from the pipe walls were detached due to splashing and diluting effect. VSS/TSS ratio also increased from T7-T11, where other laterals such as L8, L9 and L10 were connected to the main trunk.

In the second round of field work [Figure 5-4(b)], the variation of water content was mainly reflected in the ratio of DCOD/TCOD and NH_4^+/TN. The DCOD/TCOD of locations L9 and L8 were higher, being 0.57 and 0.56, respectively. The results could be due to the merging effects from the wastewater of other laterals upstream and downstream. The highest NH_4^+/TN occurred at L13, which is 0.94 and could be from the discharge of the surrounding neighborhood and a lateral from south area.

VFA is indicators of decomposition of organic matter and the gases such as methane and carbon dioxide that may be produced. The main components of VFA are acetic acid, propionic acid, and

butyric acid. It is also used along with COD for determining the organic loading rates and reflecting microbial growth potential. The VFA also had shown different trends in each fieldwork. The VFA content slowly decreased from 106 to 81 mg/L across the trunk in Figure 5-5(a). However, there were no trends of VFA that can be observed in the lateral samples of second fieldwork except for two significant spikes at locations of L5 and L9 [as shown in Figure 5-5(b)], whose origins were pump station PS 525162 (in Westview Village) and pump station PS 254801 (in Norwester Industrial). The spikes could be due to the surge of wastewater or the slough from sewer biofilm. Additionally, The VFA only represents a certain amount of organic nutrients in the wastewater that microbes can utilize, while DCOD implies the total dissolved organic matters. Therefore, observing the organic loading rate of the VFA/DCOD ratio would indicate the organic differences within the wastewater and show a clearer understanding of the wastewater characteristic. The absolute values of these two parameters showed the same phenomenon as other water quality parameters: VFA/DCOD contents were more stable in the trunk than in the laterals (Table 5-2 and Table 5-3), which was reflected in the sulfide production rates in the next section.

The water qualities of the two rounds of fieldworks offered a general overview of the wastewater characteristic in the trunk and laterals. It is noticed that the wastewater characteristic in the trunk was more stable than laterals. The phenomena in laterals could be due to the pump stations upstream, connected joints, or branched pipelines and the inflow from the surrounding neighborhoods interfering with the wastewater contents.

5.3.2. Sulfide generations by SRB in sewer biofilms

Sulfur compounds are presented in high concentrations in municipal sewage. The increased sulfide concentrations are due to the digestion of easily biodegradable organic compounds and sulfur

compounds. Sulfates are converted to sulfides by SRB in the sewer biofilms under the anaerobic condition (Gutierrez et al. 2009). SRB gain energy by oxidising organic nutrients and using sulfate compounds as terminal electron acceptors (Cord-Ruwisch et al. 1987). The organic compounds were both the carbon and energy sources. The reaction of SRB can be viewed as:

$$SO_4^{2-} + \text{organic matter} = HS^- + H_2O + HCO_3^- \quad (5\text{-}1)$$

To effectively estimate sulfide generation in a sewer system, a prediction model of WATS for the sulfide production in sewer biofilm was described by Hvitved-Jacobsen et al. (2013). The equation shows the sulfide formation rate from the surface of the sewer biofilm to the wastewater phase using readily biodegradable organic matter, as listed below:

$$r_a = k\sqrt{S_F + S_A + X_{S1}}\,\frac{K_{DO}}{C_{DO} + K_{DO}}\,\frac{1}{R}\,1.03^{(T-20)} \quad (5\text{-}2)$$

where r_a represents the sulfide formation rate from biofilm surface (mg/L/h), k is the rate constant for sulfide formation ($g^{0.5}/m^{0.5}/h$), S_F is the fermentable substrate concentration, S_A represents the fermentable product concentration (i.e. VFA), X_{S1} is the fast hydrolysable substrate concentration, C_{DO} represents the DO concentration in wastewater, K_{DO} represents the saturation constant for DO, R is the hydraulic radius in pipes, and T is the wastewater temperature (°C).

Furthermore, as seen from the sulfide formation in biofilm Eq. (5-1), all organic substrates and products are fractions of TCOD, which equals the sum of fermentable substrate (S_F), fermentable product (S_A), heterotrophic biomass in water phase (X_{HW}), and fast (X_{S1}) and slow hydrolysable substrate (X_{S2}):

$$\text{TCOD} = S_F + S_A + X_{HW} + X_{S1} + X_{S2} \quad (5\text{-}3)$$

The term, $S_F + S_A$, can be viewed as one entity- biodegradable fraction, which accounted 23.4 to 28% of TCOD in domestic wastewater, according to the literature (Kappeler et al. 1992; Makinia 2006; Drewnowski et al. 2020). In our case, by taking the average of the abovementioned percentages, we assumed the biodegradable fraction to be 25.7% of the TCOD measured from the fieldwork. Thus, S_F can be calculated by knowing the value of the biodegradable fraction of TCOD followed by subtracting S_A (VFA). X_{HW} values from fieldwork investigation were approximately by VSS. The term ($X_{S1} + X_{S2}$) was calculated based on TCOD – ($S_F + S_A$) – X_{Hw}. Due to the limitation in the testing environment, we assumed that X_{S1} and X_{S2} were 40% and 60% out of the total hydrolysable substrate ($X_{S1} + X_{S2}$), as the slow hydrolysable substrate (X_{S2}) is always in higher concentration when compared with the fast X_{S1} because of its biological properties (Hvitved-Jacobsen et al. 2013; Drewnowski et al. 2020). The estimated values of S_F and X_{S1} and X_{S2} are listed in Table 5-2 and 5-3 for both fieldworks.

As shown in Table 5-4, in the trunk of T2-T3, T3-T4, T4-T5, T7-T8 and T11-T12, r_a was from 0.1 - 0.6 mg/L/h, with average of 0.3 mg/L/h; while r_a of other parts of the trunk cannot be simulated without relevant data. r_a was also simulated in the laterals of L5-T5, L9-T9 and L10-T10, as their length was over 0.8 km. r_a in L5-T5 reached 3.6 mg/L/h, which was very high because of high concentration of COD and low concentration of DO. In L9-T9 and L10-T10, r_a was 0.1 and 0.3 mg/L/h. By multiplying r_a with retention time Δt, sulfide generation rate transformed to the water phase ΔC_s was calculated:

$$\Delta C_S = r_a \times \Delta t \tag{5-4}$$

where Δt = water volume V divided by flow rate Q. ΔC_s in T2-T3 was 0.8 mg/L, as the high retention time (1.4 h); ΔC_s in T4-T5 and L5-T5 was 0.4 and 0.6 mg/L, respectively. In other pipes,

it was less than 0.2 mg/L (see Table 5-4). Therefore, as shown in Eqs. (5-2) and (5-4), sulfide generation is related to COD, DO concentration, water depth and retention time. Higher concentration of COD, lower concentration of DO, more water depth and retention time could increase sulfide generation; as opposite, lower concentration of COD, higher concentration of DO, less water depth and retention time could decrease sulfide generation.

The reasons for the sulfide concentration variation between two manholes could be sulfide generation, dilution, and other system changes (including H_2S emission and oxidation). The mass balance of sulfide between two manholes is described with the following equation:

$$F_u + F_G = F_d + \Delta F \tag{5-5}$$

where F_u is the sulfide flux from upstream manhole, F_G is the sulfide flux of generation in biofilms, F_d is the sulfide flux to downstream manhole, and ΔF is the system change.

Here Pipes T2-T3 and T11-T12 are taken as examples to study the mass balance of sulfide, as TS in upstream and downstream were both measured. At T2, TS was 9.7 mg/L; at T3, TS was 1.6 mg/L after the dilution of L3-1 and L3-2. The system change in T2-T3: $\Delta F = F_u + F_G - F_d = (C_{TS,T2}Q_{T2}) + (\Delta C_s Q_{T2}) - (C_{TS,T3}Q_{T3} - C_{TS,L3\text{-}1}Q_{L3\text{-}1} - C_{TS,L3\text{-}2}Q_{L3\text{-}2}) = (9.7 \times 51) + (0.8 \times 51) - (1.6 \times 114 - 0.6 \times 3.4 - 0.5 \times 59) = 495 + 41 - 149 = 387$ g S/h. $\Delta F/(F_u + F_G) = 72\%$, which means that in T2-T3 the system change, including H_2S emission and oxidation, accounted for 72% of sulfide flux, and 28% of sulfide went downstream. For T11-T12, the flow rate in the lateral of T12 could be neglectable as they were about 4 m^3/h (< 0.1%). In T11-T12, the system change accounted for 24% of sulfide flux, and 76% of sulfide went downstream. In T2-T3, TS was 9.6 mg/L, much high than 3.1 mg/L in T11-T12. Higher sulfide concentration triggers high percentage of H_2S emission, which explains that less percentage of sulfide would go to downstream.

5.3.3. Sulfide and DO levels in the pipes

In the study area, TS varied from 0.5 - 9.7 mg/L and DS was from 0.5 - 9.2 mg/L (Table 5-2 and Table 5-3). The average ratio of DS/TS was 0.8 with the only exemption that DS/TS was 0.3 in L5. Figure 5-6 shows the variation TS and DS in the trunk. Both TS and DS in T2 were always the largest because T2 was closed to the force main, which is the main source of sulfide. TS and DS decreased heavily in T2-T3 from 9.7 to 1.6 and 9.2 to 1.5 mg/L (shown in Figure 5-6 and Table 5-2), respectively, because of H_2S emission and the merging and dilution effect of wastewater from laterals of L3-1 and L3-2, whose TS and DS was around 0.5 mg/L. TS and DS decreased to the lowest in T7 by dilution of L5 (DS = 0.7 mg S/L) and emission on the large drop structure T6-T7. It then increased in T11, as T11 was in the downstream of L10. In L10, DS concentration was as high as 3.3 mg S/L (Table 5-3) and the flow rate in L10 accounted for 50% of the trunk in the downstream (Table 5-1). L8 also had high DS concentration, but as the flow rate was so small (0.0002 m^3/s in Table 5-1), its contribution (0.5 mg S/s in Table 5-3) was neglected. In the other lateral manholes, DS < 1 ppm. Therefore, L10 is the main source of sulfide in the trunk of downstream, whose DS flux accounted for 56% in T12. Although T2 had the highest DS concentration, the small flow rate made its contribution accounted for only 6% in T12.

O_2 concentration level in manhole air was above 96% (i.e. the oxygen partial pressure was at 96% of its maximum partial pressure at given temperature and 1 atm), except that it is 92% in T2. DO was less than 3.5 mg/L in the trunk, averaged to be 2.0 mg/L (Table 5-2). However, it was 7.43 mg/L in the lateral of L9 (Table 5-3). The reason was that the wastewater fell across large drop structures in the upstream. Specifically, after the wastewater was pumped out from the pump station, it fell into a drop structure with a drop height of 14 m. This drop structure was 1854 m upstream of L9, and three other drop structures with a drop height of 12 - 14 m were located in

between. These four drop structures increased the DO level in the wastewater. Because of the high DO, sulfide was hard to generate and thus, gaseous H_2S concentration in the air of L9 was too low (< 1 ppm) to be detected by Odalog. Nevertheless, the drop structure was not the only reason for the high DO in the wastewater. At L8, DO concentration reached 6.32 mg/L (Table 5-3). That is because the pipe was only 3 m deep and with a diameter of 200 mm and a small discharge of 0.0002 m^2/s (Table 5-1), some part of the wastewater was just discharged from the surrounding neighborhood.

It was found that the variation of TS and DS was opposite with DO in most pipes (shown in Figure 5-6), except T4-T6. The distance from T4 to T6 was over 3 km (shown in Table 5-1), with only one drop structure of 1.0 m at T5 and some laterals. The reasons for the decrease of TS and DS were complex: there could be the dilution of laterals, the emission of H_2S and its oxidation. The reason for decrease of DO could be that the oxidation of sulfide consumed the DO in the wastewater.

5.3.4. Emission of H_2S

Gaseous H_2S concentrations in the trunk and laterals

The discharge rate (Q) of the Big Lake Pump Station was obtained from the Supervisory Control and Data Acquisition (SCADA) at the intervals of 20 s. In the study period of Oct. 4 - 19, 2021, the data showed that the pump station dealt with the average of 705 m^3 wastewater from the nearby neighborhood everyday. For the convenience of comparison, only the data on Oct. 5 was shown in Figure 5-7. There was a total of 26 pumping events in that day and every event lasted for 3 - 4 mins, with the maximum discharge rate of 143 L/s. Therefore, it was intermittent flow from T1 to T2. In the day, the gaseous H_2S level in the downstream manhole of T2 fluctuated strongly from

0 to 165 ppm. Almost every time the pump operated, gaseous H_2S concentration in T2 soared up with that then it decreased with a slower rate. In T3, the effect of the pump operation on the gaseous H_2S level was much weaker. The distance from T1 to T2 was 0.5 km while it was 2.2 km from T2 to T3 (see Table 5-1); also, the ventilation effect of two laterals (L3-1 and L3-2) brought the wastewater from other neighborhoods, so the effect of the pump operation was not so obvious in T3.

The monitoring results of gaseous H_2S concentration in the trunk were shown in Figure 5-8. H_2S was not evenly distributed along the trunk, which was high in the upstream (T2 and T3) and downstream (T12), and low in the middle part (T6 and T7). In the upstream of the trunk, T2, the maximum gaseous H_2S concentration was over 300 ppm. Such high concentration was due to the long force main connecting the Big Lake Pump Station. In its downstream, H_2S concentration reached 71 and 30 ppm in the T3 and T4, respectively. In the middle part of the trunk, the maximum gaseous H_2S concentration in T6 was only 4 ppm and H_2S was not even detected in T7. In T11 and T12, it rose again to 6 and 16 ppm, respectively. From T4 to T12, the H_2S concentration had apparent diurnal pattern, with high values near midnight. The demand of water in the families closed to midnight (such as showers) was high, therefore, the flow rate was the main factor for high H_2S concentration other than the pump cycle of the Big Lake Pump Station in the upstream.

In the laterals, H_2S was detected larger than 1 ppm only in three manholes, L3-1, L3-2, and L8 (shown in Figure 5-9). In L3-1 and L3-2, the maximum gaseous H_2S concentration was 27 and 8 ppm, respectively. As the TS and DS level in their wastewater was as low as 0.5 mg/L, the gaseous H_2S in the two lateral manholes should come from the trunk. In L8, H_2S in the air had some sudden peaks whose maximum was 35 ppm, but the average in the minoring days was < 1 ppm. As of the

very small flow rate (Table 5-1), the possible sudden air flow may cause the H_2S concentration peaks in the air.

$H_2S_{(L)}$ concentrations in the trunk and laterals

The basic sulfide system follows the acid–base equilibria in the water phase (Yongsiri et al. 2004):

$$H_2S \uparrow \rightleftharpoons HS^- + H^+ \quad pK_1 = 7.0 \qquad HS^- \rightleftharpoons S^{2-} + H^+ \quad pK_2 = 17.1 \quad (20\ ^\circ C)$$

where $pK_1 = -\log K_1 = 6045.2/T - 106.67 + 37.744 \log T$, with the wastewater temperature T in K (Rao and Hepler 1977). Because of the high pK_2 value and pH = 7 - 9, S^{2-} is generally negligible in wastewater (Matias et al. 2017a). So, it is often assumed that only H_2S and HS^- are present in wastewater (Hvitved-Jacobsen et al. 2013). The percentage of dissolved H_2S concentration (f) in the wastewater is:

$$f = \left(10^{\mathrm{pH}-pK_1} + 1\right)^{-1} \tag{5-6}$$

Therefore, the concentration of dissolved H_2S (C_L) in sulfur is

$$C_L = C_{DS} f \tag{5-7}$$

where C_{DS} is the concentration of DS, which is obtained by analysing the wastewater sample.

Dissolved H_2S was calculated by Eqs. (5-6) and (5-7), which ranged from 0.01 to 6.03 mg S/L (Table 5-2). Its equilibrium H_2S concentration in the air, $C_{G,eq}$, was calculated by Henry's Law and could be regraded theoretically as the theoretical maximum H_2S concentration at the sampling moment, which varied 3-1384 ppm. $C_{G,ave}$ is the average H_2S concentration in the air at the time of sampling in the following two weeks, which ranged from 0 to 137 ppm. The ratio of $C_{G,ave}/C_{G,eq}$ stands for the percentage of H_2S emissions from the wastewater. In the trunk, it changed from 0 -

10%, which meant less than 10% of H_2S emitted to the air and over 90% of H_2S stayed in the wastewater. $C_{G,max}$ is the maximum gaseous concentration in the monitoring period. The variation of $C_{G,ave}$, $C_{G,max}$, and C_L concentration in the trunk are shown in Figure 5-10. Those parameters had similar trends with TS and DS in Figure 5-6. They peaked in T2, decreased to the lowest in T7, then increased in T11.

Mass transfer of H_2S and O_2 in drop structures

For the emission of H_2S, the driving force is the gas concentration difference between the liquid and the air (Clift et al. 1978). To better understand the mass transfer of a falling drop in air, the two-film theory (Lewis and Whitman 1924) has been used. For H_2S studied in this work, over 80% of the overall mass transfer resistance exists in the liquid film (Matias et al. 2018) because of their low solubility in water (Amokrane et al. 1994), so the emission of H_2S is controlled by liquid phase. The mass transfer process can be expressed as:

$$-\frac{dC_{DS}}{dt} = K_{L,H_2S}a\left(C_L - C_G/H\right) = K_{L,H_2S}a\left(fC_{DS} - C_G/H\right) \tag{5-8}$$

where t is the time of mass transfer, $K_{L,\,H_2S}$ is the mass transfer coefficient, a is the surface-area-to-volume ratio, H is Henry's law constant. Eq. (5-8) can be integrated with t as:

$$\ln\left(\frac{C_G/H - fC_{DS,u}}{C_G/H - fC_{DS,d}}\right) = fK_{L,H_2S}a\Delta t \tag{5-9}$$

where $C_{DS,u}$ and $C_{DS,d}$ are the DS concentration in the upstream and downstream, respectively, and Δt is the falling time in the drop structure. Also, a deficit ratio r is introduced (Gulliver et al. 1990; Rahmé et al. 1997):

$$r = \frac{C_{a,H_2S} / H_{H_2S} - fC_{DS,u}}{C_{a,H_2S} / H_{H_2S} - fC_{DS,d}} \tag{5-10}$$

If K_L is obtained at different temperatures, it is usually adjusted to standard temperature (20℃) (Elmore and West 1961):

$$K_{L,20} = K_{L,T}\left[1.0241^{(20-T)}\right] \tag{5-11}$$

where $K_{L,\ T}$ and $K_{L,20}$ are the mass transfer coefficients determined under the test temperature T (℃) and 20℃, respectively.

T6 and T7 are the upstream and downstream of a drop structure, respectively, with a drop height of 8.0 m (Figure 5-3). The discharge rate is 0.193 m^3/s. When wastewater falls in the drop structure, it generates jets and breaks up into small water droplets (Ma et al. 2016). When the jet or droplets jet impinge on the bottom pool, the air is entrained into the pool at the bottom, causing large number of bubbles and strong turbulence created there. It will enhance the mass transfer of H_2S and O_2. After the wastewater hitting the bottom of T7, it was not mixed with other wastewater. From Table 5-2, H_2S concentration C_L decreased from 0.16 to 0.06 mg S/L when wastewater fell from T6 to T7, which means that the H_2S concentration in the upstream was 2.6 times of that in the downstream because of emission. r and fK_La were calculated with Eqs. (5-9), (5-10) and (5-11) at the onsite temperature and their results adjusted to 20 ℃ are presented in Table 5-5, where f is 0.17. At 20℃, r for H_2S was 2.01. As for O_2, DO increased from 1.94 to 2.85 mg/L (Table 5-2) from T6 to T7 and r for O_2 was 1.15 (20 ℃).

5.4. Conclusions

In the west area of Edmonton, two rounds of field work were carried out in the sanitary sewer systems, including the trunk and laterals, from the Big Lake Pump Station to the Glenora area. This research presented the results of water quality, H_2S generation and emission in the sewers of study area. Here are the conclusions:

1. The wastewater qualities had shown to be relatively stable along the trunk. In contrast, in the laterals, the wastewater qualities had larger range than the truck, which could be due to the pump stations upstream, connected joints, or branched pipelines and the inflow from the surrounding neighborhoods interfering with the wastewater contents.
2. Empirical model was employed to predict sulfide generation, which is related to COD, DO concentration, wastewater depth and retention time. For addressing the sewer odor and corrosion issues, we should minimize the condition of sulfide generation in future sewer design, such as trying to increase the slope and size of gravity pipes and avoid long distance force main.
3. In the nearby downstream of the Big Lake Pump Station, the pump operation played a significant role that it could cause the sudden increase of H_2S in the sewer air. The long force main connecting to Big Lake Pump Station was the reason of high H_2S level (343 ppm) in the upstream. L10 is the main source of sulfide (56%) in the trunk to the Glenora area. Although the upstream had the highest sulfide concentration, the small flow rate made its contribution account for only 6%.
4. Over 90% of H_2S stayed in the liquid phase when wastewater flowed in the sewer pipes. In the drop structure of 8 m, the concentration of H_2S in the wastewater changed heavily.

The H_2S concentration in the upstream was 2.6 times of that in the downstream, which proves the enhancement to the emission of H_2S in drop structures.

Table 5-1 Characteristics of the trunk and main laterals

Pipe	Length (m)	Diameter	Pipe slope	Flow rate (m^3/s)
T1 – T2	464	525-675	1.5%	0.008
T2 – T3	2247	1200	0.2%	0.014
T3 – T4	1065	1200	0.3%	0.032
T4 – T5	2418	900-1200	0.4%	0.033
T5 – T6	784	1950	0.3%	0.193
T6 – T7	1.1	1200	-	0.193
T7 – T8	1602	1200-1950	0.4%	0.193
T8 – T9	1099	1500	1.3%	0.194
T9 – T10	178	1200-1500	2.6%	0.264
T10 – T11	3.8	1200	10%	0.568
T11 – T12	1099	1500	0.1%	0.569
T12 – T13	1.2	1500	0.1%	0.570
L3-1 – T3	21	375	0.6%	0.001
L3-2 – T3	21	750	1.0%	0.016
L5– T5	794	1950	0.9%	0.152
L8– T8	30	200	0.4%	0.0002
L9 – T9	966	1500	0.7%	0.071
L10 – T10	1621	1200	0.1%	0.304
L13 – T13	2	1200	0.1%	0.011

Table 5-2 General wastewater quality in the trunk

Location (MH)	Time*	TN (mg/L)	NH_4^+ (mg N/L)	NO_3^- (mg N/L)	TP (mg/L)	TCOD (mg/L)	DCOD (mg/L)	TSS (mg/L)	VSS (mg/L)	SO_4^{2-} (mg S/L)	VFA (mg/L)	S_F (mg/L)	X_{S1} (mg/L)	X_{S2} (mg/L)	VFA/ DCOD
T2	11:10	96.9	52.8	1.0	22.4	867	320	224	191	185	107	116	185	278	0.334
T3	11:47	78.8	53.5	0.8	25.7	895	291	217	194	147	108	122	188	283	0.372
T4	12:23	91.7	58.1	0.9	30.0	809	303	255	210	145	88.5	119	156	235	0.292
T6	13:44	69.1	55.7	1.1	25.1	620	258	336	205	186	91.9	67	102	153	0.356
T7	14:05	97.3	52.3	0.9	21.5	621	270	312	212	205	78.2	81	100	150	0.289
T11	14:42	83.5	50.1	0.8	25.6	611	234	195	172	168	75.8	81	113	169	0.324
T12	15:27	67.4	39.4	0.9	25.8	717	272	211	168	169	80.9	103	146	218	0.297

Location (MH)	pH	T (°C)	TS (mg/L)	DS (mg/L)	C_L (mg S/L)	DO (mg/L)	DS Flux (mg S/s)
T2	6.94	15.0	9.7	9.2	6.03	2.00	74
T3	7.72	15.0	1.6	1.5	0.33	3.47	21
T4	7.77	16.1	2.0	1.8	0.35	2.35	57
T6	7.75	16.4	1.0	0.8	0.16	1.94	148
T7	7.92	16.1	0.6	0.4	0.06	2.85	78
T11	7.42	18.0	3.1	2.7	0.95	0.49	1559
T12	7.32	17.2	2.4	2.0	0.83	0.52	1160

***:** The water samples were collected on Oct. 4th, 2021.

Table 5-3 General wastewater quality in the laterals

Location (MH)	Time*	TN (mg/L)	NH_4^+ (mg N/L)	NO_3^- (mg N/L)	TP (mg/L)	TCOD (mg/L)	DCOD (mg/L)	TSS (mg/L)	VSS (mg/L)	SO_4^{2-} (mg S/L)	VFA (mg/L)	S_F (mg/L)	X_{S1} (mg/L)	X_{S2} (mg/L)	VFA/ DCOD
L3-1	14:27	49.5	29.5	0.7	13.8	452	133	258	223	284	55.9	60	45	67.7	0.420
L3-2	14:48	64.7	44.1	0.8	18.3	545	205	227	173	167	67	73	93	139	0.327
L5	14:39	163.3	70.2	2.6	58.1	7817	638	5183	4303	533	301	1708	602	903	0.471
L8	13:52	64.7	19.0	1.6	12.7	2092	1149	339	289	125	33.2	504	506	759	0.029
L9	13:19	51.5	20.2	1.7	59.4	1051	794	360	297	264	150	120	194	290	0.189
L10	11:48	98.4	69.0	0.7	29.4	578	156	189	171	148	61.9	60	103	155	0.396
L13	10:42	70.3	74.18	0.8	28.7	315	163	185	159	159	72.9	8	30	45	0.447

Location (MH)	pH	T (°C)	TS (mg/L)	DS (mg/L)	C_L (mg S/L)	DO (mg/L)	DS Flux (mg S/s)
L3-1	8.59	16.1	0.6	0.4	0.01	3.62	0.3
L3-2	8.17	13.3	0.5	0.5	0.04	3.60	8
L5	7.43	18.8	2.7	0.7	0.26	0.2	112
L8	6.99	18.0	3.6	3.3	1.84	6.32	0.5
L9	7.74	15.2	1.0	1.0	0.19	7.43	71
L10	8.38	12.7	2.5	2.1	0.12	0.44	652
L13	8.45	13.8	1.0	0.9	0.05	3.76	10

***:** The water samples of L5 and L8 were collected on Oct. 10th, 2021, and the others were on Oct. 5th, 2021.

Table 5-4 Sulfide generation from wastewater biofilms

Pipe section	r (mg/L/h)	ΔC_s (mg/L)
T2 – T3	0.6	0.8
T3 – T4	0.3	0.1
T4 – T5	0.4	0.4
T7 – T8	0.1	0.02
T11 – T12	0.3	0.1
L5 – T5	3.6	0.6
L9 – T9	0.1	0.03
L10 – T10	0.3	0.2

Table 5-5 Results of r and K_La at onsite temperature (16 ℃) and 20 ℃

Gas	r	fK_La (s^{-1})	r_{20}	$fK_{L,20}a$ (s^{-1})
H_2S	1.89	0.50	2.01	0.55
O_2	1.15	0.11	1.17	0.12

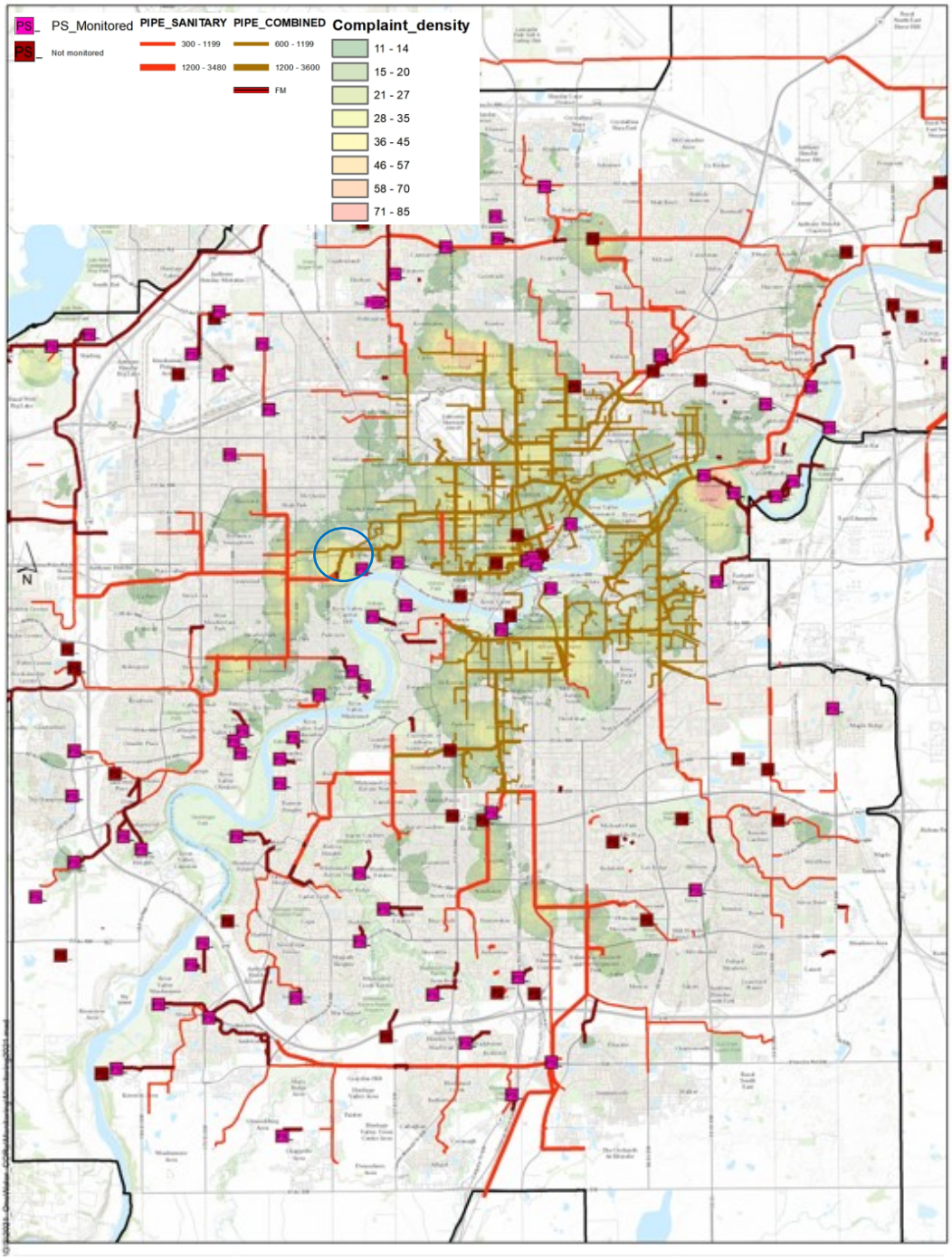

Figure 5-1 Sewer odor complaint density map in Edmonton (from EPCOR).

(a)

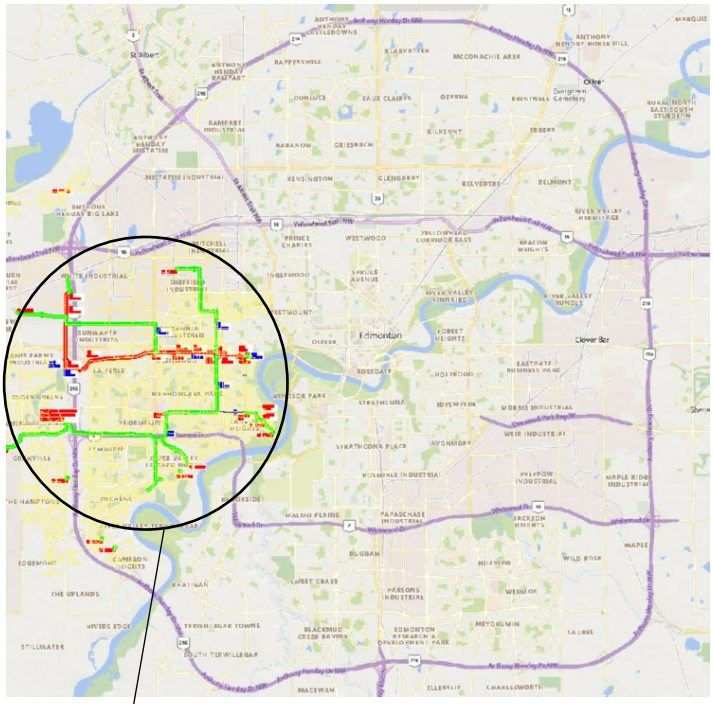

(b)

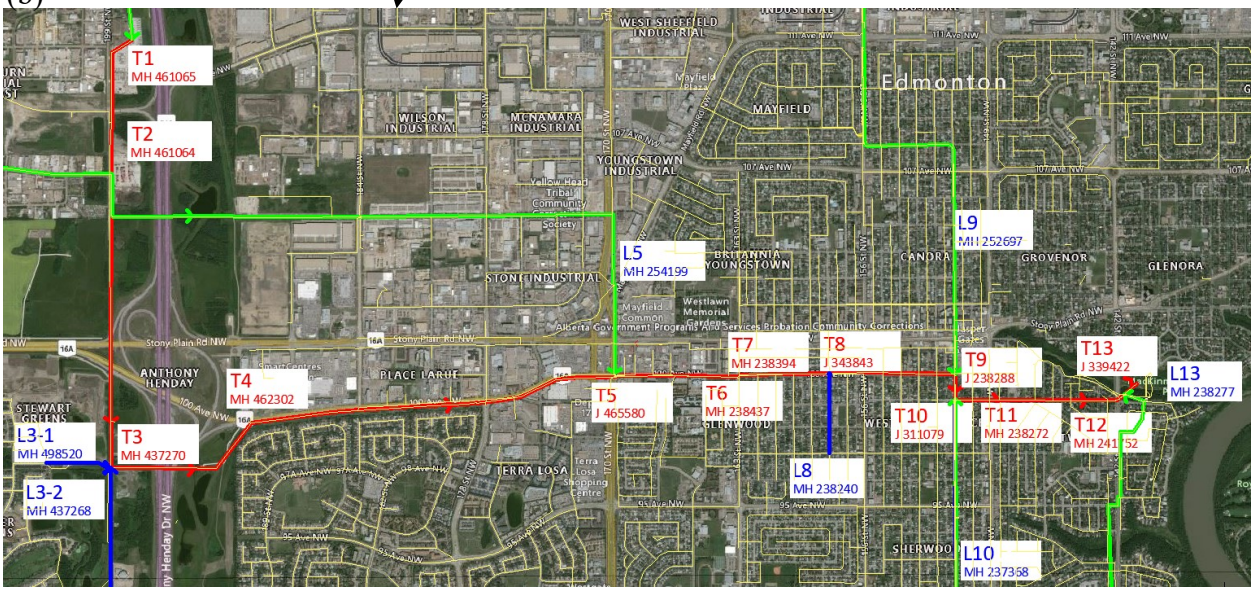

Figure 5-2 The study area of the field work (Green lines are the main laterals originating from the pump stations; blue lines are the laterals originating from the nearby neighborhood; and red lines are the trunk).

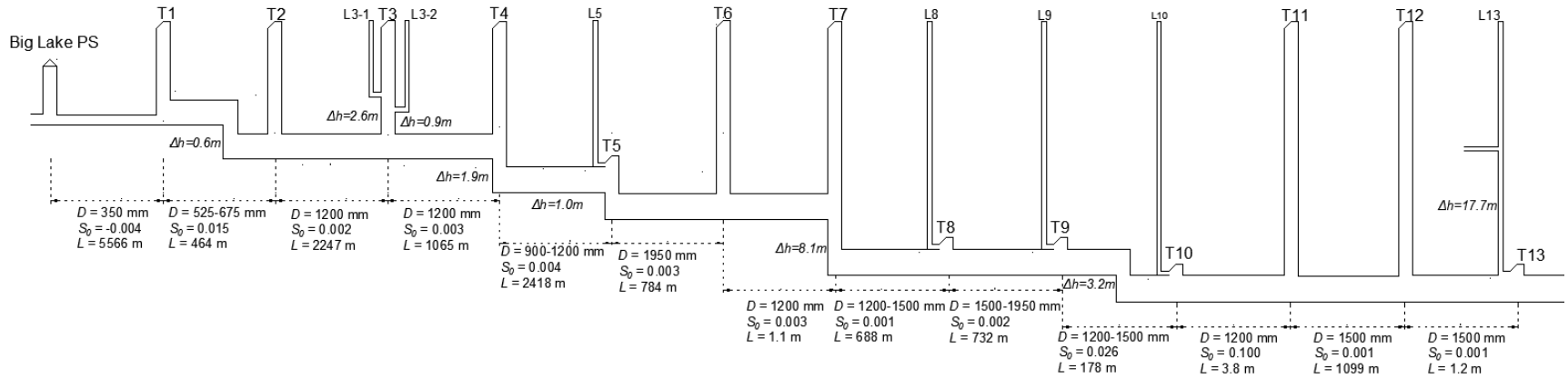

Figure 5-3 Profile of the studied sewer network.

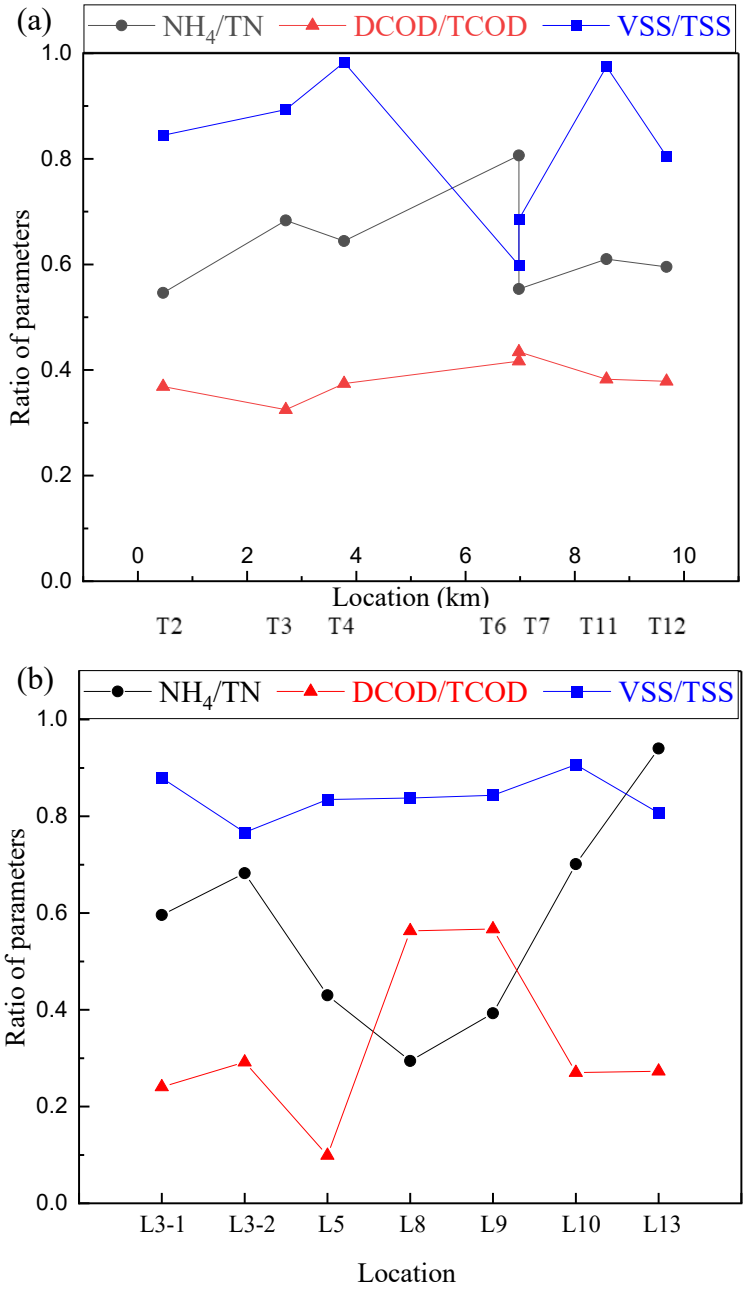

Figure 5-4 Water quality comparisons: (a) in the trunk; (b) in the laterals.

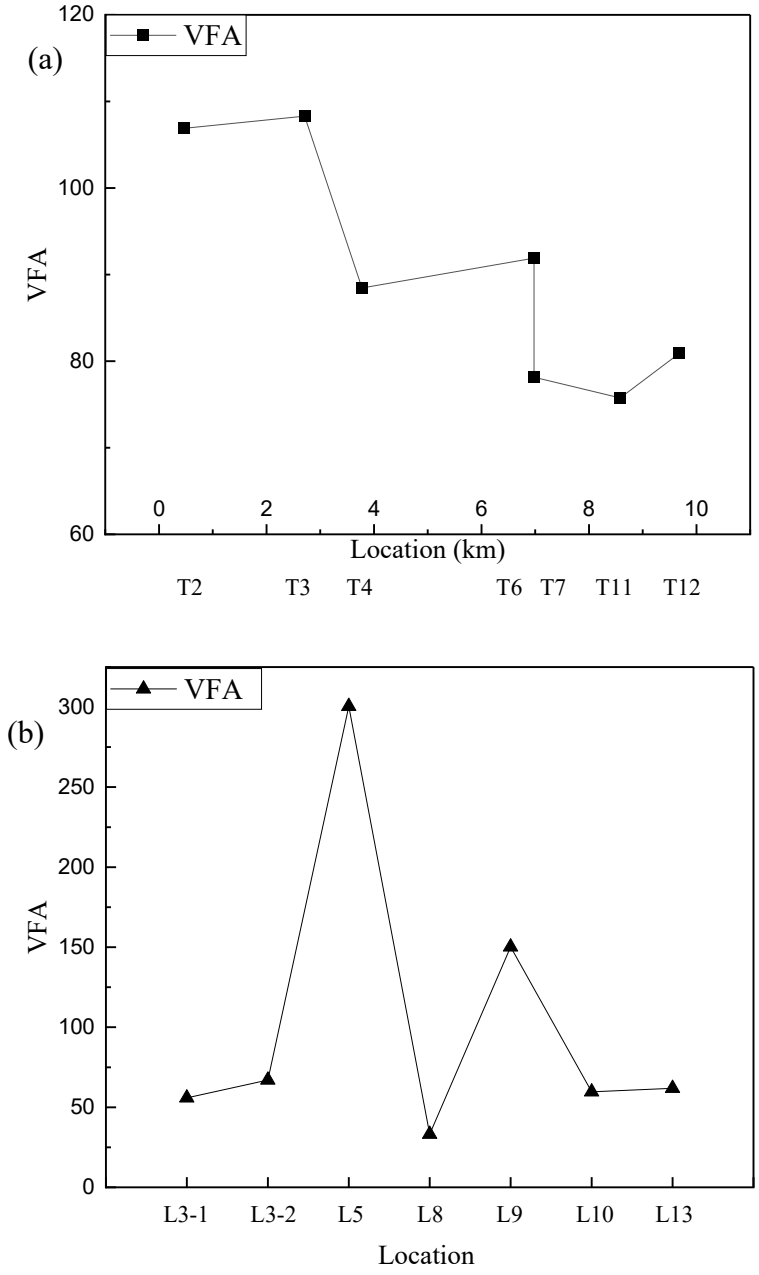

Figure 5-5 VFA across locations (a) in the trunk; (b) in the laterals.

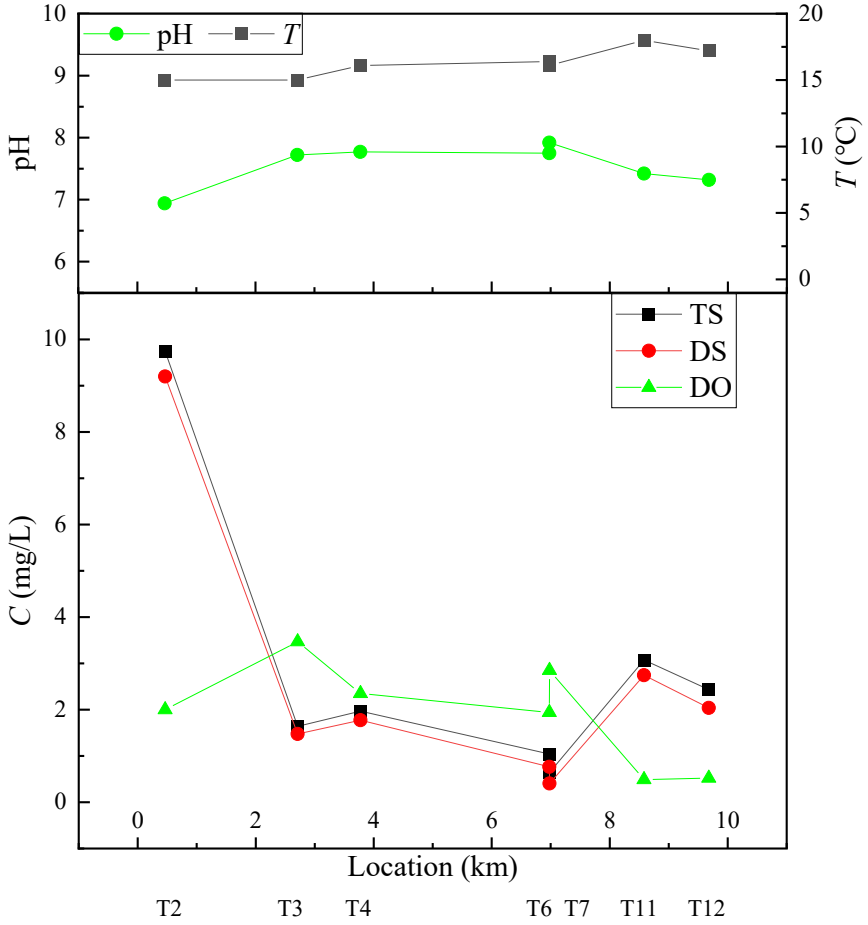

Figure 5-6 pH, temperature, TS, DS, DO concentration development along the trunk.

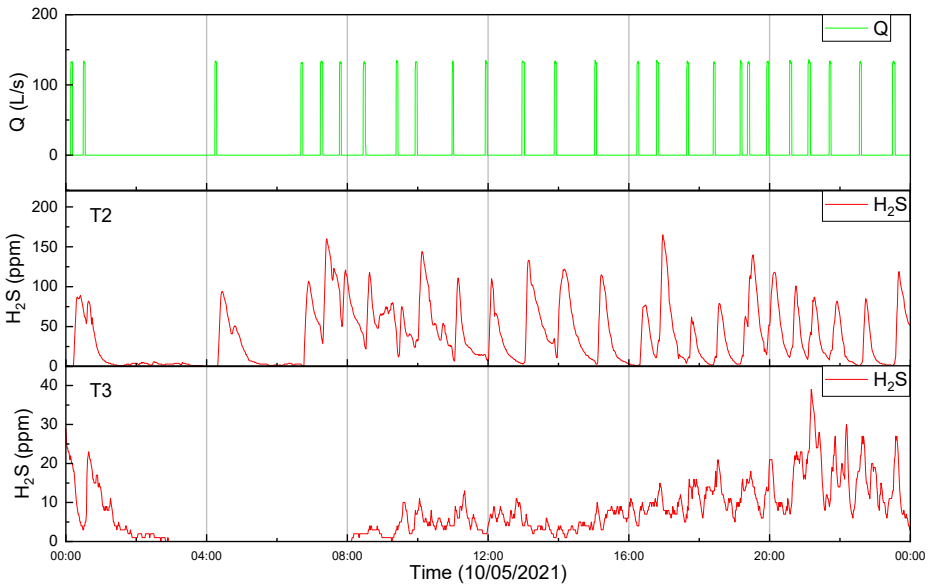

Figure 5-7 Monitoring results in the two downstream manholes of the Big Lake Pump Station.

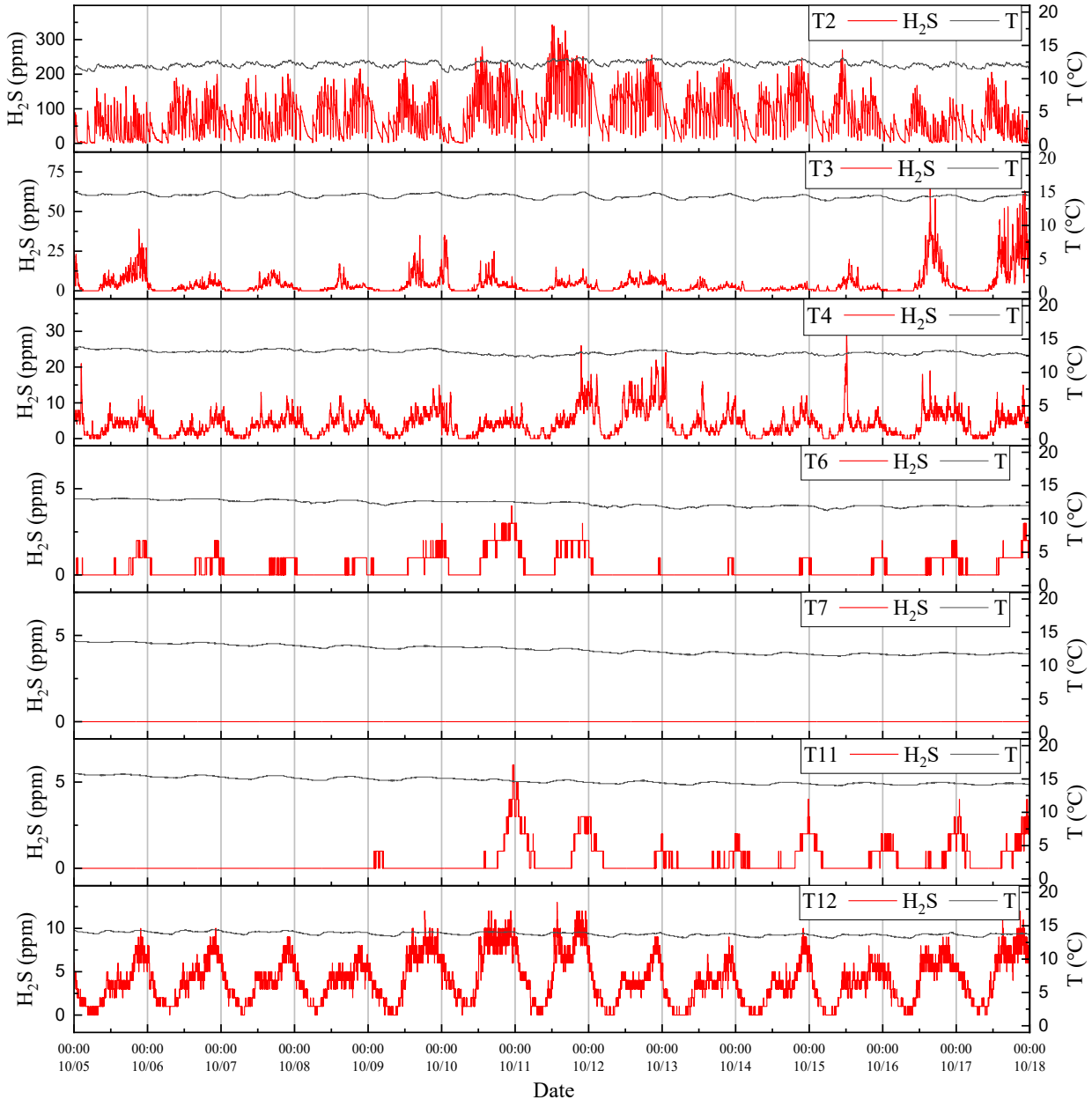

Figure 5-8 Monitored diurnal pattern of gaseous H_2S concentration in the trunk.

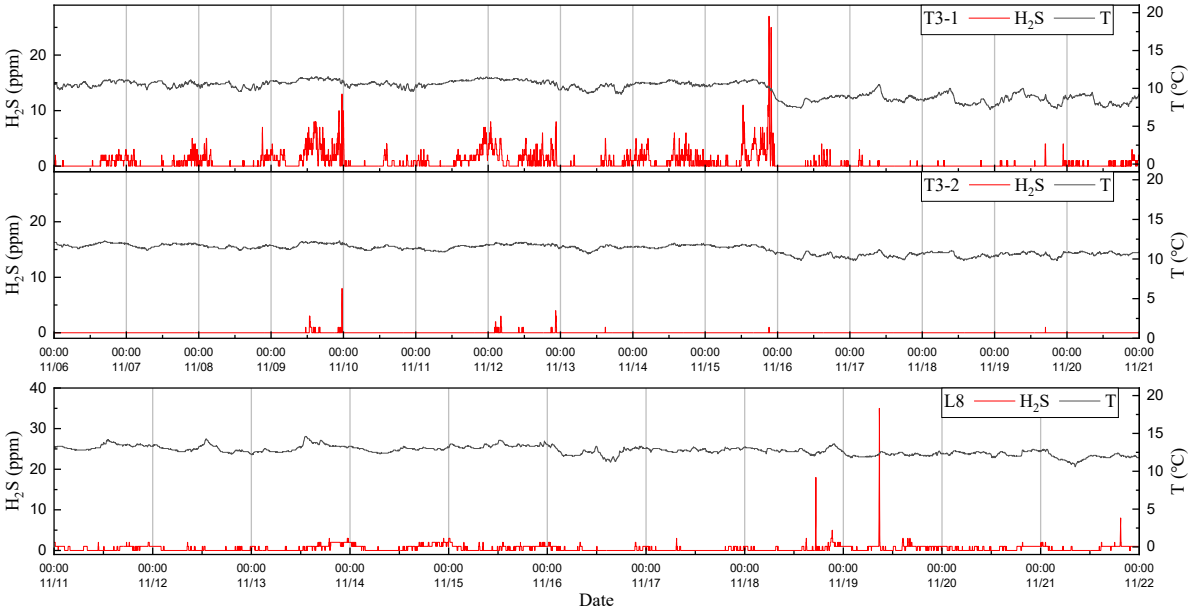

Figure 5-9 Monitored diurnal pattern of gaseous H_2S concentration in the laterals (L5, L9, L10, L13: 0 ppm).

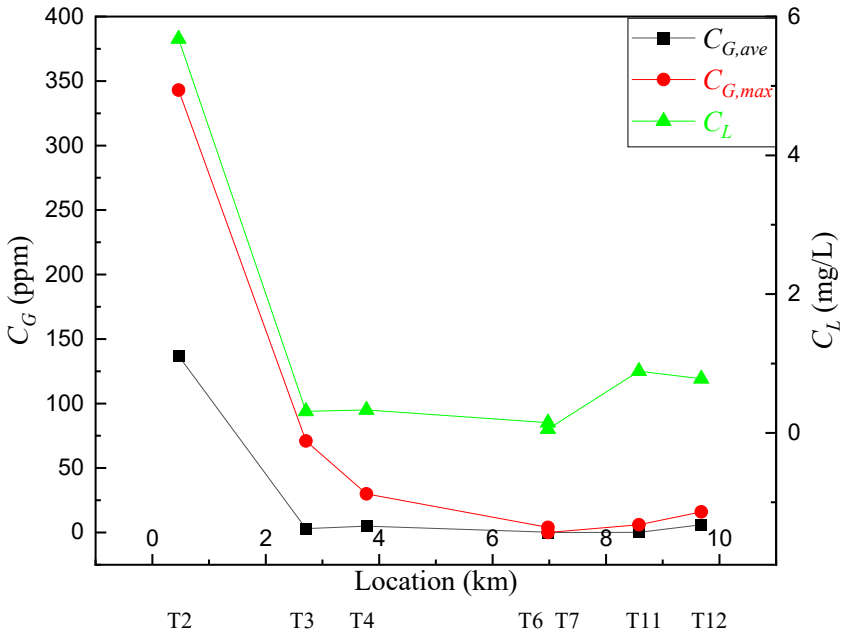

Figure 5-10 H_2S distribution in the air and wastewater along the trunk.

6. General Conclusions and Recommendations

The mass transfer of H_2S in the sewer drop structures is studied in this thesis. There are three chapters of on the experiments of mass transfer of H_2S: Chapter 2, from falling droplets; Chapter 3, at turbulent water surface; and Chapter 4, in drop structures. Chapter 5 reports a field work in the west region of Edmonton, Canada. Specific conclusions can be found in each chapter. The following are the general conclusions for this study.

1. In Chapter 2, laboratory experiments were conducted on the mass transfer of single falling droplets. K_L increases with the droplet falling height (or velocity) but decreases with the droplet size. A modified equation was proposed to reasonably predict K_L, which can be used to approximately model the complex H_2S emission in small drop structures. In large drop structures, more than 70% to equilibrium of H_2S emission can be achieved after falling 15 m. CO_2 was found to be a suitable surrogate for H_2S.
2. In Chapter 3, two series of laboratory experiments were conducted for falling drops and jet, which impinged half of the receiving water pool. K_L increased with KEF. K_L at the turbulent water surface due to falling drops was 76% larger than those of single jet. K_L was larger in the side that received the drops or jet. The increase of pool water depth promotes the mass transfer, especially for the scenario of falling jet. Two equations were proposed to reasonably predict K_L. O_2 is another safe surrogate gas for studying H_2S mass transfer in sewer drop structures.
3. In Chapter 4, the laboratory experiments were conducted with two scenarios of jets: free-falling and attached-falling jets. The nonlinear correlations between r and h_d, Q, h_t was proposed for both jet scenarios. r increased with an increase of h_d and a decrease of Q. The

mass transfer between the entrained bubbles and tailwater was vital, especially with free-falling jet. A flow chart and method for modeling mass transfer in drop structure prototypes was proposed. Furthermore, the mass transfer in drop structures is 3-13 times compared with that in gravity pipes.

4. In Chapter 5, two rounds of field work were carried out in the sanitary sewer systems in the west area of Edmonton. The wastewater qualities had shown to be relatively stable along the trunk. Empirical models can predict sulfide generation in gravity pipes. Over 90% of H_2S stayed in the liquid phase when wastewater flowed in the sewer pipes. In the drop structure of 8 m, the H_2S in the upstream was 2.6 times of that in the downstream and the deficit ratio for H_2S was 2.0, which proves the enhancement to the emission of H_2S in drop structures.

In general, this thesis covers different physical process of the mass transfer of H_2S in urban sewer drop structures. It is concluded that in real design, the drop height of drop structures should be minimised to avoid the jet breakup; and attached-falling jet should be applied in design instead of free-falling. Also we should increase the slope and size of gravity pipes, and avoid force main. However, a few aspects still exist for further studies, and the recommendations are listed below:

1. pH and the complex chemical constitutions in wastewater have effect on the mass transfer of H_2S. In the future study, pH's effect should be invested cautiously; and the chemical reaction between some constitutions and sulfide, such as oxidation and precipitation, should be studied further.

2. A complete prediction model that involves all the physical processes of mass transfer and air flow's effect in sewer drop structures should be further developed.
3. To take more tests in real drop structures with in-situ sensors other than sampling for long term measuring, and compare the difference between winter and summer, weekdays and weekend, day and night, can help calibrate the prediction model.
4. To take experiments with larger cylinder and drop height than this study, and other forms of drop structures such as vortex drop structures, retrofitted drop structures (with steps and baffles) and drop structures in series.
5. To study H_2S emission in other parts of sewer networks, such as gravity sewer pipes and WWTP, in order to have a better knowledge of the percentage of mass transfer in drop structures and the challenging issue of sewer odor and corrosion control.

Bibliography

Altwicker, E. R., and Lindhjem, C. E. (1988). “Absorption of gases into drops.” AIChE Journal, 34(2), 329–332.

Amokrane, H., Saboni, A., and Caussade, B. (1994). “Experimental study and parameterization of gas absorption by water drops.” *AIChE Journal*, 40(12), 1950–1960.

Angelo, J. B., Lightfoot, E. N., and Howard, D. W. (1966). “Generalization of the penetration theory for surface stretch: Application to forming and oscillating drops.” *AIChE Journal*, 12(4), 751–760.

APHA, AWWA, and WEF (American Public Health Association, American Water Works Association, and Water Environment Federation). (2017). *Standard methods for the examination of water and wastewater*. 23th ed. Washington, DC: APHA, AWWA, and WEF.

Ashton, I. G., Shutler, J. D., Land, P. E., Woolf, D. K., and Quartly, G. D. (2016). “A Sensitivity Analysis of the Impact of Rain on Regional and Global Sea-Air Fluxes of CO_2.” *PLOS ONE*, (M. deCastro, ed.), 11(9), e0161105.

Banks, R. B., G. B. Wickramanayake, and B. N. Lohani. (1984). “Effect of Rain on Surface Reaeration.” *Journal of Environmental Engineering*, 110 (1): 1–14.

Belanger, T. V., and Korzun, E. A. (1990). “Rainfall-Reaeration Effects.” *Journal of Irrigation and Drainage Engineering*, 116(4), 582–587.

Brunson, R. J., and Wellek R. M. (1970). “Mass transfer within oscillating liquid droplets.” *Can. Chemical Engineering Journal*, 48(3): 267-274.

Cadena, F., and Peters, R. W. (1988). “Evaluation of chemical oxidizers for hydrogen sulfide control”. *Journal (Water Pollution Control Federation)*, 1259-1263.

Carrera, L., F. Springer, G. Lipeme-Kouyi, and P. Buffiere. (2017a). “Influence of relative air/water flow velocity on oxygen mass transfer in gravity sewers.” *Water Science and Technology*, 75 (7): 1529-1538.

Carrera, L., F. Springer, G. Lipeme-Kouyi, and P. Buffiere. (2017b). “Sulfide emissions in sewer networks: focus on liquid to gas mass transfer coefficient.” *Water Science and Technology*, 75 (8): 1899–1908.

Carrera, L., Springer, F., Lipeme-Kouyi, G., and Buffiere, P. (2016). “A review of sulfide emissions in sewer networks: overall approach and systemic modelling.” *Water Science and Technology*, 73(6): 1231–1242.

Choi, M., Cho, M., and Lee, J. W. (2016). “Empirical formula for the mass flux in chemical absorption of CO_2 with ammonia droplets.” *Applied Energy*, 164, 1–9.

Chu, C. R., and G. H. Jirka. (2003). “Wind and Stream Flow Induced Reaeration.” *Journal of Environmental Engineering*, 129 (12): 1129–1136.

Clift, R., Grace, J.R., and Weber, M.E. (1978). *Bubbles, drops and particles*. New York: Academic Press.

Cord-Ruwisch, R., Kleinitz, W., and Widdel, F. (1987). “Sulfate-reducing bacteria and their activities in oil production.” *Journal of Petroleum Technology*, 39(01), 97-106.

Cussler, E. (2009). *Diffusion: Mass transfer in fluid systems*. New York: Cambridge University Press.

Dankwerts, P. V. (1951). “Significance of liquid-film coefficients in gas absorption.” *Industrial* and Engineering Chemistry, 43(6), 1460–1467.

Drewnowski, J., Szeląg, B., Xie, L., Lu, X., Ganesapillai, M., Deb, C. K., Szulżyk-Cieplak, J. and Łagód, G. (2020). “The Influence of COD fraction forms and molecules size on hydrolysis process developed by comparative our studies in activated sludge modelling.” Molecules, 25(4), 929.

Elmore, H. L., and West, W. F. (1961). “Effect of water temperature on stream reaeration.” *Journal of the Sanitary Engineering Division*, 87(6), 59-71.

EPCOR. (2022). *EDMONTON’S CAPITAL REGION: Water Treatment Process*. Online. https://www.epcor.com/products-services/water/Documents/edmonton-water-treatment-process.pdf

Ferrell, R. T., and D. M. Himmelblau. (1967). “Diffusion coefficients of nitrogen and oxygen in water.” *Journal of Chemical and Engineering Data*, 12 (1): 111-115.

Ganigué, R., Jiang, G., Sharma, K., Chen, J., Vuong, L., and Yuan, Z. (2016). “Online control of magnesium hydroxide dosing for sulfide mitigation in sewers: algorithm development, simulation analysis, and field validation.” *Journal of Environmental Engineering*, *142*(12), 04016069.

Garner, F. H., and Lane, J. J. (1959). “Mass transfer to drops of liquid suspended in a gas stream. Part II: Experimental work and results.” *Transactions of the Institution of Chemical Engineers*, 37, 162-172.

Global NEWS. (2021). “61 Avenue intersection’s closure due to massive sinkhole extended to end of July.” Online. https://globalnews.ca/news/7717109/edmonton-epcor-61-avenue-intersection-sinkhole-july/

Gulliver, J. S. (1990). “Introduction to air-water mass transfer” in *Air-Water Mass Transfer*, Wilhelms, S. C. and Gulliver, J. S. eds, New York: ASCE, 1-6.

Guo, S., Qian, Y., Zhu, D.Z., Zhang, W., and Edwini-Bonsu, S. (2018). “Effects of drop structures and pump station on sewer air pressure and hydrogen sulfide: Field investigation.” *Journal of Environmental Engineering*, *144*(3), 04018011.

Gutierrez, O., Park, D., Sharma, K.R., and Yuan, Z. (2009). “Effects of long-term pH elevation on the sulfate-reducing and methanogenic activities of anaerobic sewer biofilms.” *Water Research*, 43(9): 2549-2557.

Handlos, A. E., and Baron, T. (1957). “Mass and heat transfer from drops in liquid-liquid extraction.” *AIChE Journal*, 3(1), 127–136.

Hao, O. J., Chen, J. M., Huang, L., and Buglass, R. L. (1996). “Sulfate-reducing Bacteria.” *Critical Reviews in Environmental Science and Technology*, 26(2), 155-187.

Harrison, E. L., F. Veron, D. T. Ho, M. C. Reid, P. Orton, and W. R. McGillis. (2012). "Nonlinear interaction between rain- and wind-induced air-water gas exchange." *Journal of Geophysical Research: Oceans*, 117(C3).

Haynes, W. M., Lide, D. R., and Bruno, T. J. (2014). *CRC Handbook of Chemistry and Physics*. 95th edition. CRC press.

Higbie, R. (1935). "The rate of absorption of a pure gas into still liquid during short periods of exposure." *Trans. Am. Inst. Chem. Eng.*, 31, 365-389.

Ho, D. T., L. F. Bliven, R. I. K. Wanninkhof, and P. Schlosser. (1997). "The effect of rain on air‐water gas exchange." *Tellus*, 49 B: 149-158.

Hvitved-Jacobsen, T., Vollertsen, J., and Matos, J. S. (2002). "The sewer as a bioreactor–a dry weather approach." *Water Science and Technology*, 45(3), 11-24.

Hvitved-Jacobsen, T., Vollertsen, J., and Nielsen, A. H. (2013). *Sewer processes: Microbial and chemical process engineering of sewer networks*. Boca Raton, USA: CRC press.

Jähne, B., K. O. Münnich, R. Bösinger, A. Dutzi, W. Huber, and P. Libner. (1987). "On the parameters influencing air‐water gas exchange." *Journal of Geophysical Research: Oceans*, 92 (C2): 1937-1949.

Jensen, H. S., Nielsen, A. H., Hvitved-Jacobsen, T., and Vollertsen, J. (2009). "Modeling of hydrogen sulfide oxidation in concrete corrosion products from sewer pipes." *Water Environment Research*, 81(4), 365-373.

Jensen, N. A. (1995). “Empirical modeling of air-to-water oxygen transfer in gravity sewers.” *Water Environment Research*, 67(6), 979–991.

Jiang, G., Keating, A., Corrie, S., O'halloran, K., Nguyen, L., and Yuan, Z. (2013a). “Dosing free nitrous acid for sulfide control in sewers: results of field trials in Australia.” *Water Research*, 47(13), 4331-4339.

Jiang, G., Melder, D., Keller, J., and Yuan, Z. (2017). “Odor emissions from domestic wastewater: A review.” *Critical Reviews in Environmental Science and Technology*, 47(17), 1581-1611.

Jiang, G., Sharma, K. R., and Yuan, Z. (2013b). “Effects of nitrate dosing on methanogenic activity in a sulfide-producing sewer biofilm reactor.” *Water Research*, 47(5), 1783-1792.

Jiang, Z., X. Li, W. Jin, X. Yu, and Z. Zhou. (2018). “Planar optode observation method for the effect of raindrop on dissolved oxygen and pH diffusion of air–water interface.” *Experiments in Fluids*, 59 (11): 175.

Jimenez, M., N. Dietrich, J. R. Grace, and G. Hébrard. (2014). “Oxygen mass transfer and hydrodynamic behaviour in wastewater: determination of local impact of surfactants by visualization techniques.” *Water Research,* 58: 111-121.

Kappeler, J., and Gujer, W. (1992). “Estimation of kinetic parameters of heterotrophic biomass under aerobic conditions and characterization of wastewater for activated sludge modelling.” *Water Science and Technology*, 25(6), 125-139.

Kaushal, V., Najafi, M., Love, J., and Qasim, S. R. (2020). “Microbiologically induced deterioration and protection of concrete in municipal sewerage system: Technical Review.” *Journal of Pipeline Systems Engineering and Practice* ,11(1), 03119002.

Kientzler, C. F., A. B. Arons, D. C. Blanchard, and A. H. Woodcock. (1954). “Photographic Investigation of the Projection of Drops by Bubbles Bursting at a Water Surface.” *Tellus* 6 (1): 1–7.

Labocha, M., Corsi, R. L., and Zytner, R. G. (1996). “Parameters Influencing Oxygen Uptake at Clarifier Weirs.” *Water Environment Research*, 68(6), 988–994.

Lahav, O., Lu, Y., Shavit, U., and Loewenthal, R. E. (2004). “Modeling hydrogen sulfide emission rates in gravity sewage collection systems.” *Journal of Environmental Engineering*, *130*(11), 1382-1389.

Lahav, O., Sagiv, A., and Friedler, E. (2006). “A different approach for predicting $H_2S_{(g)}$ emission rates in gravity sewers.” *Water Research*, 40(2), 259–266.

LeClair, B. P., Hamielec, A. E., Pruppacher, H. R., and Hall, W. D. (1972). “A theoretical and experimental study of the internal circulation in water drops falling at terminal velocity in air.” *Journal of Atmospheric Sciences*, 29(4), 728-740.

Lewis, W. K., and W. G. Whitman. (1924). “Principles of gas absorption.” *Ind. Eng. Chem.* 16 (12): 1215–1220.

Liss, P. S., and Slater, P. G. (1974). “Flux of gases across the air-sea interface.” *Nature*, 247(5438), 181-184.

Luther, G. W., Findlay, A. J., MacDonald, D. J., Owings, S. M., Hanson, T. E., Beinart, R. A., and Girguis, P. R. (2011). "Thermodynamics and kinetics of sulfide oxidation by oxygen: A look at inorganically controlled reactions and biologically mediated processes in the environment." *Frontiers in microbiology*, 2:62.

Ma, Y., D. Z. Zhu, and N. Rajaratnam. (2016). "Air entrainment in a tall plunging flow dropshaft." *Journal of Hydraulic Engineering*,142 (10): 04016038.

Makinia, J. (2006). "Performance prediction of full-scale biological nutrient removal systems using complex activated sludge models." ISAH, Inst. für Siedlungswasserwirtschaft und Abfalltechnik der Univ. Hannover.

Mandal, B. (2018). *Mass Transfer Operations-I*. Lecture notes. Indian Institutes of Technology. Guwahati, India. Online. https://www.youtube.com/watch?v=Yc2eSffzhBI&list=PLwdnzlV3ogoVX_S_8DyKa7RudEazDL0o_&ab_channel=NPTELIITGuwahati

Matias, N. M., Matos, J. S., and Ferreira, F. (2014). "Hydrogen sulfide gas emission under turbulent conditions – an experimental approach for free-fall drops." *Water Science and Technology*, 69(2), 262–268.

Matias, N., Ferreira, F., Matos, J. S., Nielsen, A. H., and Vollertsen, J. (2018). "Liquid-gas mass transfer of volatile substances in an energy dissipating structure." *Water Environment Research*, 90(3), 269–277.

Matias, N., Matos, R. V., Ferreira, F., Vollertsen, J., and Matos, J. S. (2017a). "Release of hydrogen sulfide in a sewer system under intermittent flow conditions: the Ericeira case study, in Portugal." *Water Science and Technology*, 75(7): 1702-1711.

Matias, N., Nielsen, A. H., Vollertsen, J., Ferreira, F., and Matos, J. S. (2017b). "Liquid-gas mass transfer at drop structures." *Water Science and Technology*, 75 (10), 2257–2267.

Millero, F. J., S. Hubinger, M. Fernandez, and S. Garnett. (1987). "Oxidation of H_2S in seawater as a function of temperature, pH, and ionic strength." *Environmental Science and Technology*, 21 (5): 439–443.

Nielsen, A. H., Lens, P., Vollertsen, J., and Hvitved-Jacobsen, T. (2005). "Sulfide–iron interactions in domestic wastewater from a gravity sewer." *Water Research*, 39(12), 2747-2755.

Nielsen, A. H., Vollertsen, J., Jensen, H. S., Madsen, H. I., and Hvitved-Jacobsen, T. (2008). "Aerobic and anaerobic transformations of sulfide in a sewer system—field study and model simulations." *Water Environment Research*, 80(1), 16-25.

Nielsen, P. H., Raunkjær, K., Norsker, N. H., Jensen, N. A., and Hvitved-Jacobsen, T. (1992). "Transformation of wastewater in sewer systems – A review." *Water Science and Technology*, 25(6), 17–31.

Pan, G., Wang, B., Guo, S., Zhang, W., and Edwini-Bonsu, S. (2020). "Statistical analysis of sewer odour based on 10-year complaint data." *Water Science and Technology*, 81(6), 1221-1230.

Park, K., Lee, H., Phelan, S., Liyanaarachchi, S., Marleni, N., Navaratna, D., Jegatheesan, V. and Shu, L. (2014). "Mitigation strategies of hydrogen sulphide emission in sewer networks–a review." *International Biodeterioration and Biodegradation*, 95, 251-261.

Pérez, A., Manjón, C., Martínez, J. V., Juárez-Galan, J. M., Barillon, B., and Bouchy, L. (2013). "Odours in sewer networks: nuisance assessment." *Water Science and Technology*, 67(3), 543-548.

Pincince, A. B. (1991). "Transfer of Oxygen and Emissions of Volatile Organic Compounds at Clarifier Weirs." *Research Journal of the Water Pollution Control Federation*, 63(2), 114–119.

Pomeroy, R. D., and Lofy, R. J. (1977). "Feasibility study on in-sewer treatment methods." *U. S. National Technical Information Service*. Springfield, Va., PB 271 445,(3 POM), 118.

Prata, A. A., J. M. Santos, S. P. Beghi, I. F. Fernandes, L. L. C. Vom Marttens, L. I. Pereira Neto, R. S. Martins, N. C. Reis, and R. M. Stuetz. (2016). "Dynamic flux chamber measurements of hydrogen sulfide emission rate from a quiescent surface – A computational evaluation." *Chemosphere* 146: 426–434.

Qian, Y., Zhu, D. Z., and Edwini-Bonsu, S. (2018). "Air flow modeling in a prototype sanitary sewer system." *Journal of Environmental Engineering*, 144(3), 04018008.

Qian, Y., Zhu, D. Z., and Yue, D. (2021). "Effect of pump operation on headspace air pressure variation in sanitary sewer systems." *Journal of Environmental Engineering*, 147(3), 06021001.

Rahmé, Z. G., R. G. Zytner, R. L. Corsi, and M. Madani-Isfahani. (1997). "Predicting Oxygen Uptake and VOC Emissions at Enclosed Drop Structures." *Journal of Environmental Engineering*, 123(1): 47–53.

Rao, S. R., and Hepler, L. G. (1977). "Equilibrium constants and thermodynamics of ionization of aqueous hydrogen sulfide." *Hydrometallurgy*, 2(3), 293–299.

Ruckenstein, E. (1967). "Mass transfer between a single drop and a continuous phase." *International Journal of Heat and Mass Transfer*, 10(12), 1785-1792.

Santos, J. M., V. Kreim, J. M. Guillot, N. C. Reis Jr, L. M. de Sá, and N. J. Horan. (2012). "An experimental determination of the H_2S overall mass transfer coefficient from quiescent surfaces at wastewater treatment plants." *Atmospheric Environment*, 60: 18–24.

Seader, J. D., Henley, E. J., and Roper, D. K. (2010). "Chapter 3: Mass Transfer and Diffusion." in *Separation Process Principles: Chemical and Biochemical Operations*. 3rd Edition. New York: Wiley.

Shao, T., Feng, X., Wang, W., Jin, Y., and Cheng, Y. (2012). "Visualization of coupled mass transfer and reaction between gas and a droplet using a novel reactive-PLIF technique." *Chemical Engineering Journal*, 200–202, 549–558.

Sherwood, T. K., Pigford, R. L. and Wilke, C. R. 1975. *Mass Transfer*. New York: McGraw-Hill.

Shypanski, A. (2020). "Review: Potential Odour Generation Sources Impacting 109 Street and 61 Avenue." Report for EPCOR, Edmonton, AB.

Skelland, A. H. P. (1974). *Diffusional Mass Transfer*. New York: Wiley.

Sun, L., W. Zhang, and D. Z. Zhu. (2020). "Emission of hydrogen sulfide from falling drops in sewage drop structures." *Journal of Environmental Engineering*, 146 (12): 04020135.

Sun, L., W. Zhang, and D. Z. Zhu. 2022. "Mass transfer of hydrogen sulfide and oxygen at turbulent water surface by falling drops and single jet." *Journal of Environmental Engineering*. under review.

Takagaki, N., and S. Komori. (2007). "Effects of rainfall on mass transfer across the air-water interface." *Journal of Geophysical Research: Oceans*, 112: C06006.

Tamimi, A., E. B. Rinker, and O. C. Sandall. (1994). "Diffusion coefficients for hydrogen sulfide, carbon dioxide, and nitrous oxide in water over the temperature range 293-368 K." *Journal of Chemical and Engineering Data*, 39 (2): 330–332.

Tewari, P. K., and Bewtra, J. K. (1982). "Alpha and beta factors for domestic wastewater." *Journal (Water Pollution Control Federation)*,54, 1281–1287.

Thibodeaus, L. J. (2011). "Mass transport fundamentals from the environmental perspective." In Thibodeaux, L. J., and Mackay, D. eds., *Handbook of Chemical Mass Transport in the Environment*. CRC Press.

US ATSDR. (2014). *Medical Management Guidelines for Hydrogen Sulfide.* Agency for Toxic Substances and Disease Registry. Atlanta, GA. Online. https://www.atsdr.cdc.gov/mhmi/mmg114.pdf

US ATSDR. (2016). *ToxGuide for Hydrogen Sulfide (H_2S)*. Agency for Toxic Substances and Disease Registry. Atlanta, GA. Online. https://www.atsdr.cdc.gov/toxguides/toxguide-114.pdf

US Environmental Protection Agency. (1974). *Process Design Manual for Sulfide Control in Sanitary Sewerage Systems*. US Environmental Protection Agency Technology Transfer Office, Washington, DC: EPA, 625/1-74-005.

Vollertsen, J., Nielsen, A. H., Jensen, H. S., Wium-Andersen, T., and Hvitved-Jacobsen, T. (2008). "Corrosion of concrete sewers—the kinetics of hydrogen sulfide oxidation." *Science of the Total Environment*, 394(1), 162-170.

Vollertsen, J., Revilla, N., Hvitved-Jacobsen, T., and Nielsen, A. H. (2015). "Modeling Sulfides, pH and Hydrogen Sulfide Gas in the Sewers of San Francisco." *Water Environment Research*, 87(11): 1980–1989.

Walcek, C. J., Pruppacher, H. R., Topalian, J. H., and Mitra, S. K. (1984). "On the scavenging of SO_2 by cloud and raindrops: II. An experimental study of SO_2 absorption and desorption for water drops in air." *Journal of Atmospheric Chemistry*, 1(3), 291-306.

Wylock, C., Colinet, P., and Haut, B. (2012). "Gas absorption into a spherical liquid droplet: Numerical and theoretical study." *Chemical Engineering Journal*, 207, 851–864.

Yang, Z., Zhu, D. Z., Yu, T., Edwini-Bonsu, S., and Liu, Y. (2019). "Case study of sulfide generation and emission in sanitary sewer with drop structures and pump station." *Water Science and Technology*, 79(9), 1685–1694.

Yang, Z., Zhu, D. Z., Yu, T., Edwini-Bonsu, S., Shypanski, A., and Liu, Y. (2020). "Case study of H_2S release and transport in a trunk sewer with drops." *Water Science and Technology*, 82(11), 2271-2281.

Yang, Z., Zhu, D. Z., Yu, T., Shypanski, A., Edwini-Bonsu, S., and Liu, Y. (2022). "Sulfide generation in force mains and its control using nitrate dosing." *Journal of Environmental Engineering*, 148(7), 04022032.

Yeh, N. K. (2002). "Liquid phase mass transfer in spray contactors." PhD dissertation, Dept. of Chemical Engineering, The Univ. of Texas at Austin, USA.

Yongsiri, C., Hvitved-Jacobsen, T., Vollertsen, J., and Tanaka, N. (2003). "Introducing the emission process of hydrogen sulfide to a sewer process model (WATS)." *Water Science and Technology*, 47(4), 85-92.

Yongsiri, C., J. Vollertsen, and T. Hvitved-Jacobsen. (2005). "Influence of wastewater constituents on hydrogen sulfide emission in sewer networks." *Journal of Environmental Engineering*, 131 (12): 1676-1683.

Yongsiri, C., Vollertsen, J., and Hvitved-Jacobsen, T. (2004a). "Hydrogen sulfide emission in sewer networks: a two-phase modeling approach to the sulfur cycle." *Water Science and Technology*, 50(4), 161-168.

Yongsiri, C., Vollertsen, J., Rasmussen, M., and Hvitved–Jacobsen. T. (2004b). "Air–water transfer of hydrogen sulfide: An approach for application in sewer networks." *Water Environment Research*, 76 (1): 81-88.

Zhang, G., Yang, Z., Zhou, Y., Zhu, D. Z., Zhang, Y., Yu, T., and Shypanski, A. (2022). "Combination of nitrate and sodium nitroprusside dosing for sulfide control with low carbon source loss in sewer biofilm reactors." *Journal of Hazardous Materials*, 424, 127527.

Zhang, L., De Schryver, P., De Gusseme, B., De Muynck, W., Boon, N., and Verstraete, W. (2008). "Chemical and biological technologies for hydrogen sulfide emission control in sewer systems: A review." *Water Research*, *42*(1-2), 1-12.

Zhang, Q., Shao, W., Zhu, D. Z., and Xu, W. (2020). "Steady air flow model for large sewer networks: a theoretical framework." *Water Science and Technology*, 82(3), 503-512.

Zhang, W., and Zhu, D. Z. (2015). "Far-field properties of aerated water jets in air." *International Journal of Multiphase Flow*, 76, 158–167.

Zhang, W., Zhu, D.Z., Rajaratnam, N., Edwini-Bonsu, S., Fiala, J., and Pelz, W. (2016). "Use of air circulation pipes in deep dropshafts for reducing air induction into sanitary sewers." *Journal of Environmental Engineering*, 142(4), 04015092.

Zuo, Z., Chang, J., Lu, Z., Wang, M., Lin, Y., Zheng, M., Zhu, D.Z., Yu, T., Huang, X., and Liu, Y. (2019). "Hydrogen sulfide generation and emission in urban sanitary sewer in China: What factor plays the critical role?" *Environmental Science: Water Research and Technology*, 5(5), 839-848.

Appendices

Oxidation of H_2S by O_2 at Turbulent Water Surface

H_2S can be oxidised by O_2 to generate element sulfur (S^0) at acidic environment (pH < 7) and sulfate (SO_4^{2-}) if pH > 7.5 (Cadena and Peters 1988). Millero et al. (1987) suggested the overall rate constant (k) for H_2S oxidation by DO in water is:

$$\mathrm{d}C_{\mathrm{H_2S}} / \mathrm{d}t = kC_{\mathrm{O_2}} C_{\mathrm{H_2S}} \tag{A-1}$$

where oxidation rate constant k is related to pH, water temperature T, and the ionic strength I:

$$\log k = 10.50 + 0.16\mathrm{pH} - \left(3.0\times10^3\right)/T + 0.44I^{1/2} \tag{A-2}$$

In Eq. (A-2), the application range for pH is 4-8, T is 278–338 K (5-65 ℃), and I is 0-6 mol/L.

A typical example of estimating H_2S oxidation in our experiments is given below. Experimental conditions are T = 293 K (20℃), pH = 7.5 and I = 0 (in DI water). k is calculated to be 28.9 L/(mol h) from Eq. (A-2). In the collection pool, C_{DS} = 5 mg/L = 1.5 × 10^{-4} mol/L and f = 27% [Eq. (3-7)], and hence C_{H_2S} = 4.2 × 10^{-5} mol/L. Based on Eq. (A-1) (where C_{O_2} = 5 mg/L = 1.6 × 10^{-4} mol/L and Δt = 9 min), the change of H_2S concentration due to oxidation in the collection tank, ΔC_{H_2S}, is calculated to be 2.9 × 10^{-8} mol/L, which accounts for 0.02% of total DS. While in Figure 3-4, the mass-transferred ΔC_{H_2S} accounts for 42% of total DS. Therefore, the oxidation rate of H_2S is smaller than 0.1% of its total mass transfer rate. This can be further demonstrated in Figure A-1, where K_L for O_2 in tap water is not larger that in H_2S solution under the drop or jet scenario. If the oxidation in H_2S solution were important, the oxidation would consume a certain part of O_2 and

slow the increase of DO concentration, and thus cause K_L for O_2 in tap water obviously larger than that in H_2S solution. In brief, the oxidation of H_2S did not play an important role in our experiments.

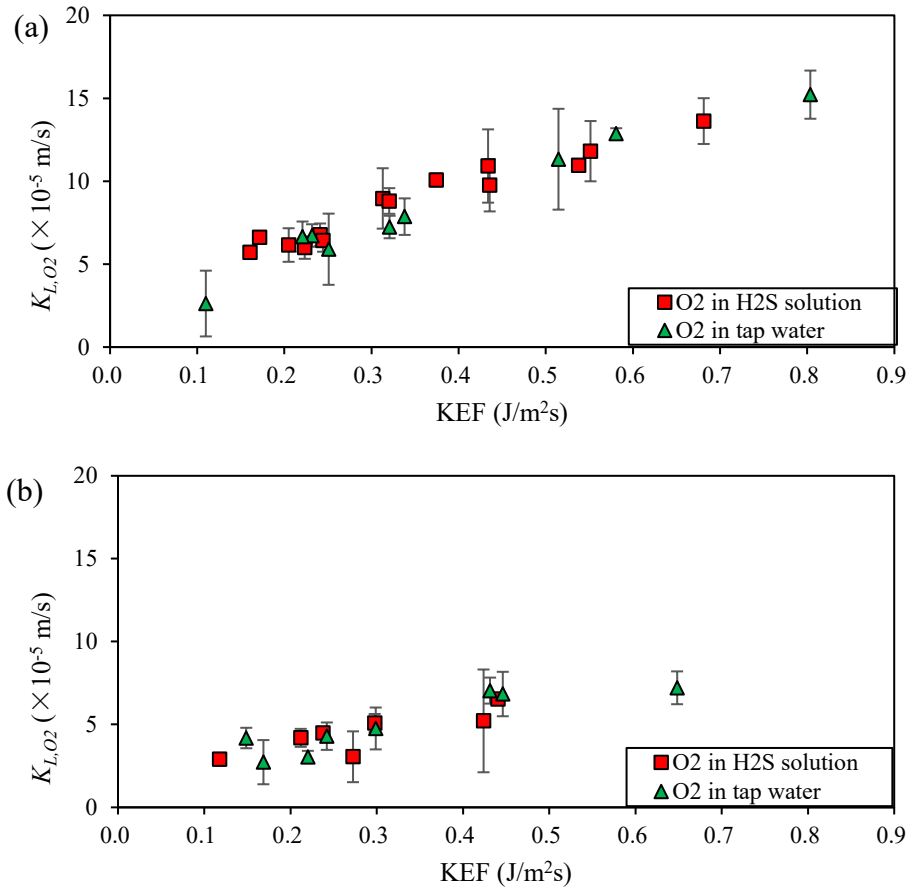

Figure A-1 Comparison of K_L for O_2 in the H_2S solution (with oxidation) and tap water (without oxidation) under scenarios of (a) falling drops; and (b) falling jet. Error bars show ±1 standard deviation.

Oxidation of H_2S by O_2 in Drop Structures

H_2S is oxidised by O_2 to generate element sulfur (S^0) at acidic environment (pH < 7) and sulfate (SO_4^{2-}) if pH > 7.5 (Cadena and Peters 1988). Millero et al. (1987) suggested the overall rate constant (k) for H_2S oxidation by DO in water is

$$\mathrm{d}C_{\mathrm{H_2S}} / \mathrm{d}t = kC_{\mathrm{O_2}} C_{\mathrm{H_2S}} \tag{A-3}$$

where oxidation rate constant k is related to pH, water temperature T, and the ionic strength I,

$$\log k = 10.50 + 0.16\mathrm{pH} - \left(3.0\times10^3\right)/T + 0.44I^{1/2} \tag{A-4}$$

In Eq. (A-4), the application range for pH is 4-8, T is 278–338 K (5-65 ℃), and I is 0-6 mol/L.

A typical example of estimating H_2S oxidation in the experiments is given below. Experimental conditions are T = 294.4 K (21.4℃), pH = 5.9 and I = 0 (in DI water). k is calculated to be 17.7 L/(mol·h). C_{DS} = 6.3 mg/L = 1.8 × 10^{-4} mol/L and f = 94% [Eq. (4-5)], hence C_{H_2S} = 4.2 × 10^{-5} mol/L. Based on Eq. (A-3) (where C_{O_2} = 2.9 mg/L = 9.0 × 10^{-5} mol/L, C_{H_2S} = 6.2 mg/L = 1.8 × 10^{-4} mol/L and Δt = 20 min), ΔC_{H_2S} is calculated to be 3.3 × 10^{-3} mg/L, which accounts for 0.05% of total DS. The mass-transferred ΔC_{H_2S} (2.7 mg/L) accounts for 43 % of total DS. Therefore, the oxidation rate of H_2S is around 0.1% of its mass transfer rate. This can be further demonstrated in Figure A-2 where r for O_2 in water is similar to that in H_2S solution. If oxidation in H_2S solution were important, the oxidation would consume a part of O_2 and slow the increase of DO concentration, and thus cause r in clean water obviously larger than that in H_2S solution. In brief, the oxidation of H_2S in our experiments did not play an important role for the mass transfer in drop structures.

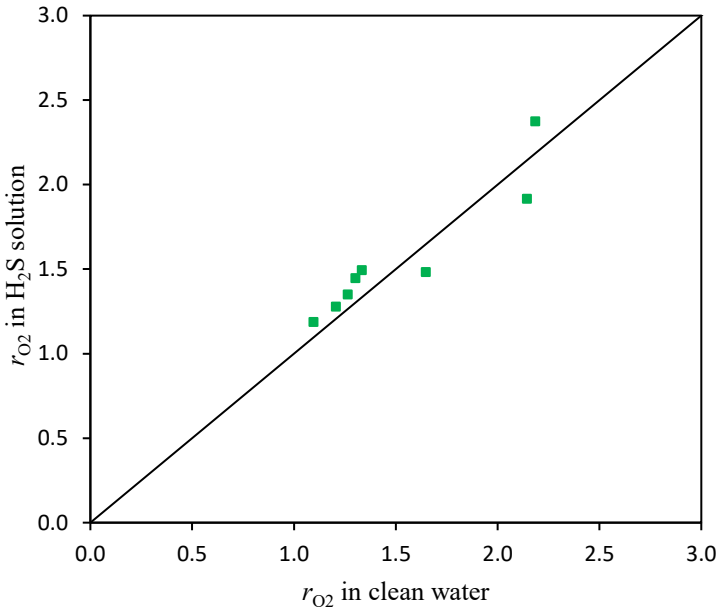

Figure A-2 Comparison of r_{O_2} in water and H_2S solution.